1-1-2003

Self-consolidating concrete : rheology, fresh properties and structural behaviour

Vasilios Bill Lambros
Ryerson University

Follow this and additional works at: http://digitalcommons.ryerson.ca/dissertations

Part of the Civil Engineering Commons

Recommended Citation

SELF-CONSOLIDATING CONCRETE: RHEOLOGY, FRESH PROPERTIES AND STRUCTURAL BEHAVIOUR

By

Vasilios Bill Lambros, B.Eng.

Ryerson University, 2001

A thesis

presented to Ryerson University

In partial fulfillment of the

requirements for the degree of

Master of Applied Science

in the program of

Civil Engineering

Toronto, Ontario, Canada, 2003

National Library
of Canada

Bibliothèque nationale
du Canada

Acquisitions and
Bibliographic Services

Acquisisitons et
services bibliographiques

395 Wellington Street
Ottawa ON K1A 0N4
Canada

395, rue Wellington
Ottawa ON K1A 0N4
Canada
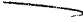
Canada

AUTHOR'S DECLARATION

I hereby declare that I am the sole author of this thesis.

I authorize Ryerson University to lend this thesis to other institutions or individuals for the purpose of scholarly research.

Vasilios B. Lambros

I further authorize Ryerson University to reproduce this thesis by photocopying or by other means, in total or in part, at the request of other institutions or individuals for the purpose of scholarly research.

Vasilios B. Lambros

ii

BORROWERS PAGE

Ryerson University requires the signatures of all persons using or photocopying this thesis. Please sign below, and give address and date.

Name   **Address**   **Date**

ABSTRACT

SELF-CONSOLIDATING CONCRETE: RHEOLOGY, FRESH PROPERTIES AND STRUCTURAL BEHAVIOUR

Vasilios Bill Lambros
2003, MASc., Department of Civil Engineering, Ryerson University

Self-consolidating concrete (SCC) is known for its excellent deformability, high resistance to segregation and bleeding and can be obtained by incorporating viscosity modifying agents (VMA). Identifying and proposing a new low-cost VMA, and developing and testing the fresh and mechanical properties of such a concrete are essential. This thesis presents the performance of four new polysaccharide-based VMAs in enhancing the rheological and fresh properties of cement paste, mortar and concrete. An experimental study on the structural properties of two SCC and one normal concrete (NC) mixtures with varying proportions of coarse aggregate content (713-1030 kg/m^3) and maximum aggregate size (12 and 19-mm) is presented. Eighteen reinforced concrete beams were tested to study the comparative shear resistance of SCC and NC. Sixteen SCC and NC filled steel tube columns with and without additional steel reinforcement were tested. A design equation for peak load capacity of CFST columns is proposed and validated

ACKNOWLEDGEMENTS

I would like to express my deepest gratitude to my supervisors, Dr. Mohamed Lachemi and Dr. Anwar Hossain, for their guidance, support and patience during the development of this thesis. A special thanks to Dr. Mohamed Lachemi whom for the past four years has always given me the encouragement, support and wisdom to grow and excel in all my endeavors, I am indebted to you.

Many thanks to Nidal Jaalouk and Dan Peneff for their technical assistance during the experimental program of this thesis.

To my colleagues and friends, thank you for the memorable moments we shared together over these past six years at Ryerson.

Finally, special gratitude goes to my family. Without your constant love, support and sacrifices my successes would not be possible

DEDICATION

To My Family

TABLE OF CONTENTS

LIST OF TABLES

LIST OF FIGURES

NOTATION

A_c	net area of concrete
A_{cc}	area of the confined concrete subtract rebar reinforcement
A_{cch}	is the area confined by the hoop confinement.
A_{ct}	cross area of concrete core measured center-to-center of outer tie
A_{ra}	total area of longitudinal reinforcement
A_{rv}	total area of steel rebar taken as and equivalent concrete area by the volumetric ratio of total rebar to total concrete.
A_s	steel tube cross sectional area
A_{sc}	area of embedded steel
A_{sr}	area of the steel bar
A_{st}	cross sectional area of longitudinal steel area of embedded steel
a	shear span
b	width of beam base
d	diameter of the confined concrete section
d_b	effective depth of beam
d_r	rebar diameter
D	outside diameter of steel tube
DI	ductility index
D_r	diameter of the concrete from center-to-center of the confining rebar
E_c	elastic modulus of concrete
E_s	elastic modulus of the steel tube
f_2	lateral confining pressure at tube yield
f_{2max}	maximum uniaxial lateral pressure
f_c	concrete stress
f'_c	compressive strength of the unconfined concrete
f_{cu}	in-situ compressive strength (air-cured strength)
f'_{cu}	compressive strength of the concrete cubes.
f'_{cc}	compressive strength of the confined concrete
f'_{cch}	compressive strength of the hoop confined concrete
f_p	unconfined compressive strength of concrete (factored)
f_r	modulus of rupture of concrete
f_{rp}	lateral confining pressure at rebar (hoop) yield
f_s	yield strength of the steel bar
$f_s{}'$	equivalent stress acting on the steel tube
f_T	axial stress applied to the concrete core
f_y	uniaxial steel yield strength.
f_{yr}	yield strength of reinforced steel
f_{ys}	Von Mises' stress
H	height of steel tube
h	height of beam
I	moment of inertia of beam section
K	effective length factor
l_8	bonded length

M_a	theoretical cracking moment
N_u	axial capacity of thin walled confined columns
P	axial load on the concrete core
P_b	applied load on beam
P_{85}	load at 85% the peak load
P_{max}	maximum column or confined column load
P_o	calculated ultimate strength
P_{obs}	observed axial capacity of CFST
P_{r1}	axial capacity of CFST
P_{r2}	axial capacity of CFST
P_s	load carried by the steel
P_{ys}	axial load CFST corresponding biaxial steel yield
s	lateral spacing of the confining hoops
t	is the thickness of the steel tube
V	applied shear force at critical section
V_c	shear cracking resistance
V_r	shear resistance based on CSA flexural design method
V_u	ultimate shear force
y_t	distance from the centroid to extreme tension layer of the section

α	hoop stress factor
β	axial stress factor
ε_{85}	axial strain in the column at 85% of the peak load on the descending branch of the stress strain curve
ε_a	axial steel strain of tube
ε_h	circumferential/hoop steel strain of tube
ε_p	axial strain of CFST at axial peak load
ε_{ys}	axial strain CFST corresponding biaxial steel yield
λ	slenderness
ν	Poisson ratio
ρ	ratio of tension reinforcement
σ_a	axial stress in steel tube
σ_h	hoop stress in steel tube
τ_1	average tensile strength
τ_{max}	maximum tensile strength

CAN/CSA S16.1-1984

C_r	factored compressive resistance of the steel tube
C_r'	factored compressive resistance of confined concrete
C_{rc}	factored compressive resistance of composite section
L	length of steel tube
r_c	radius of gyration of the concrete area
S	sort term load

T	total load on column
λ_s	slenderness of steel tube
λ_c	slenderness of concrete
τ	modifier for length effect of steel tube
τ'	modifier for length effect of concrete
ϕ_s	steel material resistance factor
ϕ_c	concrete material resistance factor

AISC/LRFD 1994

E_m	elastic modulus of the composite section
F_{cr}	critical stress
f_{my}	compressive strength of the composite section
P_{cr}	critical load
r_m	radius of gyration of the steel tube
λ	slenderness

1.0   Introduction

1.1   General

Many types of construction materials are used in building infrastructure. Concrete, undoubtedly, is the most widely used of all building materials and it is the largest consumer of natural resources such as water, sand, gravel and crushed rock. Portland cement is the commonly used binder for modern concrete mixtures. Besides the large amount of natural resources required in the production of cement, considerable amount of energy is required for the process, which results in large quantities of CO_2 emissions into our atmosphere. Poor workmanship, quality of materials and management of our infrastructure are the main causes of premature deterioration in concrete structures. It has been proven that normal concrete of the past does not satisfy the needs of structures in harsh and even mild climates. Deterioration due to poor durability is an issue and it is imperative that the construction industry use more sustainable materials to increase the efficiency of modern structures.

The required workability for casting concrete depends on the type of construction, selected placement, consolidating methods, and the complex shape of the reinforcement. With the increased use of congested reinforced concrete there is a growing need for highly flowable concrete to ensure proper filling of the formwork. Congested elements restrict the access of vibrators required to adequately consolidate normal concrete. Moreover, excessive vibration can cause undesirable segregation and bleeding in non-flowable concrete. Therefore, skilled labour and strict quality control are required to ensure sufficient compaction and adequate homogeneity of the concrete to avoid the degradation of infrastructure. Ensuring proper placement and consolidation of non-flowable concrete increases the cost of construction and time required to complete a project.

Self-consolidating concrete (SCC) is a highly flowable concrete that can flow into place under its own weight. SCC achieves good consolidation without internal or external vibration and without defects due to segregation and bleeding. SCC can be employed to

1

facilitate the filling of congested structural elements within a restricted area, it can be used as a repair material for structural rehabilitation, and it can also be used in casting non-congested elements to reduce construction time and improve the overall productivity of a project. SCC can also reduce labour cost, and improve the working environment by eliminating the noise and pollution caused by vibrators.

SCC was first developed in Japan in the early 1980's. The roots of the development were dictated by three main factors, one being the need for flowing concrete to compensate proper filling within the intricate reinforcement design in seismic members. The others are the decreasing number of skilled craftsmen in Japan and the need to reduce the cost and time of construction. With the growing use of concrete in special architectural configurations and closely spaced reinforcing bars, it is very important to produce concrete that ensures proper filling ability, good structural performance, and adequate durability (Hayakawa et al., 1993).

1.2   Statement of the Problem

There are several different approaches used to develop SCC. One method to achieve self-consolidating property is to increase significantly the amount of fine materials, for example fly ash or limestone filler (Sakata et. al, 1995 and Bouzoubaa and Lachemi, 2001, Lachemi et al., 2003a) without changing the water content compared to common concrete. An alternative approach consists of incorporating a viscosity modifying admixture (VMA) to enhance stability (Sari et. al, 1999; Lachemi et al., 2003a).

Viscosity modifying admixtures (VMA) are water soluble polymers that increase the viscosity of mixing water and enhance the ability of cement paste to retain its constituents in suspension. VMAs are used to enhance the stability of SCC (Rols et al. 1999; Khayat and Guizani, 1997, Lachemi et al., 2003a). The use of VMA along with adequate concentration of superplasticizer can ensure high deformability and adequate workability leading to good resistance to segregation. The use of VMAs have proven very effective (Sakata et. al., 1996), but they tend to be costly and increase the overall price of the SCC.

2

A cost-effective VMA can significantly reduce the price of SCC which would encourage the use of the concrete in new construction.

If the use of SCC is to evolve beyond the current prominence of being a concrete for highly congested members only, along with the development of cost-effective SCC, application and the structural performance involving the material should be explored. Currently, there are many publication related to research on the fresh properties, mix proportions and some applications of SCC. However, there is little research on the structural performance of SCC. The lack of published research related to the structural behaviour of SCC may deter engineers from using the concrete in the construction of new structures. There is a need for more studies on the application of the concrete in ductile elements such concrete filled steel tube (CFST) columns, and to study the effect of SCC in the structural performance of elements.

1.3   Objectives

The objectives of this study were to:

- Investigate the performance of four different types of new VMAs, based on various tests on rheological properties. A series of tests were carried out using viscometer to obtain rheological data such as yield stress, apparent and plastic viscosity. This was performed in an attempt to determine the robust mixture proportions for the cement pastes/mortars incorporating various dosages of superplasticizer (SP) and VMA.
- Develop and test two mixtures of SCC with VMA and one normal concrete (NC) mix, with different aggregate size and content to use in structural elements.
- Examine the effect of SCC, aggregate content and size on the shear strength of reinforced concrete beam elements through a comparative study of initial shear cracking and ultimate shear strength of two types of SCC and one NC mixtures.
- Study the behaviour of SCC with different aggregate contents in CFST columns and CFST columns with congested reinforcement. This phase also

3

included the study of existing peak strength models for confined columns, and to develop and propose a new peak load model for confined columns with SCC and NC which accounts for additional hoop confinement and longitudinal reinforcement.

1.4   Scope

Chapter two comprises of a review of available literature on the properties and applications of SCC, the mechanical properties of SCC in beam and column elements, the mechanical properties of concrete and steel tubes in CFST, and existing models used to develop and predict the peak loads of CFST.

Chapter three presents the experimental investigation carried out on the rheology of various cement pastes and mortar mixtures with four new VMAs and a commercial VMA. The chapter presents the experimental program, the materials used in the study, the results of the test program and the analysis of the washout and rheology test results for cement pastes and mortars with VMAs.

Chapter four presents the fresh and hardened properties of SCC and NC used in the structural investigation. These include the mix proportions, mix procedures, tests and results on the flowability of SCC and the mechanical properties of SCC and NC.

Chapter five presents the experimental program for reinforced concrete beam elements studying in shear behaviour failure. Eighteen reinforced beams manufactured from SCC and NC, with shear-span-to-depth ratios of 2.16, 1.55, and 1.06 were tested to failure under four-point loading. A comparative analysis was conducted on the effect of SCC with 12-mm aggregate, SCC with 19-mm aggregate and NC with 12-mm aggregate (with a higher aggregate content than both SCCs) on the shear resistance of beam elements.

Chapter six presents the experimental program for confined columns with SCC and NC. Sixteen columns with height-to-diameter ratios (H/D) of 3.1, 4.8, 6.8 and 9.5 were

constructed using SCC and NC, instrumented and tested to failure in concentric uniaxial compression. The data gathered from the tests was used to analyze the effect of different types of concrete (SCC or NC) on the behaviour of CFST and to develop the peak strength model.

Conclusions and recommendations from the investigations are presented in chapter seven.

2.0   Literature Review

The required workability for casting concrete depends on the type of construction, selected placement and consolidating methods, and the complex shape of the reinforcement. With the increased use of heavily reinforced concrete elements there is a growing need for highly flowable concrete to ensure proper filling of the formwork as well as need for decrease in production time with no increase in man power. Providing adequate consolidation of such congested elements can be difficult with the restricted access for vibrators. Also excessive vibration to fluid concrete can cause undesirable segregation and bleeding in the concrete. Therefore, skilled labour and strict quality control are required to ensure sufficient compaction and adequate homogeneity of the concrete. Ensuring proper placement and consolidation of concrete increases the cost of construction and time required to complete the project.

Self-Consolidating Concrete (SCC) is a highly flowable High Performance Concrete (HPC) that can flow into place under its own weight and achieve good consolidation without internal or external vibration and without exhibiting defects due to segregation and bleeding (Lachemi et al, 2003). SCC can be employed to facilitate the filling of congested structural elements with restricted access for consolidation and can be used as a good repair material and for repair and rehabilitation. SCC can also be used in casting non-congested structures where it can reduce construction time, hence improving overall productivity at the construction site. Additional benefits in using SCC include reduced labour cost, and improved working environment by eliminating the noise and pollution caused by the vibrators (Campion and Jost, 2000).

There are limited published studies on the structural performance of SCC. Many researchers of SCC concentrated on the fresh properties and mix proportions to produce a cost effective and more efficient product. Consequently, the lack of research on the structural applications of SCC deters engineers from using such a concrete in design, as no reliable design guidelines are available.

2.1   Self Consolidating Concrete (SCC)

SCC is gaining worldwide acceptance as a high performance construction material. The growing interest in SCC is leading concrete suppliers/manufactures, researchers and engineers into investigations to understand and develop new cost effective and high performance materials.

The primary advantage associated with SCC is the improvement of productivity mainly in the transport and placement of fresh concrete. Development of SCC can also offer an increase in automation of the concrete construction process (Skarendahl, 1999). Also the improved working environment can be improved with the use of SCC. Operating a vibrating poker creates a disturbance in the blood circulation of the worker causing what is known as "white fingers". It also causes noise and air pollution. SCC eliminates the use of vibrators creating improved working conditions and in-turn increases the cost-efficiency of concrete construction. The improved working environment may attract more skilled people into concrete construction, a worldwide problem the construction industries is facing today.

Durability of structures is a major issue with conventional concrete. Thus, high performance materials are required to produce more durable structures. Proper filling and consolidation associated with the use of SCC can eliminate voids and insufficient bonding of concrete to the reinforcement, which in turn, can increase the durability of the concrete and reduce future rehabilitation costs.

The benefits of incorporating SCC in new construction projects are the most convincing aspect. SCC has not yet gained the confidence of construction industry and lack of case studies delays the situation further. Incorporating SCC in construction projects can reduce the cost and time of concrete construction as reported by Okamura (1996). Use of SCC in the construction of a liquefied natural gas tank decreased the number of lifts required and increased the height of the lift, for slip-form casting, resulting in faster productivity. The number of concrete workers was decreased from 150 to 50 and the construction period was decreased from 22 to 18 months.

2.1.1 SCC Applications

Lacombe et al (1999) investigated the application of SCC as an overhead repair material. The study tested three types of repair materials such as normal concrete, SCC and shotcrete. Three concrete blocks were repaired at a depth of approximately 40 mm on one surface of each block. The SCC used in the experiment included a Viscosity-Modifying Agent (VMA) to reduce bleeding and segregation in the mixture. Following seven days from the repairs, observations were made for each repair method. Results indicated that the normal concrete did not possess suitable rheological properties and filling capacity to be used as an overhead repair material. It also developed considerable segregation and large air pockets. This technique required skilled labour and was expensive. SCC performed well as a repair material creating a good bond and showed good rheological properties essential for a quality repair material. But unfortunately, SCC was expensive due to the use of chemical admixtures. Furthermore, labour was not a major factor in the placement of the SCC as it consolidated under its own weight. Shotcrete bond to old concrete was almost perfect, but skilled labour was required to perform the work and the cost was increased significantly. The research also suggested the need for more investigations to develop cost-effective SCC in order to increase its use as a repair material.

Other applications for SCC as a repair material were described by Campion and Jost (2000). SCC was used to repair a chloride-induced deteriorated cast-in-place bridge built in the 1960's in the Swiss Alps. The concrete structure had lost a substantial amount of concrete and steel reinforcement on its underside. Formwork and placement of concrete followed the replacement of the steel reinforcement under the deck. The only poured concrete available to accommodate the task at hand was SCC, and it was pumped in the formwork through the underside. Air holes were drilled at the top of the deck to allow the release of pressure generated when concrete is pumped in the formwork. SCC allowed the project to be finished on time while maintaining the required concrete quality throughout the entire project (Campion and Jost, 2000).

Khayat and Aïtcin (1999) investigated projects in Canada where SCC was used. These included the rehabilitation of the Webster parking garage in Sherbrooke, the rehabilitation of the Beauharnois Dam near Montreal, the casting of experimental residential basement walls, and the construction of a reaction wall at the Université de Sherbrooke. The use of SCC in these projects showed SCC to be an effective material for the repair of damaged structural sections. SCC also enhanced reliability and durability of newly constructed concrete walls.

Other applications included self-consolidating high-performance concrete as discussed by Okamura (1996). The use of SCC in structures has gradually increased over the last few years. The Akashi Straits Bridge is one of the longest suspension bridge in the world, and SCC was used in the construction of the two anchorages of the bridge. The concrete was batched in an onsite plant and transported by pump through 200 m of pipes. The maximum size of coarse aggregate was 40 mm and despite the large size of aggregate, no segregation was observed. The use of SCC shortened the construction period of the two anchorages by 20%, from 2.5 to 2 years.

Li (1995) discussed the use of SCC in Japan and the competitive edge gained by the firms when producing their own. Two projects in particular were highlighted as examples. One being the Kiba-Park Large Bridge, a 151-m cable-stayed prestressed concrete bridge, only required two workers to pour 650 m^3 of SCC in nine months. The incentive to use SCC was the difficulty and high labour cost of placing normal concrete in heavily reinforced concrete structures. The second was a 70-storey building, the tallest high–rise in Japan, that used 885 m^3 of SCC pumped into steel tubular columns. The concrete was pumped in from the bottom at a maximum filling height of 40 m.

2.1.2   Achieving Self-Consolidation

SCC concrete requires a high slump that can easily be achieved by superplasticizer addition to a concrete mixture (Bouzoubaâ and Lachemi, 1999). The superplasticizer alone can increase the fluidity of the concrete but also increase segregation and bleeding.

9

One method adopted to resolve the problem of segregation and bleeding is the use of supplementary cementing material (SCM) such as fly ash, silica fume and blast furnace slag Lachemi et. al., 2003a, Bouzoubaâ and Lachemi, 1999). The second option is to incorporate a VMA to stabilize the concrete mixture. VMA will be reviewed in more detail in the following section.

Previous investigations had shown that the use of blast furnace slag and fly ash in SCC reduced the dosage of superplasticizer needed to obtain similar slump flow as for concrete made with Portland cement only (Bouzoubaâ and Lachemi, 1999). Sakata et al. (1995) incorporated limestone powder as a SCM in SCC. The study investigated the characteristics and the proportioning of SCM for this type of concrete as it demonstrated to be within the allowable parameters for SCC. Research demonstrates that it is possible to produce a successful SCC with SCM although, as with any concrete with SCM the early strength development can be slow.

2.1.3   Viscosity-Modifying Admixtures

VMAs are used in SCC to enhance the stability of the concrete by reducing the segregation and bleeding. The cost of these concretes with VMA is about 20% higher than normal concrete (Li, 1995). Researches were conducted on the use of various types of VMAs in SCC.

Mantagazza and Alberti (1994) incorporated polysaccharide syrups derived from enzymatic hydrolysis of starch. This is an organic material used with five different variations. They discovered that a dosage of 0.1% did not affect the flow or mechanical characteristics of the concrete, but a dosage of 0.8% increased the setting time. However, it increased the compressive strength by permitting better hydration due to delayed setting time. Dosages from 0.2 to 0.4% were desired as they proved to be a good balance among all properties of SCC. Mantagazza and Alberti (1994) also combined many theories to explain the effects of polysaccharides. From their analysis, it was shown that the time of initial set increased with the increase of D.E. (equivalent dextrose) for all the

syrups used. This proved that polysaccharides could be used to maintain the workability by delaying set.

Welan gum, a type of polysaccharide, is one of the earliest forms of VMA. Welan gum is extremely effective in stabilizing the fluidity of concrete (Sakata et al., 1996). Welan gum has the ability to prevent segregation, maintain good viscosity and flow ensure adequate ability for proper filling of concrete. However, the cost associated with the use of welan gum is relatively high.

Sari et al. (1999) conducted tests using two VMAs in a high performance concrete. Precipitated silica slurry was used for one test and a polysaccharide containing hydrocolloid for the other. Hydrocolloid is used to suspend other particles when added to the mixture. Tests revealed both admixtures performed adequately to provide an excellent control over final concrete performance.

Research by Rols et al (1999) involved the use of starch, precipitated silica, and a by-product from the starch industry as an alternative to welan gum. The study determined that the starch products could be a good alternative to the welan gum as it produced good strength and resistance to segregation, bleeding and drying shrinkage.

2.2   Durability

Durability of concrete is challenged by the exposure conditions it faces and the presence of chemical constituents and impurities that may react with the cement. The main factors affecting the durability of concrete are freeze-thaw cycles, de-icing salts, carbonation, sulfate attacks and alkali-reactivity. Most attack must have the presence of water and are very dependant on the quality of the concrete or more significantly the porosity of the concrete surface. Freeze-thaw cycles can create expansive behaviour of ice in pores causing cracking of concrete near the surface and de-icing salts can increase the effect. De-icing salt contains chlorides that may depassivate the reinforcement allowing it to corrode in concentrated regions. Carbonation is not a major problem in Canada since the

relative humidity is high enough to prevent carbon penetration into concrete surfaces. Sulfate attacks react with elements in the cement paste and cause expansive deterioration, which causes cracking in the concrete. Certain reactive aggregates react with alkalies in the cement and cause expansion resulting in cracks (Aïtcin, 1998).

It is well known that the reduction in the porosity of concrete decreases the possibility of deteriorating agents penetrating the concrete surface. Reduction in porosity can be accomplished by reducing the water-to-binder ratio (W/B) of the concrete mixture. The use of HPC with SCM such as fly ash, slag and silica fume can reduce the porosity of the concrete even more with low W/B.

Tumidajski and Chan (1996) performed experiments on six concrete mixes exposed to magnesium brine to determine the durability of HPC. The HPC mixtures incorporated ground granulated blast furnace slag, silica fume and fly ash. All HPC showed to be more durable than the normal concretes when exposed to magnesium, chloride and sulfate attacks. The HPC with slag had the best overall durability.

2.3   Mechanical Properties of Self-Consolidating Concrete

The performance of reinforced concrete is significantly influenced by the quality of the concrete. The quality of structural concrete is dependant on the properties of the materials and the concrete mix properties. Each constituent within the concrete has an effect on the properties of the structural concrete. Water influences the strength and durability of the concrete. High quantities of Portland cement can increase heat of hydration and cause high rates of drying shrinkage, leading to early cracking in concrete. Aggregate strength and type can have an effect on strength and can contribute to other undesired problems such as alkali aggregate reactions in the concrete. Proportioning structural concrete is dependant on the application and conditions it will be subjected to. High quality concrete will ensure that the structural performance of the concrete will not be affected by the loss of durability due to deterioration and poor construction practices. Being a fairly new concrete, SCC does have an abundant resource for future research on

durability and structural performance. The majority of structural construction with SCC has taken place within the last decade in which all performance related issues are only within a short time frame. The mechanical properties of SCC must be clearly understood in order to determine the design constraints or improvements that can be applied to the design of structural elements with SCC.

2.3.1 Strength and Elastic Modulus of SCC

One of the most important properties of structural concrete is its compressive strength. When designing concrete structures, engineers must specify the compressive strength (f'_c). The compressive strength of normal concrete ranges from 20 to 40 MPa (CPCA, 1995). Usually, the compressive strength is determined by testing 150 x 300 mm or 100 x 200 mm cylinders under axial compression at 28 days. The consistency of the concrete and its rheological properties are important to produce a concrete without significant variations in strength within a structural element such as a column or beam. The VMAs used in SCC are required to retard the effects of superplasticizer (SP) on segregation and bleeding of concrete. The segregation of aggregates can significantly affect the structural performance of the concrete.

Persson (2001) performed a study on the mechanical properties of SCC such as strength, elastic modulus, creep and shrinkage. The data used in the study was taken from experimental studies performed in Japan (Ehara, 1998; Klevbo, 1999) and Sweden (Byfors and Grauers, 1997; Grauers, 1998; Dieden, 1999; Andersson and Sjökvist, 1999). Various mixes of concrete were designed for their use in beams, piles, slabs, T-beams and in tunnel construction. The study included a total of 88 cylinders, half made with normal concrete as reference samples and the other half with SCC. The SCC samples used various forms of viscosity fillers such as fly ash, glass fiber, limestone powder, silica fume and quartzite, and the w/c ranged from 0.24 to 0.80. One half of the samples tested were sealed airtight with foil to avoid moisture loss and the others were air-cured. Persson (2001) determined that the strength of the concrete tend to be significantly higher with the quartzite filler and low water-to-cement ratios. He also noted that the

comparison between normal concrete and SCC at constant porosity showed small differences in strength. The elastic modulus for both SCC and normal concrete exhibited similar curves regardless of the samples being air-cured or sealed.

Researchers from the University of Paisley had provided the concrete industry with valuable information for the properties of hardened concrete with several publications and online reports (Sonebi et al, 2000). The studies evaluated the properties of two types of SCC, incorporating limestone powder in the housing concrete (SCCH) and ground granulated blast slag in the civil concrete (SCCC). The reference concretes used Portland cement only. A third type of SCC incorporated steel fibres and limestone powder (FSCC). The W/B was 0.36 for both SCCH and SCCC and 0.68 and 0.43 for the reference concretes (RH and RC), respectively.

The compressive strength of SCC is generally high when incorporating viscosity-modifying agents (VMA), as compared to normal concrete. This is believed to be attributed to the slight delay of hydration due to the addition of VMA. Sonebi et al (2000) noted that the fine limestone powder developed high early strength due to the accelerated effect on C_3S hydration, where the blast furnace slag delayed hydration in the SCCH to produce lower early strengths than the reference concrete. The average 28-day compressive strength of the SCCH and SCCC were 47 and 79.5 MPa, respectively. The reference concretes RH and RC had compressive strengths of 37 and 61.5 MPa, respectively. Sonebi et al (2000) also noted that the difference in air-cured 90-day compressive strength was related to the type of filler used in SCC. The limestone powder was less affected by air-curing due to the accelerated affect on curing and water retentiveness of SCCH. The opposite was found for SCC with blast slag when compared to the reference concrete.

Sonebi et al. (2000) found the same relationship between modulus of elasticity and compressive strength for both SCC and normal concrete. Two cylinders for each type of concrete were tested at ages varying from 4 to 13 months. The comparison was calculated as a relationship in the form of:

$$\frac{E_c}{\sqrt{f'_c}} \qquad (2.1)$$

where E_c and f'_c are in units of GPA and MPa, respectively.

The recommended ACI 318-89 value is 4.73 for structural calculations with normal weight concrete (Sonebi et al, 2000). All the results found for both SCC and reference concretes were similar.

2.3.2 Bond Strength

The relevance of bond strength of SCC with deformed steel reinforcing rebar is important in terms of durability and bonding properties of reinforced SCC. The bond strength should not be significantly lower than that of normal concrete to avoid the degradation of structural performance.

Sonebi et al (2000) performed bond tests with 12 and 20 mm deformed reinforcing steel placed in concrete specimens with dimensions of 100 x 100 x 150 mm. Tensile forces were applied on the bar while the concrete was placed in compression. The average tensile forces (τ_1) were calculated as follows:

$$\tau_1 = \frac{P}{\pi d_r l_8} \qquad (2.2)$$

Where P, d_r and l_8 correspond to the applied load, bar diameter and bonded length, respectively (Sonebi, 2000). In general the bond strength of the SCCH and SCCC were higher than RH and RC, respectively. The analysis used normalized ratios of the tensile strength with compressive strength:

$$\frac{\tau_{max}}{\sqrt{f'_c}} \qquad (2.3)$$

15

And were used in comparison of SCC and reference concrete. Testing showed the normalized ratios of SCCH and SCCC were about 10% and 18-38% higher, respectively, than that of the reference mixes.

The lack of available data and research on various types of SCC limits the understanding of bond properties of SCC. From the limited resources available, bond of SCC shows positive results as it increases the bond strength of reinforcement to concrete (Sonebi, 2000).

2.3.3 Creep

Creep is the time-dependant increase of strain in concrete under sustained loading. Creep decreases with time at a decreasing rate and is expressed in terms of the creep coefficient (C_t). The amount of creep is dependant upon (1) the magnitude of stress, (2) The age and strength of the concrete when the stress is applied, and (3) the length of time the concrete is stressed (Kosmatka et al, 2002). Other factors that may affect creep include the materials used in the concrete, size and shape of concrete, temperature, exposure conditions, prior curing conditions and amount of reinforcing steel in the concrete. The creep strain begins when the elastic strain stops and only part of the creep strain is recoverable in old concrete never in new concrete.

Persson (2001) used 64 of the 88 cylinders used to study creep. The study proved that the creep coefficient of mature SCC coincided well with the corresponding property of normal concrete for both air-cured and sealed samples.

2.3.4 Shrinkage

Shrinkage is referred to the decrease in the volume of hardened concrete with time. The decrease of volume is attributed to the moisture loss caused by drying, hydration and chemical changes in cement paste. Shrinkage is not dependant on externally applied loads and strains begin immediately after exposing concrete to a drying environment.

Shrinkage is relatively small in reinforced normal concrete ranging between 200 and 300 microstrain (Kosmatka et al, 2002).

Persson (2001) presented the variation in shrinkage between samples of SCC and normal concrete. The shrinkage testing was performed on air-cured and sealed samples for 0.5 years and 1.5 years. Results showed less shrinkage for sealed samples for both normal concrete and SCC. The air-cured samples did not diverge between normal concrete and SCC when the relative humidity was held constant.

Drying shrinkage is not a significant problem in SCC. Many of the fillers and VMA used in SCC actually reduce the amount of shrinkage in hydrated paste as compared to normal concrete. SCC, which uses SCMs such as fly ash and slag, has reduced quantity of Portland cement and sometimes reducing the amount of shrinkage in the concrete. SCC with VMA does not increase the use of PC and may even limit the amount required therefore, maintains similar shrinkage characteristics as normal concrete. Sonebi et al (2000) found that the SCCH and SCCC concrete had lower shrinkage values than the reference concrete (NC) when measured at 28-day and 150-day. The reference mixes had more drying shrinkage of up to 35% higher than the SCC.

Research performed by Yasumoto et al (1998) on shrinkage cracking resistance of SCC reported the effects of various powdered additives on the drying shrinkage of SCC. Experimental tests showed that the SCC resistance to shrinkage was higher when limestone powder was used as an additive. SCC with Portland cement and blast furnace slag showed reduced shrinkage cracking over SCC with low-heat Portland cement.

2.4   Performance of Structural Elements Made with SCC

Proper placement of concrete in construction practices is vital to the performance and durability of concrete structures. Congested and heavily reinforced structural elements often are subjected to difficulties related to proper consolidation of the concrete. Construction practices utilize vibrators in consolidating concrete but may be insignificant

in confined structural elements. Heavily reinforced design is usually found in moment resistant frames in seismic areas. Inadequate consolidation of the concrete can result in low ductility, structural defects and poor bond with the reinforcing steel. Vibration and surface finishing of concrete can also delay construction time and overall completion time of projects. Developing a SCC that will satisfy the needs in terms of congested reinforcement should also be cost-effective for the construction industry. The research in SCC to date revolved around the mix proportions and fresh concrete properties. There is a major lack of research and information on SCC in structural elements and its mechanical and structural performance. Engineers are reluctant to use such a concrete that lacks sufficient data on its structural performance. Providing an affordable and durable SCC can open the doors to all types of construction projects especially where proper placement is a concern.

Sonebi et al (2000) demonstrated the use of in-situ testing for SCC structural elements using non-destructive testing (NDT). Tests were performed on columns and beams cast with both SCC and reference normal concrete and were tested along various locations of the elements. The elements made with normal concrete were vibrated to ensure proper consolidation. The SCC was not vibrated, allowing it to consolidate under its own weight. The significance of the results revealed the consistency between normal concrete and SCC in practical use. The columns with RH and RC reference concretes demonstrated higher strengths at the bottom, as expected for compacted concrete. Comparisons of the results suggested that the compressive strength in the SCC mixes was less variable along the column as compared to the reference concretes and much smaller in the beams. The in-situ strength achieved in the columns (all mixes) varied between 80 and 100% of the standard cube strength, which was above the average value of 65% reported for such elements. The average relative strength for the columns was much lower than the cube samples at 75 % because of different exposure and curing conditions. The in-situ surface testing confirmed the consistencies found with the core test results. A statistical analysis was performed to determine the statistical significance of any differences in the beams and columns. The analysis showed the variation in strength along the beams was statistically insignificant but was significant for the columns. Also,

there was a marginal increase in uniformity for in-situ properties of SCC as compared to the corresponding reference mixes.

2.4.1 Columns

Sonebi et al (2001) refers in his study of SCC columns at Paisley University to the reinforcement arrangements as house concrete (SCCH) and civil engineering concrete (SCCC) as shown in Fig. 2.1(a) and 2.1(b). The reinforcement arrangement for the SCCH consisted of 1.4% of longitudinal reinforcement (4 No. 12 and 4 No. 16) and 0.66% for lateral reinforcement (No. 10). The SCCC column utilized 1.9% (4 No. 16 and 8 No. 12) of longitudinal reinforcement and 1.53% of lateral reinforcement (No. 10). The longitudinal reinforcement stirrup spacing was 100 mm for the SCCH and 75 mm for the SCCC. The SCCH incorporated limestone powder as the viscosity filler and the SCCC incorporated ground granulated blast slag. Reference concrete was also used in column fabrication for comparison for each reinforcement configuration. Three columns, 300 x 300 x 3000 mm (Fig. 2.2) for each concrete mix were cast, where one was loaded to failure after 90-day, one was used for in-situ testing and one was put outdoors for future durability assessment. The reference concrete was cast and consolidated using an external vibrator while the SCC was allowed to consolidate under its own weight.
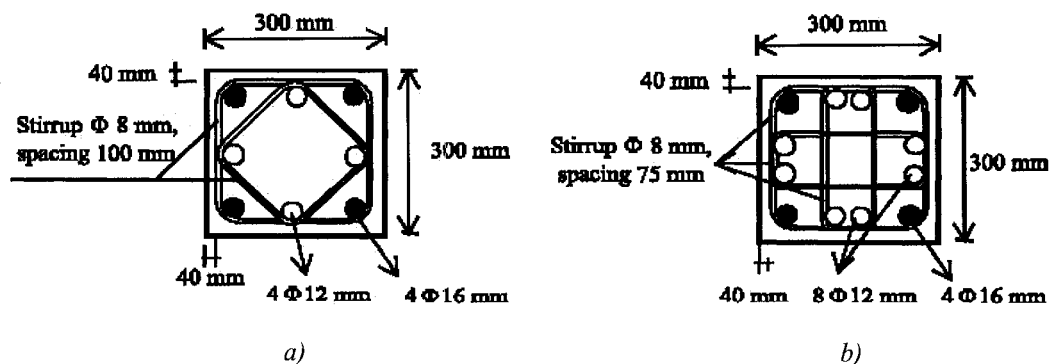
Fig. 2.1 – Detail of Column Reinforcement Configuration: (a) SCCH Application; (b) SCCC Application. (Zhu et al, 2001)

19
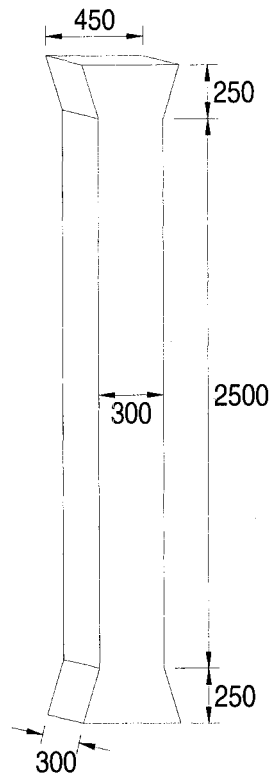
Fig. 2.2 – Column Dimensions, in mm
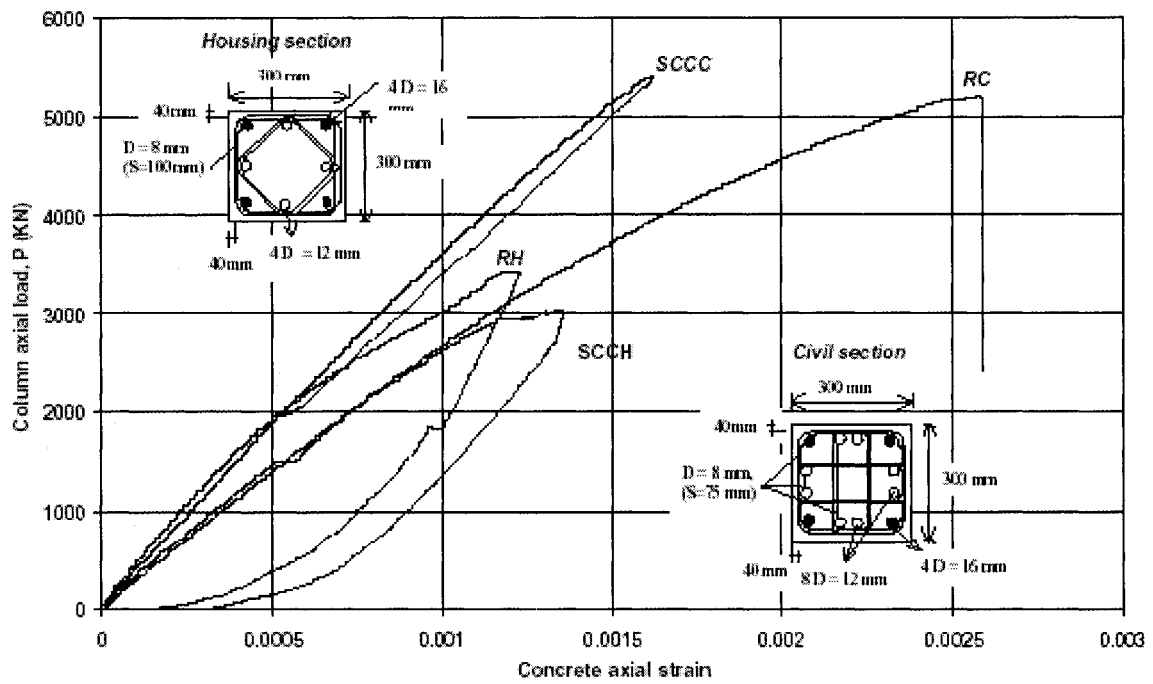
Fig. 2.3 – Comparison of Concrete Axial Load vs. Axial Strain for Columns (Sonebi et. al., 2000)

20

Axial loads were applied to each column until failure after a 90-day period and the results were plotted in an axial load vs. strain curves as shown in Fig. 2.3. The maximum load P_{max} of reinforced columns ranged from 3020 to 5415 kN. The ratio,

$$\frac{P_{max}}{P_o} \qquad (2.4)$$

was used for comparison of axial load of failure to calculate axial strength (as per Eq. 2.5):

$$P_o = 0.67 f_{cu} A_c + f_{yr} A_{sc} \qquad (2.5)$$

where

P_o is the calculated ultimate strength

f_{cu} is the in-situ compressive strength (air-cured strength)

f_{yr} is the yield stress of reinforced steel in compression

A_c is the net area of concrete

A_{sc} is the area of embedded steel

The ratio P_{max}/P_o were 2.07 and 1.18 for the reference concrete (RH) and the SCCH respectively, and were 1.4 and 1.35 for RC and SCCC respectively. Sonebi and Bartos (2001) noted that the SCC had lower ratios as compared to the reference concrete. All concrete mixes exceeded their design loads. Both SCC and RH housing concretes had lower axial load capacity of approximately 2000 kN less than those of the civil concrete. This could be attributed to the less lateral confinement for the housing concrete. The RC exhibited greater toughness than the SCCC. The SCCH and RH showed similar behaviour although results were slightly lower for SCCH.

The results from the experimental trails for SCC at the University of Paisley indicated the structural performance of SCC could vary for different types of SCC and might be less as compared to elements made with normal concrete.

Khayat et al. (2001) of the Université de Sherbrooke showed promising results in experiments performed on SCC with welan gum VMA. The experimental program consisted of two highly reinforced concrete columns with SCC and two others with normal concrete (NC) with compressive strengths of 40 to 50 MPa. Two unreinforced columns were also used to determine the overall load carrying capacity under monotonic axial loading. Two more unreinforced columns were cast to extract cores for in-situ compressive strength and modulus of elasticity of the SCC and NC. One column with unreinforced SCC of 60 MPa was cast to determine compressive strength under uniaxial compression. All columns had similar dimension of 235 x 235 x 1400 mm with similar configurations of reinforcement. Fig. 2.4 shows the column dimensions, reinforcement configuration and core sample extraction as described by Khayat et al. (2001). The water–to–binder ratio (W/B) was kept relatively low for the SCC mixes, ranging from 0.41 to 0.42 for SCC and 0.5 for the normal concrete.
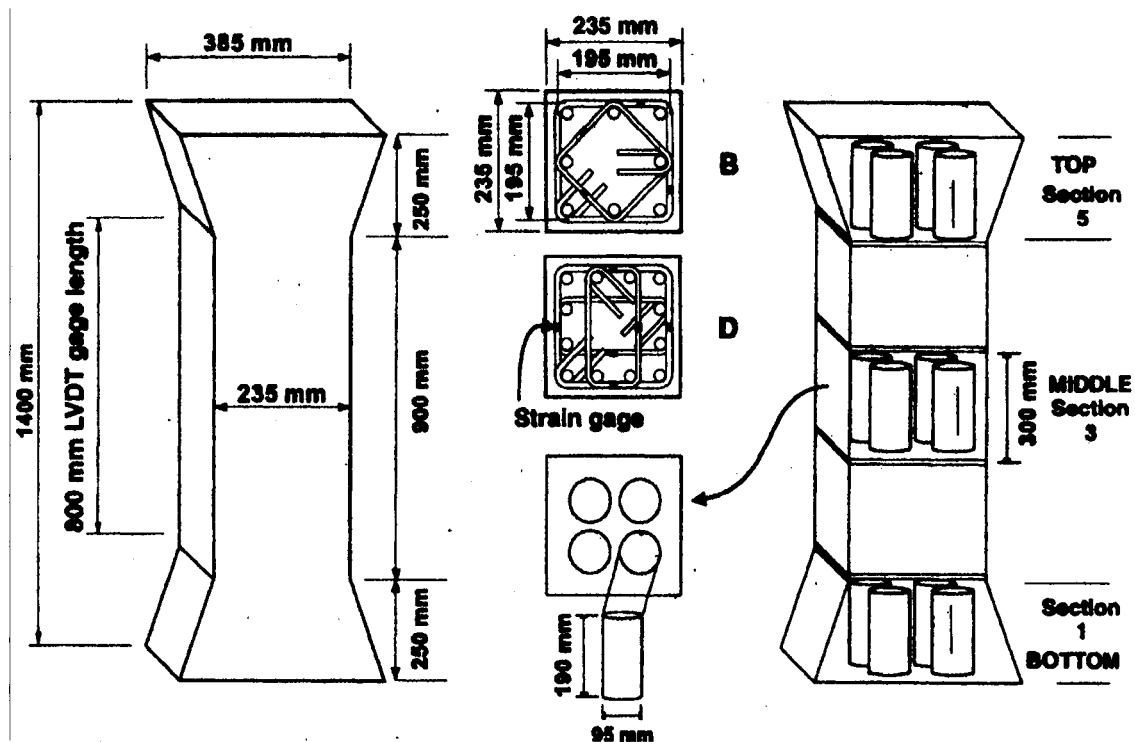
Fig. 2.4 – Column Specifications used by Khayat et al. (2001).

Configuration B had 3.6 % longitudinal reinforcement (4 No. 20 and 4 No. 15) with 4.9% lateral reinforcement (No. 10) at 50 mm spacing (Fig. 2.3). Configuration D had 3.6 % longitudinal reinforcement (4 No. 20 and 8 No. 10) with 4.8% lateral reinforcement (No. 10) at 50 mm spacing. Deformed bars were used for the longitudinal reinforcement and undeformed bars were used for the lateral reinforcement.

The columns fabricated with normal concrete were vibrated using a poker vibrator to ensure proper consolidation and the columns with SCC were not externally or internally vibrated allowing them to consolidate under their own weight. An acrylic plate was used on one side of the form to observe consolidation during placement. Several standard cylinders were cast along with the columns and cured for 14 days.

Results of the four reinforced columns for axial load vs. axial strain were plotted and compared using the same P_{max}/P_o ratio as used in the University of Paisley program, where the calculated ultimate strength (P_o) is the given by:

$$P_o = 0.85 f_c' A_{ct} + f_{yr} A_{sc} \tag{2.6}$$

where:

f_c'' is the maximum compressive strength of cylinders

A_{ct} is the cross area of concrete core measured center-to-center of outer tie

f_{yr} is the yield stress of longitudinal reinforced steel in compression

A_{st} is the cross sectional area of longitudinal steel area of embedded steel.

The results of the confined columns were also normalized with the unconfined columns to plot the relative concrete load vs. axial strain, and column axial load vs. axial strain in Fig. 2.5 and 2.6 respectively.
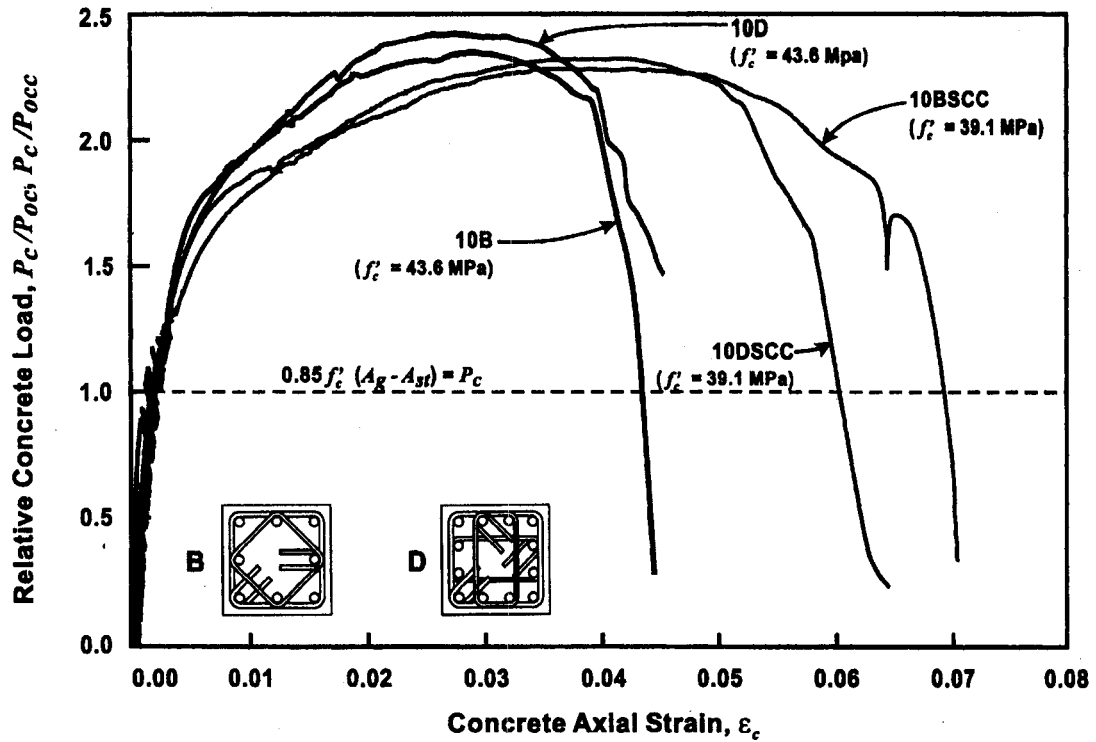
Fig. 2.5 – Comparison of Concrete Axial Load Versus Axial Strain for NC and SCC Columns (results normalized in terms of load on concrete with respect to unconfined section and confined section) (Khayat et. al., 2001).
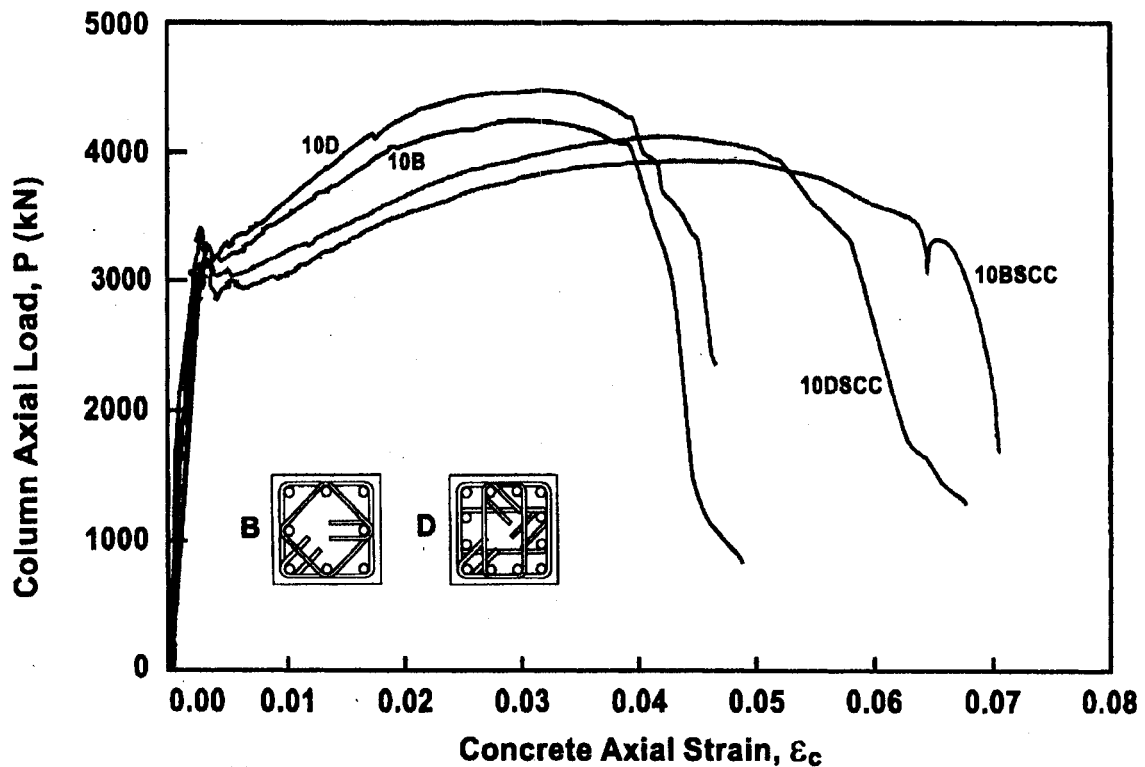
Fig. 2.6 – Comparison of Concrete Axial Load Versus Axial Strain for NC and SCC Columns (Khayat et. al., 2001)

24

The normalized values for the SCC and normal concrete were 1.5, 1.5 and 1.51, 1.53, respectively. Results showed that SCC and normal concrete had no significant difference in responses to axial loads. However, the curves clearly indicated that SCC was significantly more ductile with slightly lower ultimate compressive resistance than the normal concrete. Khayat et al (2001) also noted that the SCC exhibited better confinement than the normal concrete according to the determined strain ratios. The ratios also proved confinement B and D with SCC are 62% and 33% respectively indicating a more ductile behaviour than the corresponding normal concretes. The concrete ductility was affected by the elastic modulus of the concrete which was found to be 30.3 GPa for SCC and 37.0 GPa for the normal concrete.

Other significant results by Khayat et al (2001) confirmed the need for a 10% reduction when estimating the in-place strength of SCC members in compression. This confirmation was made when strength tests from unconfined columns and cores were compared to lab cast cylinders. Other researchers found similar results for members under axial loading therefore, justifying the required reduction in estimating in-place strength of SCC.

The experimental programs performed at both Universities suggested the adequacy of structural performance of SCC as compared to elements with normal concrete. Both programs also emphasized on the greater homogeneity of SCC on in-place compressive strength, which indicated more stable concrete than vibrated conventional concrete. Although maximum load-carrying capacity were comparable, the ductility of SCC between the two programs were opposite when compared with the reference mixes. Thus, the need for more research on structural performance of SCC is greatly needed to reduce the uncertainty of such results.

2.4.2 Beams

The lack of research on the application of SCC in beams was noted from the literature review. The only research used in this section was provided by the University of Paisley

where several beams with SCC and normal concrete were tested for flexural strength. Again, as in the columns the beams used two different configurations for steel reinforcement for the housing concrete and the civil engineering concrete. All beams used in the program were 3800 mm in length with a width of 200 mm and a height of 300 mm. Details of the reinforcement configurations are shown in Fig. 2.7. The housing SCC was the only concrete not cast for beam testing.
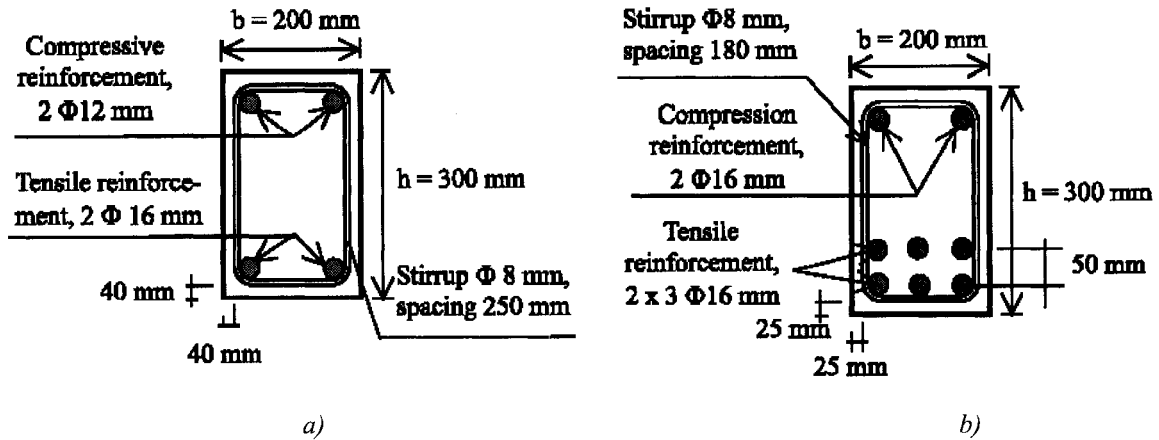
Fig. 2.7 – Details of Beam Reinforcement Configuration (a) for Housing Applications; (b) for Civil Engineering Applications (Zhu et al., 2001)

The flexural tests were performed using the third point flexural strength test. At the service load level, cracking in the flexural span was composed predominantly of vertical cracks perpendicular to the direction of maximum principal stress induced by pure moment. Cracking outside the pure bending zone started similarly to flexural cracking but, as the load was increased, other cracks were formed. The average crack spacing at 90% ultimate load ranged from 82 to 270 mm, the lowest being for the SCCC (Sonebi and Bartos, 2001). Eq. 2.7 was used to determine the theoretical cracking moments (M_a) of the beams:

$$M_a = \frac{f_r I}{y_t} \tag{2.7}$$

where:

f_r is the modulus of rupture of concrete

f'_{cu} is the compressive strength of the concrete cubes.

I is the moment of inertia of beam section

y_t is the distance from the centroid to extreme tension fiber of the section

For the civil engineering category, the cracks were wider in the reference beam than those in the SCCC with increased loading. Also, the moment required to initiate cracking in the beams was relatively similar. The maximum deflection for the SCC beam was higher at the ultimate load than the reference concrete (Sonebi and Bartos, 2001).

Based on the results, it was found that SCC beams performed similar to reference concrete beams in terms of axial strain at the maximum load and toughness.

2.5   Confined Columns

There exists two categories of confined columns; one being reinforced concrete with hoop or spiral confinement, and the other being concrete filled steel tubes (CFST). There are many advantages in using composite columns of concrete steel tubes filled with concrete, as columns in a structure. Some of these include architectural, economic and structural performance.

2.5.1   Biaxial Stresses and CFST

Confined columns that are axially loaded on the concrete portion only, expose the concrete to triaxial confinement. The increase in concrete strength outweighs the reduction in yield strength of the steel in vertical compression due to the confinement tension needed to contain the concrete (Shanmagam and Lakshmi, 2001). Typically these columns have a higher peak strength capacity than columns axially loaded on both the steel and concrete. Axial steel strain arises as a result of interfacial friction between the concrete and steel tube. The tube is in a state of biaxial stress and this affects the degree of confinement provided to the concrete section (McAteer, 2002).

The combination of axial stress (σ_a) and circumferential/hoop (σ_h) stress in the steel tube shell is shown in Fig. 2.8, where the hoop stress σ_h is a direct result of lateral pressure acting on the steel tube from the confined concrete f_2. The two stresses, axial and circumferential, define the yield criteria as outlined by Von Mises yield Criterion. The biaxial stress path of Von Mises criterion for 300 MPa is illustrated in Fig. 2.9.
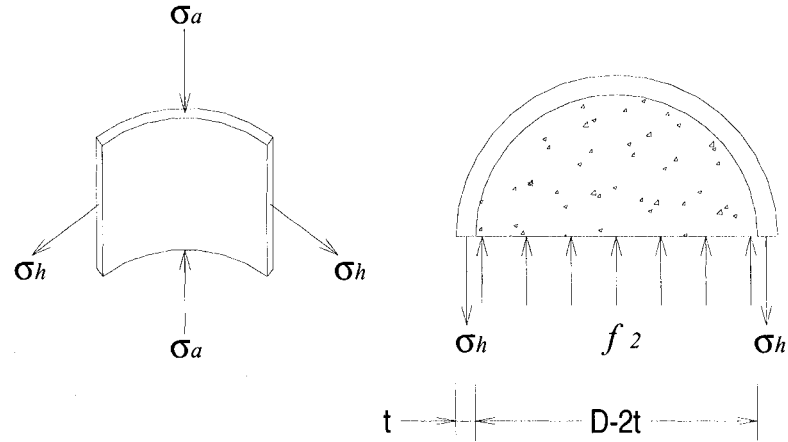
Fig. 2.8 – Equilibrium Lateral Pressure and Stresses in Confined Column
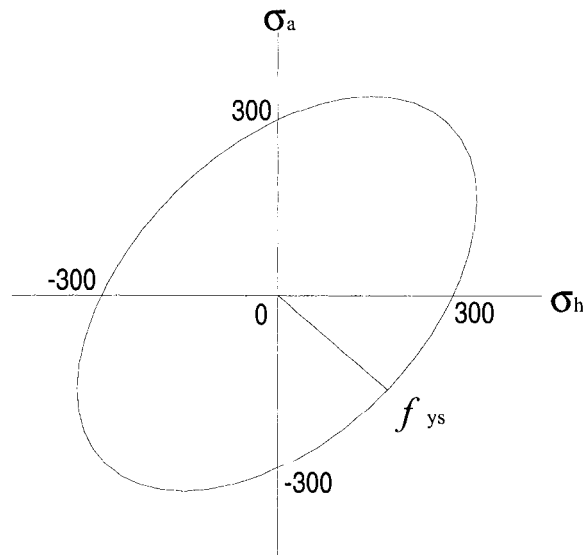
Fig. 2.9 – Von Mises Stress Path, f_{ys} = 300 MPa

Von Mises yield criterion of the CFST is interpreted by the biaxial stresses in the steel tube and is defined as:

$$f_{ys}^2 = \sigma_a^2 + \sigma_h^2 - \sigma_a \sigma_h \qquad (2.8)$$

The stresses of CFST would fall in the fourth quadrant of the curve given that the forces acting on the tube are axial compression and the circumferential tension (outward pressure by confined concrete). The axial and hoop stresses are dependant on the configuration of the CFST, materials and interfacial bond of concrete and steel. These stresses are always lower than the uniaxial yield strength when loaded on the concrete only. The strains are used to interpret these parameters and define the conditions of the confined concrete.

When the CFST is loaded the confinement affect does not begin until the concrete starts to dilate. The confinement pressure increases when the lateral expansion due to Poisson's effect and microcracking take place (Légeron, 2003). Therefore, confining stresses should reach peak values when the confinement, in this case steel, has yielded. Lateral pressure (f_2) developed by the dilation of concrete in the confined column can be obtained by Eq. 2.9 where the equilibrium in Fig. 2.8 is satisfied:

$$f_2 = \frac{2t}{D - 2t} \sigma_h \qquad (2.9)$$

where

t is the thickness of the steel tube

D is the outside diameter of the of the tube

σ_h is the circumferential stress developed in the tube during axial loading and concrete deformation. It can be obtained by $E_s \varepsilon_h$, which is the elastic modulus of the tube multiplied by the circumferential strain.

Spiral and hoop confinement is not continuous along the height of columns and therefore, Eq. 2.9, may not properly represent the confining action. A lateral pressure model based on rebar confinement (f_{rp}), spacing and diameter is recommended (Eq. 2.10):

$$f_{2h} = \frac{2A_{sr}f_s}{D_c s}$$

(2.10)

where

A_{sr} is the section area of the steel bar

f_s is the yield strength of the steel bar

D_r diameter of the concrete from center-to-center of the confining rebar

s is the lateral spacing of the confining hoops

2.5.2 Axial Load Sharing

When the CFST is axially loaded on the concrete alone, the biaxial stress actions in the steel tube indicate a portion is carried by the steel itself. The strength of the interfacial bond and tube configurations will determine the magnitude of axial load transfer from the concrete to the steel tube. It is believed that the bond strength has a significant effect on the behaviour of the CFT column. Johansson and Gylltoft (2002) studied the bond effect of CFST sub columns with three loading conditions; concrete only, steel only and both. The study determined that the columns with load applied to the concrete core had a higher interfacial bond which effectively increased the stiffness and stress capacity of the CFST. Aïtcin (1998) recommended further study of the bond to further develop analysis and modeling of CFST with high-performance concrete.

Since the biaxial stresses do occur it is possible to determine the load carried by the steel and concrete through stress-strain measurement in the steel. The equivalent axial stress applied to the concrete core can be taken as (McAteer, 2002):

$$f_T = \frac{P}{A_c} = f_c + \frac{\sigma_a A_s}{A_c}$$

(2.11)

30

where

σ_a the axial stress applied to the steel determined by Von Mises failure criterion

f_T The axial stress applied to the concrete core

P is the axial load on the concrete core

f_c is the concrete stress

P_s is the load carried by the steel

A_c is the concrete area

A_s is the steel tube cross sectional area

Therefore, to determine the stress of the confined concrete, Eq. 2.11 can be re-written as:

$$f_c = \frac{P}{A} - f_s'$$
(2.12)

where f'_s is the equivalent stress acting on the steel tube

$$f_s' = \frac{A_s \sigma_a}{A_c}$$
(2.13)

2.5.3 Confinement models

The confined compressive strength of the concrete had been examined and modeled by many researchers. Generally, the models are based on two types of confinement, active confinement and passive confinement. Active confinement consists of a constant lateral stress acting on the concrete as the axial load is applied. Passive confinement is achieved through the use of circular hoops, spirals, or tubing as a kinematic restraint (McAteer, 2002).

Richart et. al. Confinement Model - Active Confinement

The earliest investigations of these models were conducted by Richart et al. (1928) on plain concrete cylinders with active confinement. This model was developed by the use

of hydrostatic fluid pressure as the confining action and was based on normal strength concrete. Richart et al. (1928) discovered that the peak stress was 4.1 times greater than the confining stresses in the concrete and is written as follows:

$$f_{cc}^{'} = f_{c}^{'} + 4.1 f_{2}$$ (2.14)

where

f'_{cc} is the compressive strength of the confined concrete

f'_{c} is the compressive strength of the unconfined concrete

Mander's Confinement Model – Passive Confinement

The model developed by Mander et al (1988) is particularity popular with many researchers. The parameters used to calibrate the model included the confined concrete strength, the strain at peak confined concrete strength, the shape of the confined concrete curve and the confined pressure. The model is represented by Eq. 2.15:

$$f_{cc}^{'} = f_{c}^{'}\left(2.254\sqrt{1 + 7.94\frac{f_{2}}{f_{c}^{'}}} - 2\frac{f_{2}}{f_{c}^{'}} - 1.254 \right)$$ (2.15)

It should be noted that the model was developed for predicting the uniaxial stress-strain curve of hoop and spiral confined concrete. As discussed in the previous section, concrete loaded confined columns develop biaxial stresses and the tube will not reach its uniaxial yield stress. Therefore, Mander's model may over estimate the confined strength of the concrete for CFST.

O'Shea and Bridge Confinement Model – Passive Confinement

O'Shea and Bridge (2000) accounted for the biaxial stresses developed in the steel confining tube. The equation of Mander et. al. (1988) was used with new constants calibrated to tests conducted by O'Shea and Bridge (2000) for 50 MPa unconfined concrete strength. The modified model is:

$$f'_{cc} = f'_c \left(2.172 \sqrt{1 + 7.46 \frac{f_2}{f'_c}} - 2 \frac{f_2}{f'_c} - 1.228 \right) \tag{2.16}$$

The model was tested against 50 MPa concrete thin walled confined tubes and was found to provide a good estimate of the confined concrete strength (O'Shea and Bridge, 2000).

2.5.4 CFST Peak Load Models

Peak load models are based on the axial capacity of the confined concrete and the steel confining tube. Two models proposed by Hossain (2003) for thin walled columns (TWC) were selected for investigation in this study. The models were proposed and validated through tests on TWC columns with volcanic pumice concrete (VPC) and normal concrete (NC). A comparative study showed that the models predicted the axial capacity of the columns better than some existing codes and models (Hossain, 2003).

The models developed were based on Von Mises failure criterion where the stresses axial (σ_a) and hoop (σ_h) stresses are reduced as given by:

$$\sigma_a = \beta f_y \tag{2.17}$$

$$\sigma_h = \alpha f_y \tag{2.18}$$

where

$\quad f_y \quad$ is the uniaxial steel yield strength.

$\quad \alpha \quad$ is the hoop stress factor

$\quad \beta \quad$ is the axial stress factor

The values of α and β are based on the biaxial yield of the confining steel tube evaluated through experimental tests.

33

Hossain (2003) proposed a model for axial capacity of concrete filled steel tubular columns where confined concrete strength (f'_{cc}) was determined by using Eq. 2.19:

$$f'_{cc} = f_p + 4.1 f_2 = f_p + 4.1 \frac{2t}{D - 2t} \alpha f_y = f_p + \frac{1.56}{D/t - 2} f_y \qquad (2.19)$$

where f_p is the unconfined compressive strength. The value of f_p can be taken as $0.85 f'_c$ for 100 mm diameter cylinder. Study on the size effect of column on f_p revealed that 0.85 is rational average of the f_p for the columns with diameter, d, ranging from 300 mm to 600 mm, but would overestimate the f_p when the diameter of the column is larger than 700 mm. To maintain wide application, the following equation was proposed (Sun and Sakino, 1998) for f_p:

$$f_p = 1.61(d)^{-0.1} f'_c \qquad (2.20)$$

where d is the diameter of the confined concrete section in mm.

The proposed axial capacity of TWC columns (Nu) was:

$$N_u = \beta A_s f_y + A_c f'_{cc} \qquad (2.21)$$

By substituting Eq. 2.17 and $A_s = \pi(D - 2t)t$ and $A_s = \pi(D - 2t)^2 / 4$ in Eq. 2.18, Hossain derived the axial capacity equation as:

$$N_u \approx A_c f_p \left[1 + (4\beta + 8.2\alpha) \frac{t}{D - 2t} \frac{f_y}{f_p} \right] \qquad (2.22)$$

Hossain[2]

Hossain suggested a modification to Kato's formula (1996) by removing 'γ' and using f'_{cc} in place of f'_c. The proposed modified equation is written as:

$$N_u = A_s f_y + A_c f'_{cc} \tag{2.23}$$

2.5.5 Code Provisions CFST

CAN/CSA S16.1-94

The axial load is assumed to be carried by the concrete and steel tube independently when acting as a composite column. Where the axial load carried by the concrete is only the portion of the load applied directly to the concrete area. The factored resistance C_{rc} of the composite column can be taken as:

$$C_{rc} = \tau C_r + \tau' Cr' \tag{2.24}$$

where:

C_r = factored compressive resistance of the steel tube

$$C_r = \varphi A_s F_y \left(1 + \lambda_s^{2n}\right)^{-1/n} \tag{2.25}$$

ϕ_s = steel material resistance factor = 0.9

$$\lambda_s = \frac{KL}{r_s} \sqrt{\frac{f_y}{\pi^2 E_s}} \tag{2.26}$$

r_s = radius of gyration of the steel tube

$n = 1.34$

$$\tau = \frac{1}{\sqrt{1 + \rho + \rho^2}} \qquad \text{if L/D} < 25, \text{ or } \tau = \tau' = 1 \tag{2.27}$$

$$\rho = 0.02(25 - L/D) \tag{2.28}$$

and:

35

Cr' = factored compressive resistance of concrete acting at the centroid of the concrete area in compression.

$$Cr' = 0.85\phi_c f_c' A_c \lambda_c^{-2} \left[\sqrt{1 + 0.25\lambda_c^{-4}} - 0.5\lambda_c^{-2} \right] \tag{2.29}$$

ϕ_c= concrete material resistance factor = 0.6

$$\lambda_c = \frac{KL}{r_c} \sqrt{\frac{f_c'}{\pi^2 E_c}} \tag{2.30}$$

r_c = radius of gyration of the concrete area

$$E_c = \left(1 + \frac{S}{T}\right) 2500 \left(\sqrt{f_c'}\right) \quad (S \text{ is the sort term load}, T \text{ is the total load on column}) \tag{2.31}$$

$$\tau' = 1 + \left(\frac{25\rho^2\tau}{D/t}\right)\left(\frac{F_y}{0.85 f_c'}\right) \tag{2.32}$$

AISC-LRFD 1994

This is based on the same principles as the ACI code which is based on the design equations of steel columns. Both the steel tube and concrete core are converted to equivalent members, and then reduced by a factor based on the slenderness of the column. The equations used in the design are taken as:

$$\lambda^2 = \left(\frac{kL}{r_m \pi}\right)^2 \left(\frac{f_{my}}{E_m}\right) \tag{2.33}$$

where:

r_m is the radius of gyration of the steel tube

$$f_{my} = f_y + 0.85 \frac{A_c}{A_s} f_c' \qquad \text{(compressive strength of the composite section)} \tag{2.34}$$

$$E_m = E_s + 0.4 E_c \frac{A_c}{A_s} \qquad \text{(elastic modulus of the composite section)} \tag{2.35}$$

The critical stress F_{cr} is computed from the slenderness parameters λ

$$F_{cr} = \left(0.658^{\lambda^2}\right)f_{my} \qquad \text{for } \lambda \leq 1.5 \quad \text{(critical stress)} \tag{2.36}$$

$$F_{cr} = \left(\frac{0.877}{\lambda^2}\right)f_{my} \qquad \text{for } \lambda > 1.5 \tag{2.37}$$

The critical load P_{cr} is then calculated as:

$$P_{cr} = A_s F_{cr} \tag{2.38}$$

Eurocode 4: 1994

The plastic resistance of the cross section of the composite column with concentric loading is given by the sum of all the components, steel tube, concrete and longitudinal reinforcements. The Code is recommended for composite sections with concrete not exceeding an unconfined strength of 50 MPa. The Code assumes full interaction of all the components and the ultimate load ($N_{Pl.Rd}$) can be taken as:

$$N_{pl.Rd} = A_s f_y + A_c f_c' + A_{sz} f_{yr} \tag{2.39}$$

where:

A_s, A_c and A_{sz} are the cross-sectional area of the steel tube, concrete and reinforcement in the axial direction, respectively

f_y, f'_{cc} and f_{yr} are the yield strength of the steel tube, concrete and reinforcing steel, respectively

3.0   Effect of VMA on the Rheology of Cement Paste and Mortar

The objective of this study was to investigate the performance of four different types of new viscosity modifying admixtures (VMAs), based on various tests of rheological properties. A series of tests were carried out using viscometer to obtain rheological data such as yield stress, apparent viscosity and plastic viscosity. This was performed in an attempt to determine the robust mixture proportions for the cement pastes/mortars incorporating various dosages of superplasticizer (SP) and VMA. Rheological properties and consistency of cement paste and mortar play an important role in controlling the rheology and consistency of concrete. The current study on cement pastes and identification of suitable new VMAs are important and will provide the foundation of developing a cost-effective SCC with adequate rheological properties.

The experimental investigation was carried out on various cement paste and mortar mixes with four new VMAs in addition to a commercial VMA largely used in Canada and designated in this thesis as "COM". The flow of fresh paste and mortar is in the domain of fluid mechanics that deals with mass in motion, namely a time-dependent parameter. Using static measurements to predict dynamic behaviour is quite disputed. For this reason, the Bingham model (Bingham and Reiner, 1933) was introduced to characterize the flow behaviour of fresh paste, mortar and concrete by measuring the rheology data such as the yield stress, viscosity, shear stress and shear rate. Additional tests were performed on the paste to observe the mixture proportions of the paste by means of the washout test.

3.1   Materials

3.1.1   Cement and Aggregate

Type 10 Portland cement (similar to ASTM Type I) with specific gravity of 3.17 and Blaine fineness of 4070 cm^2/g was used. Its chemical and physical properties are shown

in Table 3.1. Local natural sand was used as fine aggregate. The fine aggregate had a specific gravity of 2.70 and water absorptions of 0.84%.

Table 3.1 – Cement Properties

Chemical Analyses	%	Physical tests	
Calcium oxide (C_aO)	62	Specific gravity	3.17
Silica (SiO_2)	20.3	Fineness	
Alumina (Al_2O_3)	4.2	Passing 45mm, %	94
Iron oxide (Fe_2O_3)	3	Specific surface, Blaine, cm^2/g	4070
Sulfur trioxide (SO_3)	3.5	Compressive strength, MPa	
Magnesia (MgO)	2.8	7-day	26
Sodium oxide (Na_2O)	0.2	28-day	32
Potassium oxide (K_2O)	0.9	Setting time, Vicat test, min	
Loss on ignition	2	Initial setting	220
		Final setting	325
		Air content of mortar, volume %	5.5

3.1.2 Chemical admixtures

A superplasticizer (SP) composed of naphthalene formaldehyde condensates having specific gravity of 1.21 and total solid content of 40.5% was used. Four novel polysaccharide-based VMAs in liquid form classified as A, B, C and D having specific gravity of 1.42 and total solid content of about 81% were used. All the tests in this study were carried out at room temperature. A known commercial VMA widely used in Canada and designated in this paper as "COM" was also used to perform a comparative study. The specific gravity and total solid content of COM were 1.21 and 42.5% respectively. The chemical composition of COM is a proprietary secret and it is composed of a combination of SP and VMA. The percentages of VMA and SP were calculated on the basis of total solid content. Chemical and physical properties of VMAs are presented in Table 3.2.

Table 3.2 – Chemical and Physical Properties of VMA

	VMA				
	A	B	C	D	COM
Total solids (%)	80.7	80.2-81.4	80.4-81.6	82.1	42.5
pH	4.9	4.9	4.8	4.8	7
Specific gravity	1.42	1.42	1.42	1.42	1.21
Viscosity (centipoises)					
260C	81000	81000	54000	25000	-
600C	2500	2500	1600	1000	-

3.2   Experimental Program

3.2.1   Washout Test

The mix proportions of the cement paste used to investigate washout mass loss are presented in Table 3.3. All pastes had a 0.45 w/c and VMA concentrations of 0.025%, 0.05% and 0.075% by mass of cement. For each VMA concentration, three paste mixes were prepared with SP solid concentrations of 0.25%, 0.50% and 0.75% by mass of cement. The pastes also determined the effect of VMA-SP combination on washout mass loss.

The washout mass of cement paste was determined using a 750 ml paste sample and was introduced into a beaker containing an equivalent volume of water. The setup was similar to that used by (Yahia, 1997) as shown in the schematic of the washout test set up Fig. 3.1. The paste was poured from the 750 mm beaker into a funnel which was positioned at a given high (20-mm) above the water level of another 750 mm beaker that was completely filled with water. As the grout fell freely in the water beaker from a fixed distance, it displaced the water and became partially diluted. The degree of dilution depends on the ability of the grout to retain its mix water and suspended cement particles. During this process, suspended cement particles of the paste were also washed away with displaced water. The washout mass loss was determined by calculating the difference between the initial mass of the paste and the mass of the paste after pouring it in the water, the value was expressed as percentage of initial mass (Yahia, 1997). All the tests were carried out at room temperature within the range of 22-25 °C.

750 ml
paste filled
beaker

80

Funnel

50

20

750 ml
water filled
beaker
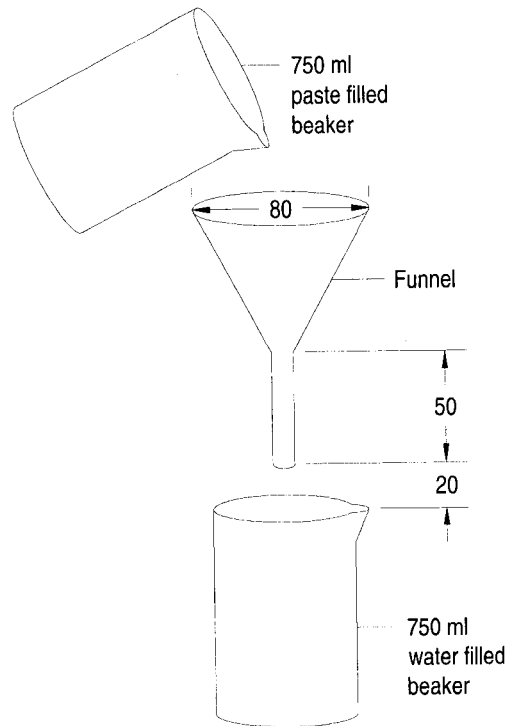
Fig. 3.1 — Schematic Representation of Washout Test Setup

Table 3.3 — Mix Design of Pastes and Mortar

	Washout Test		Reological Test	
	VMA Types A-D, COM	Control	VMA Types A-D, COM	
	Paste		Paste	Mortar
W/C	0.45	0.45	0.45	0.45
VMA (% C)	0.025 0.050 0.075	0	0.025 0.075	0.025 0.075 For COM mix: VMA: 0.075% and 0.37%
SP (%)	0.25, 0.50, 0.75	0.25, 0.50, 0.75	0.25	SP: 0.6% by weight of cement for type A, B, C and D For COM mix: SP: 0.6% and 0.74% by weight of cement
No. of mixes	45	3	10	10 + 1 (control with 0% VMA) Cement: 656kg/m^3, Water: 295kg/m^3, Aggregate: 1349 kg/m^3

3.2.2 Test Procedure for the Rheological Properties of Cement Pastes

Flow behaviour of fresh paste is a complex rheological phenomenon, which is roughly described by the Bingham model. The flow behaviour of a test sample can be quantified by the measurable parameters of torque, and rotational speed with a rheometer, as demonstrated by Bingham model (Bingham and Reiner, 1933). The purpose of using VMA in cement-based pastes is to improve the stability (bleeding) and rheological properties (viscosity, cohesion and internal friction or bond) in order to enhance the penetrability and flow characteristics.

A total of 10 paste mixes shown in Table 3.3 were used. These included eight mixes with 0.025% and 0.075% of types A-B-C-D VMA and two mixes using 0.025% and 0.075% of COM with W/C of 0.45. The SP content in the paste mixes was set at a constant dosage of 0.25% by mass of cement. The cement was weighed in a bowl; water, SP and VMA were weighed and mixed in a 750 ml beaker and then the cement was added to the solution, and was then hand mixed with a spatula for 1 minute. The paste was then mechanically mixed in a blender for 2 minutes. Following the mixing, the rheological measurements of paste were conducted by using a commercially available digital Brookfield viscometer (Model RVDV-II) equipped with disc spindles at normal room temperature of about 22-25°C.

Tests were conducted at 5, 15 and 30-minute interval following the contact of water and cement. The test samples were poured into the viscometer and the spindle was introduced in the beaker for measurement. The tests were executed stepwise at 100, 60, 50, 30, 20, 12 and 5 rpm. At each rotational speed, torque and apparent viscosity data were recorded. The results were then converted into viscosity functions such as shear stress (Pa) and shear rate (1/sec) using standard procedure (Mitschka, 1982). The linear regression analysis was carried out to determine the viscosity and yield stress as slope and intercept of the regression line drawn through the data points in shear stress vs. shear rate plot. The samples were allowed to stand and were covered after each measurement. Before starting the test for the next time interval, the samples were manually stirred for 15 seconds.

3.2.3 Test Procedure for the Rheological Properties of Cement Mortar

A total of eleven mortar mixes, Table 3.3, were prepared to study the effect of type and dosage of VMA on the rheological properties of mortar. The proportion of cement and sand was kept approximately at 1:2 by weight. Mortar with VMA (types A, B, C and D), W/C and SP content were kept constant at 0.45 and 0.6% by mass of cement respectively while VMA contents were kept at 0.025% and 0.075% of cement. The mixture with commercial VMA "COM" had W/C of 0.45, SP content of 0.74% and VMA content of 0.37% - typically used in a commercial SCC using "COM" as per recommendation from the manufacturing company. Another COM mix was also made with 0.075% VMA and 0.6% SP similar to new VMA mixes. The sand and 50% of the water was first mixed for 30 seconds. Then cement was added with the remaining water, SP and VMA and mixed for 2 additional minutes.

The rheological measurements of mortars were conducted similar to paste samples by using a commercially available digital Brookfield viscometer (Model RVDV-II) equipped with cylindrical spindles at normal room temperature of about 22-25°C. Viscosity measurements were carried out as soon as the mortars were prepared. The test samples were poured into a beaker, and then the spindle of the viscometer was introduced in the beaker for measurement. The tests were executed stepwise at 100, 60, 50, 30, 20, 12 and 5 rpm. At each rotational speed, torque and apparent viscosity data were recorded. The results were then converted into viscosity functions such as shear stress (Pa) and shear rate (1/sec) using standard procedure (Mitschka, 1982). The linear regression analysis was carried out to determine the viscosity and yield stress as slope and intercept of the regression line drawn through the data points in shear stress vs. shear rate plot.

3.3 Test Results

3.3.1 Washout Resistance of Paste

Typical washout resistance of paste with VMAs A, B and COM are compared with those of control paste without VMA (Fig. 3.2). For similar dosages of VMA and SP, the

43

washout resistance of VMA A and B were found to be better than the COM and control paste. Washout mass losses were higher in COM pastes (ranged between 12.6% and 14.9%) compared with VMA Types A (ranged between 6.7% and 12.4%) and B (ranged between 7.5% and 13%) pastes. The washout resistance of the control paste was similar to that of COM pastes. Improved washout resistance was not observed in pastes with COM when compared to control pastes for the SP–VMA combinations of dosages used in this study. VMA Types A and B pastes were found to have similar washout resistances. Similar behaviour was also observed in pastes with VMAs C and D. These results were similar to those obtained by Khayat and Yahia (1997) in their investigation on the combination of welan gum and high range water reducer (HRWR). Washout resistance improved with increasing concentration of VMA coupled with a greater content of SP to maintain the desired fluidity. Therefore, by adjusting the combination of VMA–SP, a washout-resistant paste with adequate fluidity could be obtained. The increase in the dosage of SP in paste dispersed the cement grains and increased the amount of free water in the system. The higher SP dosage might be the cause for no improvement in washout resistance of pastes with COM compared with control paste.

As COM is a combination of SP and VMA, the actual SP content in the COM paste was higher than the pastes with new VMA. This lead to a higher washout mass loss in pastes with COM. The combined addition of SP and VMA could improve both fluidity and washout resistance. The improvement in washout resistance was due to the enhancement in the degree of water retention by the VMA, whereby some of the free water made by the addition of SP can be physically adsorbed by hydrogen bonding onto polymer molecules of the VMA. Furthermore, some of the VMA polymer became adsorbed onto cement grains along with the imbibed water, resulting in further retention of suspended cement particles. The use of VMA increased the viscosity of the paste, which reduced the rate of sedimentation of cement grains, thus resulting in highly stable paste even at elevated fluidity levels (Khayat and Yahia, 1997).
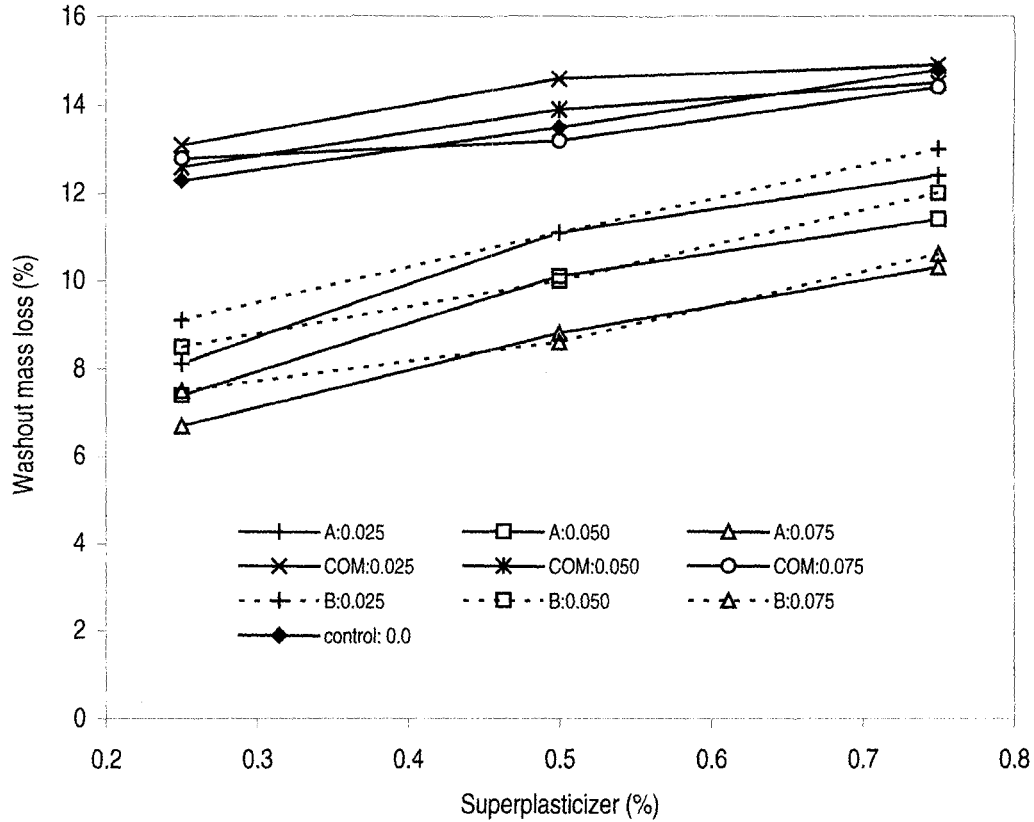
Fig. 3.2 – Washout Mass Loss of Paste

3.3.2   Rheological Properties of Cement Paste

The typical variation of apparent viscosities with shear rate for pastes with 0.025% and 0.075% of various VMAs A, B and COM at 15 minute is shown in Fig. 3.3. A, B C and D VMAs were found to give similar results for apparent viscosity, thus only results for A and B are shown in Fig. 3.2. Apparent viscosity decreases with the increase of shear rate. The apparent viscosities of pastes with type A and B-VMA were found to be slightly higher than those of the other VMAs including commercial "COM". The apparent viscosity is also increased with the increase of the dosages of VMA from 0.025% to 0.075%. For any given concentration of SP (0.25% in the current study), the increase in VMA content is expected to increase the viscosity both at high and low shear rate and this was observed in the current study. This can be attributed to the fact that the degree of water retention and the free water needed to lubricate the paste, increase with the dosage of VMA that acts on the aqueous phase. The addition of VMA also increases the

45

degree of pseudo-plasticity, or shear thinning, of the cement paste regardless of the concentration of SP (Khayat and Yahia, 1997). Pastes with VMA exhibit high apparent viscosities at low shear rates and significantly lower viscosities at greater shear rates. For the same dosage of SP, the use of VMA results in a greater apparent viscosity at low shear rate than at high shear rate (Fig. 3.3).

The increased pseudo-plastic response in the presence of VMA is believed to be due to the fact that the polymer chains of the VMA entangle or associate, resulting in an increase in apparent viscosity, especially at low shear rate. With the increase in shear rate, the entangled chains dislodge and align in the direction of flow, thus decreasing the resistance of the grout to undergo deformation. The apparent viscosity is then decreased with an obvious improvement in flowability at high shear rate regimes (Khayat and Yahia, 1997). The effect of the increase in the concentration of VMA on the viscosity depends on the shear rate. For a given concentration of SP, the increase in the dosage of VMA is more effective in increasing viscosity at low shear rate than that at high shear rate.
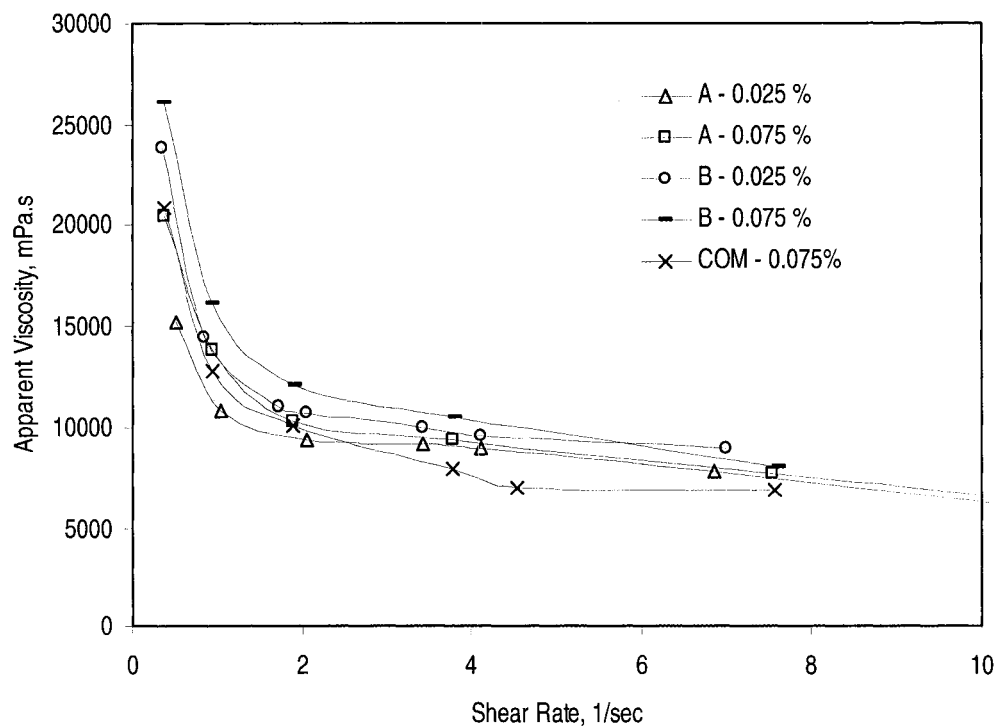
Fig. 3.3 – Variation of Apparent Viscosity of Pastes With Various Types of VMA at 15 min.

46
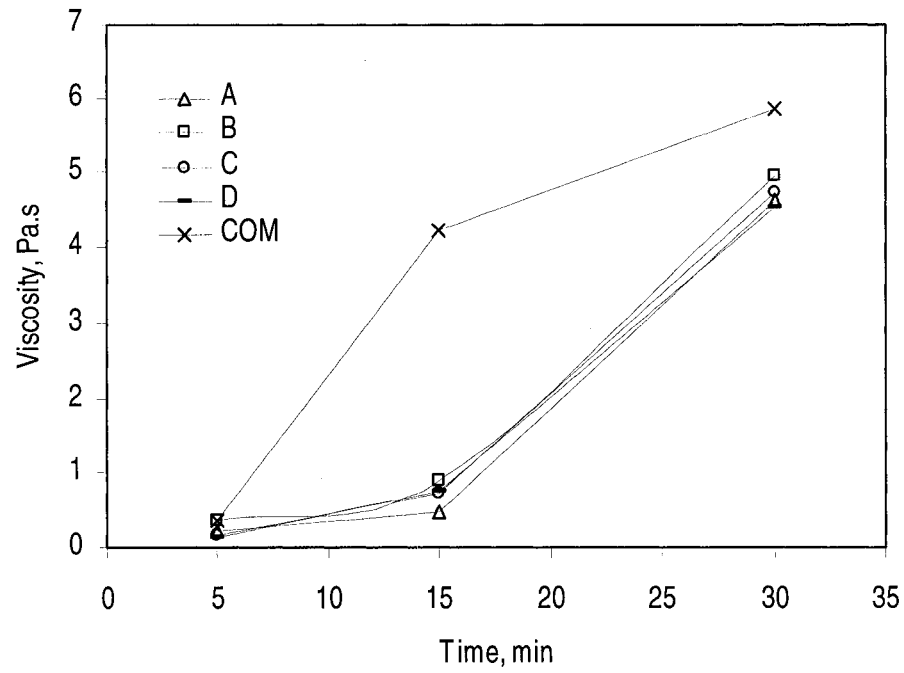
Fig. 3.4 – Typical Variation of Paste Viscosity With Time (VMA=0.025%)
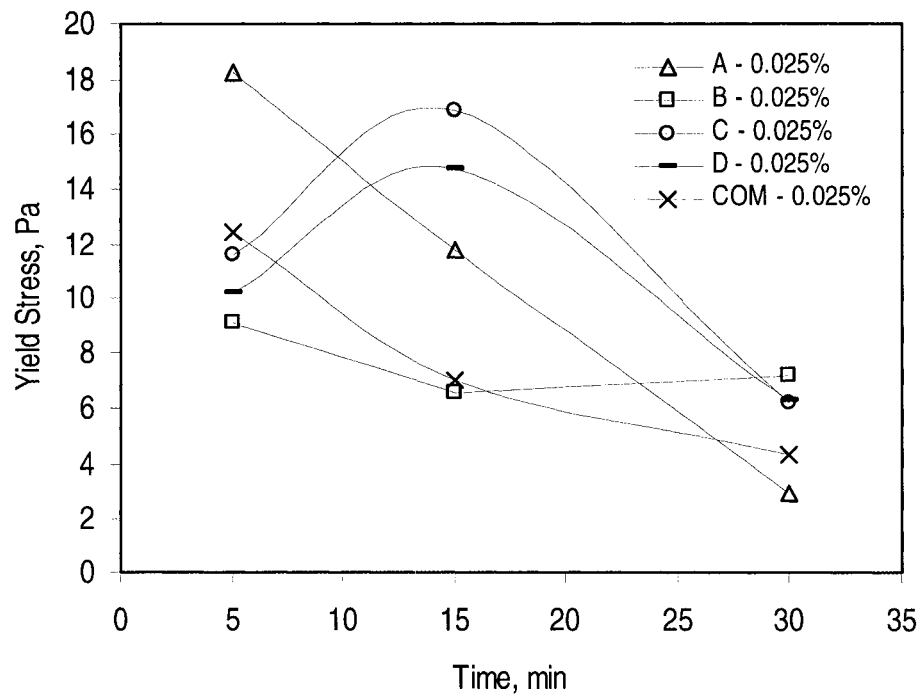
Fig. 3.5 – Typical Variation of Paste Yield Stress With Time

47

Fig. 3.4 shows a typical variation of viscosity of paste with time (elapsed between mixing and testing) for various types of VMA. Viscosity is found to increase with the increase of elapsed time. This can be attributed to the hydration of cement with time that made the paste stiffer as time progresses. This also indicates somehow that the new VMAs are not inhibitors for the cement hydration. The yield stress is decreased with the increase of time (Fig. 3.5). The yield stress, viscosity and apparent viscosity values are affected by the combination of dosages of VMA and SP. It is then important to find out the combinations of dosages of VMA and SP to secure a stable paste with required fluidity and rheological properties. This can be achieved by testing trial mixes with various combinations of dosages of SP and VMA as illustrated in this study.

3.3.3   Rheological Properties of Mortar

Apparent viscosities of the mortars with A and COM VMAs including the control mortar are compared in Fig. 3.6. Apparent viscosity is found to decrease with the increase of shear rate. The results of mortars with A-VMA are similar to mortars B, C and D-VMA and therefore only A-VMA is used in the comparative analysis.   For any given concentration of SP (0.6% in all the mortars), the increase in VMA content increases the viscosity both at high and low shear rate (Fig. 3.6). The apparent viscosity of the mortar is increased with the increase of the percentage of VMA in the mixture. The apparent viscosities of VMA mortars were found to be higher than the control mortar with 0% VMA.   The apparent viscosities of type A VMA mortars were also found to be higher than that of COM VMA with similar dosage of VMA of 0.075% and similar SP dosage of 0.6%.   The development of higher apparent viscosity in COM mortar with substantially higher percentage of VMA of 0.37% and higher SP content of 0.74% was also observed. The increase in apparent viscosity can be attributed to the fact that the degree of water retention increases with the dosage of VMA, which acts on the aqueous phase. Viscosity of mortar with new VMAs is found to increase and yield stress is generally found to decrease with the increase of VMA content from 0.025% to 0.075% (when SP content is kept constant at 0.6%). The study on mortar suggests that all new

VMAs can provide satisfactory rheological properties with less VMA dosage than commercial "COM".
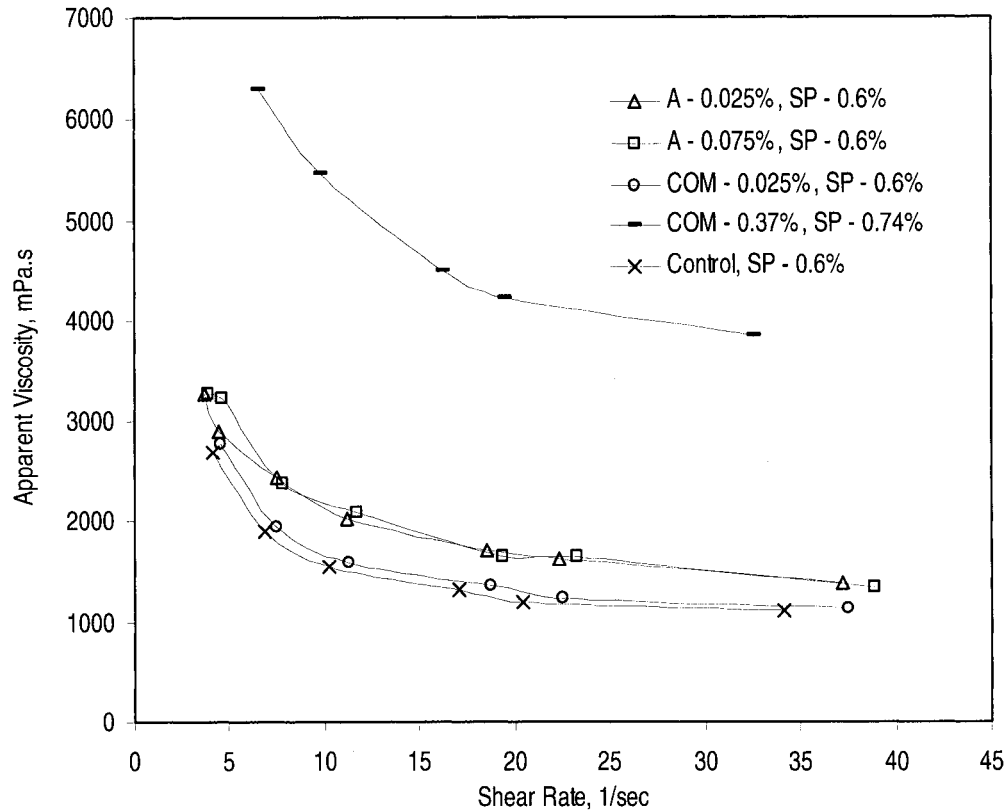
Fig. 3.6 – Variation of Apparent Viscosity of Mortar With Shear Rate

3.4 Discussion

The apparent viscosity of the cement paste/mortar is increased with the increase of dosages of VMA from 0.025% to 0.075%. The viscosity of paste/mortar with new A, B, C and D VMAs is found to be higher than that of commercial "COM" VMA. Viscosity of the paste also increases with the increase of elapsed time between mixing of paste and testing. Based on viscosity data, all new VMAs are found to be more effective and efficient than the commercial "COM" VMA and would provide better rheological properties at lower dosages. Based on the current investigation, cement paste/mortar with new VMA dosage ranging between 0.025 and 0.075% would provide better rheological properties.

The washout resistance is increased with the increase of VMA dosage and reduction in SP. However, with the right combination of A-VMA and SP, a flowable yet washout resistant mix can be secured.

The results of this study show the combination of Type A-VMA and SP can be used to develop a reliable SCC. The author selected type A-VMA of 0.05% and the dosage of SP was determined during batching, as the SP demand increases within concrete, and discussed in detail in the following chapter.

4.0 Properties of Self-Consolidating Concrete

The primary objective of the experimental program was to investigate the performance of SCC in beam and confined column elements. The SCC selected for this program was based on mix designs developed by the author in previous research studies (Lachemi et. al, 2003b), where it incorporated new cost effective viscosity-modifying agents (VMA), the same as those studied in the previous chapter. Due to the limited development and research on SCC with new VMA, it was essential to develop SCC mixtures, evaluate their fresh and hardened properties so they could meet the requirements of the structural concrete. Two types of SCC were designed for the structural elements: one mix with low content (0.7:1 to sand) 12-mm coarse aggregate, and the second mix with 19-mm coarse aggregate at normal content (1:1 to sand). A normal concrete (NC) mix was also required with similar 28-day compressive strength of 50 MPa (similar to SCCs) and with a higher content 12-mm coarse aggregate (1.6:1 to sand). This was required for the comparative study of structural properties of SCC against NC and to study the effect of aggregate content on SCC structural performance. This chapter explains the materials and methods utilized in the development of SCC and NC including the testing procedures, and the fresh and mechanical properties of the concretes.

4.1 Concrete Materials

4.1.1 Cement

Type 10 Portland cement (Similar to ASTM Type 1) with specific gravity of 3.17 and Blain fineness of 4070 cm^2/g was used. Chemical and physical properties are listed in Table 4.1.

Table 4.1 – Cement Properties

Chemical Analyses	%	Physical tests	
Calcium oxide (CaO)	62	Specific gravity	3.17
Silica (SiO2)	20.3	Fineness	
Alumina (Al2O3)	4.2	Passing 45mm, %	94
Iron oxide (Fe2O3)	3	Specific surface, Blaine, cm^2/g	4070
Sulfur trioxide (SO3)	3.5	Compressive strength, MPa	
Magnesia (MgO)	2.8	7-day	26
Sodium oxide (Na2O)	0.2	28-day	32
Potassium oxide (K_2O)	0.9	Setting time, Vicat test, min	
Loss on ignition	2	Initial setting	220
		Final setting	325
		Air content of mortar, volume %	5.5

Table 4.2 – Grading of Sand

	Seive Size (mm)							
	10 (3/8")	5 (No. 4)	2.5 (No. 8)	1.25 (No. 16)	0.63 (No. 30)	0.315 (No. 50)	0.16 (No. 100)	Pan
Cummulative % Passing	100	97	84	73	54	25	6	0

Table 4.3 – Grading of Coarse Aggregates

	Seive Size (mm)						
	40 (1-1/2")	28 (1")	20 (3/4")	14 (1/2")	10 (3/8")	5 (No. 4)	Pan
19 mm	100	100	98	57	28	1	0
12 mm	100	100	100	94	41	7	0

4.1.2   Sand

Local natural sand was used as the fine aggregate in the concrete mixtures. Standard ASTM tests methods C136-01 and C128-97 were used to find the particle size distributions and specific gravities, respectively. The grain size distribution of the sand is listed in Table 4.2. The specific gravity (SSD) of the sand was 2.71 with an absorption value of 0.75%, and a fineness modulus of 2.6. Detailed test results are given in Appendix A.

4.1.3 Coarse Aggregate

SCC can include a coarse aggregate of either 19-mm or 12-mm maximum nominal size. The flow properties of SCC and SP demand would vary for each type of aggregate, and the size of coarse aggregate is also believed to alter the structural performance of SCC in structural elements. To distinguish the effect each aggregate has on these properties, both types were adopted for the SCC in this study. Another aspect, as mentioned earlier, was to study the effect of coarse aggregate content on the fresh and structural properties of SCC.

The 19-mm coarse aggregate is made up of gravel with some crushed particles and the 12-mm aggregate was a natural pea stone. Standard ASTM tests methods C136-01 and C128-97 were used to find the gradation and specific gravities of both aggregates, respectively. The grain size distributions of both aggregates are listed in Table 4.3. The 19-mm and 12-mm aggregates have a specific gravity of 2.71 and 2.64, and an absorption value of 0.56% and 1.89%, respectively. Detailed test results are given in Appendix A.

4.1.4 Superplasticizer (SP)

The SP used is composed of naphthalene formaldehyde sulphonic acids with a solid content of 40.5% and a specific gravity of 1.21. Achieving high-fluidity with the addition of superplasticizer can make the concrete mix unstable and may cause excessive segregation and bleeding. Thus, a VMA is required to eliminate this problem and to ensure good rheological properties of the mix.

4.1.5 Viscosity Modifying Agent (VMA)

VMA is a chemical admixture that is used in SCC to help stabilize the mixture while maintaining its high fluidity. Stability is achieved by maintaining the homogeneity of the concrete during placement. A polysaccharide-based VMA in liquid form having specific gravity of 1.42 and total solid content of about 81% was used in this part of the program.

4.2 Mix Design of SCC and NC

4.2.1 Trial Mixes

Initially, the intent was to design three concrete mixes, two types of SCC and one NC each containing different coarse aggregate contents. Furthermore, the SCC mixes would contain 12-mm and 19-mm coarse aggregates and the NC mix would only contain 12-mm aggregate. The SCC mixes included one mix with new VMA and another one with slag as a supplementary cementing material. The author's familiarity with both types of SCC, from previous research, helped facilitate the selection of mix proportions required for the trial mix program (Lachemi et al, 2003). The SCC mixes included three levels of coarse aggregate content: low, medium and high. Based on their performance one level would be assigned to each mix.

SCC trial mixes

The low and high levels of aggregate content were derived by altering common mix design quantities of previous studies (Lachemi et al, 2003a). The usual coarse aggregate to sand ratio was 1:1 and based on this, the content ratio was altered to 0.7:1, 1:1 and 1.6:1. Typical slag SCC, VMA SCC and NC mix included aggregate quantities of 850, 930 and 930 kg/m^3, respectively for both coarse and fine aggregate. The VMA content in SCC was found most suitable at 0.05% of the cement mass, and the cement content in slag SCC was replaced by 50% of slag (Lachemi et al, 2003a). Typical design mixes based on a W/B of 0.40 for 28-day strength of 50 MPa are given in Table 4.4. All the trial mix designs for VMA SCC and Slag SCC are given in Table B1.1 and B1.2

Table 4.4 – Typical Design Mix of SCC

SCC Type	Nom. Agg. Size	W/B	Cement	Slag	Water	Coarse Aggregate (SSD)*	Fine aggregate (SSD)*	SP (SS)**	VMA (SS)**
	mm		kg/m^3	kg/m^3	kg/m^3	kg/m^3	kg/m^3	%	%
VMA	12	0.40	450	0	180	890	890	0.55	0.05
Slag	19	0.40	200	200	160	925	925	2.00	0.00

* Saturated Surface Dry Condition (SSD), ** Suspended Solids (SS)

A total of thirteen trial mixes were conducted for the VMA SCC and eleven mixes for slag SCC with various coarse aggregate content. Originally the W/B of the mixes was 0.45 and the cement content was 400 kg/m^3 but due to durability issues, generally with concrete structures, it was decided to reduce the W/B to 0.40. Evidently, the lower W/B produced a more stable SCC in terms of fresh properties and performance. The volumetric difference of the aggregate contents were replaced by sand content in the mix. A smaller aggregate size (12-mm) in concrete increases the surface area required to be covered by the paste and this may lower the strength and change the fresh properties of the SCC and NC. Therefore, the cement content was increased for all mixes to avoid this potential problem.

A 10-L batch was prepared, for each concrete trial, to quantify the volume required for the slump flow test and to cast three 100 x 200 mm cylinders. The slump flow test was adopted to test the mix for flowability and workability. The three cylinders were tested at 7 days to measure compressive strength of the concrete.

Problems arose with SCC with high aggregate content, and with the slag SCC. The high aggregate content for both 19-mm and 12-mm concrete produced many large voids. This can be explained by an inadequate paste content that available to compensate for the increase of aggregate surface area. The slag SCC did not poses favourable workability and showed signs of segregation and bleeding during the slump flow test. Due to the time restraint, new mix designs could not be tested for the slag SCC and therefore, were eliminated from the testing program. The mix designs selected for the SCC are given in Table 4.5.

NC Trial Mixes

The normal concrete mix was designed for 50 MPa, at 28 days, by the absolute volume method as per ACI committee 211 (Kosmatka et. al., 2002). The w/c was dependant on the required strength, aggregate size and a target slump between 100 and 150 mm to provide better workability for beam and column applications. The 12-mm normal

concrete was also re-designed for three additional mixes containing 8% more course aggregate (Table B1.3). The mix design selected for NC is given in Table 4.5.

Table 4.5 – Selected Trial Mix Design

Concrete Type	Nom. Agg. Size mm	W/B	Cement kg/m³	Water kg/m³	Coarse Aggregate (SSD) kg/m³	Fine aggregate (SSD) kg/m³	SP (SS) %	VMA (SS) %
SCC	12	0.40	450	180	715	1050	0.70	0.05
SCC	19	0.40	400	160	935	935	0.85	0.05
NC	12	0.42	481	202	1017	671	0	0

4.2.2 Beam Concrete Mix Design

The investigation on beam elements is concentrated mainly on the study of the shear resistance of SCC. The beams were investigated to study the effect of SCC, and the content and size of aggregate have on the shear resistant in beam elements. The mix designs selected include VMA SCC and NC mixes based on those given in Table 4.5. Following batching the proportions of the mix design were adjusted based on the measured contents and measured density of the fresh concrete for each batch volume. The concrete mix designs for the beam-shear study are given in Table 4.6.

The proportional values changed slightly from those of the trial mixes, and the author gives two explanations for this. The proportion of SP was adjusted during batch mixing to ensure proper slump flow (600-700 mm) of SCC. The other reason is given by the difference in batch size between the trial mix and the beam element mix which is 16 times larger in volume. This is directly related to the loss of paste/mortar which remains on the drum walls of the mixer during mixing of the concrete. When mixing small volume of concrete in a large volume drum, the percentage of paste/mortar lost to the surface area of the mixer is greater than when mixing a larger volume of concrete in a the same volume drum mixer. A low volume of concrete mixed in a large mixer will be more susceptible to the change of the concrete fresh properties affected by the lost paste/mortar volume, particularly with the flowability of SCC.

Table 4.6 – Beam Concrete Mix Proportions

Designation	Nom. Agg. Size mm	W/B	Cement kg/m³	Water kg/m³	Coarse Aggregate (SSD) kg/m³	Fine aggregate (SSD) kg/m³	SP (SS) %	VMA (SS) %
B-SCC-12a	12	0.410	449	184	713	1038	0.74	0.05
B-SCC-12b	12	0.407	455	185	722	1052	0.62	0.05
B-NC-12a	12	0.421	482	203	1018	637	0	0
B-NC-12b	12	0.420	488	205	1031	645	0	0
B-SCC-19a	19	0.411	411	169	961	947	0.97	0.05
B-SCC-19b	19	0.413	409	169	958	944	1.14	0.05

A total volume of 160-L was required to cast one set of beam elements, nine 100 x 200-mm cylinders, and to perform the fresh testing of the concrete. The capacity of the concrete drum mixer located in the Ryerson University concrete lab can only handle a maximum of 90 L at once. Therefore, two batches were required for the elements. Actually, this provided an advantage in checking the consistency of concrete between batches through the fresh test results and structural performance. The beam elements included a pair of three beam sizes, each 90-L concrete batch would accommodate a set of beams consisting of one beam for each size.

4.2.3   Confined Column Concrete Mix Design

The investigation for the confined column program examined two types of confined columns, series CI and CII. Each type required one SCC mix and one NC mix, with the same size aggregate and similar 28-day compressive strength of approximately 50 MPa. There were no special requirements for the aggregate content in each mix, only that the same strength was required for the direct comparison of SCC and NC. Therefore, the mixes given in Table 4.7 were originally based on the 12-mm aggregate SCC and NC mix design in Table 4.5

As with the beam concrete, the proportion of SP was adjusted during the batch mix for the columns thus, slightly changing the actual proportions of all the constituents in the concrete. The batch size for each set was selected to accommodate the filling of all the column tubes in a set, nine 100 x 200 mm cylinders and fresh tests. The volumes

required were 52-L and 90-L for each set of columns in the CI and CII series, respectively.

Table 4.7 – Confined Column Concrete Mix Design

Column Series	Designation	Nom. Agg. Size mm	w/b	Cement kg/m³	Water kg/m³	Coarse Aggregate (SSD) kg/m³	Fine aggregate (SSD) kg/m³	SP (SS) %	VMA (SS) %
CI	C-SCC-CI	12	0.408	453	185	729	1060	0.75	0.05
	C-NC-CI	12	0.414	486	201	1028	647	0	0
CII	C-SCC-CII	12	0.408	453	185	719	1056	0.74	0.05
	C-NC-CII	12	0.420	486	204	1028	651	0	0

4.3 Properties of SCC

4.3.1 Mixing Sequence

The mixing procedure is critical in producing and reproducing concrete to attain the same properties. The sequence of mixing must allow sufficient time for the thorough mixing of all the constituents. The rheological study revealed that the VMA delayed the hydration reaction in the paste and mortar, and additional reaction time is required for the paste and mortar to stabilize. A 90-L drum mixer, located at the Ryerson University concrete materials laboratory, was used to mix concrete materials. All materials are weighed precisely and added in a sequence to the mixer at room temperature (23°C). The mixing procedure utilized for all the concrete mix was as follows:

- The mixer was first lightly dampened with water.
- The coarse aggregate and 1/3 of the water was introduced to the mixer and mixed for approximately 20 seconds.
- The sand was then added followed by the cement and mixed for a total elapsed time of approximately 1 minute.
- The rest of the water was then gradually introduced.
- The superplastisizer was then slowly added as required, and determined by visual observation.

- The above ingredients were added within a total time frame of 2 minutes from the introduction of cement and continued to mix for an additional 1½ minutes.
- The mixer was then stopped so that the concrete could rest for 3 minutes to allow sufficient time for the superplastisizer to react with the cement.
- The mixing proceeded for an additional 2 minutes with the introduction of the diluted VMA .
- The concrete was then left to rest for an additional 3 minutes before testing. The total elapsed time of the mixing sequence was approximately 12 minutes.
- If deemed necessary to increase the slump flow of the concrete, superplasticizer may be added and mixed for an additional minute following the initial mixing sequence.

The same mixing procedure was used for the normal concrete mixes excluding the use of superplastisizer and the VMA.

4.3.2 Slump Flow

The slump flow is a simple test to observe the fluidity of SCC and to evaluate the deformability of SCC. A standard slump cone is used for the test where the concrete is poured in the cone without consolidation. Unlike the standard slump test, the diameter of the material is measured after the removal of the cone to characterize the flowability of the concrete, hence the name slump flow. The test can also be used as a visual inspection for segregation. This is observed by the flow characteristic of the aggregate, mortar and fluid or paste separation. Two types of segregation have been observed by the author through the slump flow test. One is the clustering of aggregates in the middle of the slump diameter while the paste and some mortar continue to flow outwards to the diameter rim. The other is the continuous flow of the concrete beyond 700 mm diameter with visual separation of the water from the concrete material on the outer rim of the slump flow diameter. The recommended slump flow of SCC ranges between 500 and 700 mm diameter (Nagataki and Fujiwara, 1995). The slump flow target for the SCC in

this program was between 600 and 700 mm. A typical concrete slump flow for SCC is shown in Figure 4.1.
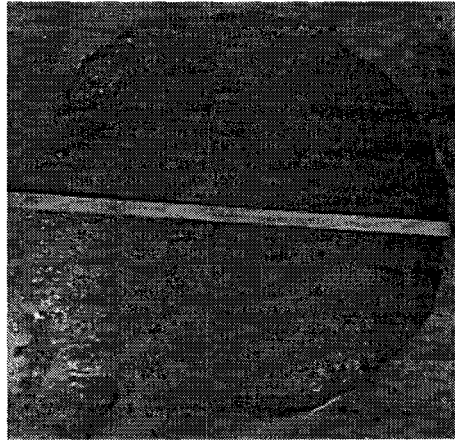
Fig. 4.1 – Slump Flow Diameter of SCC

Table 4.8 – Fresh Properties of Concrete

Concrete Type	ID	Slump	Slump Flow	Flow Time	L-Box
		mm	mm	sec	mm
SCC	C-SCC-CI		655	3.9	0.70
	C-SCC-CII		695	3.2	0.77
	B-SCC_12a		645	3.2	0.75
	B-SCC-12b		675	2.9	0.78
	B-SCC-19a		635	4.3	0.52
	B-SCC-19b		637	4.9	0.67
NC	C-NC-CI	130		-	-
	C-NC-CII	150		-	-
	B-NC-12a	155		-	-
	B-NC-12b	150		-	-

The diameter of the slump flow is the recorded average of orthogonal axis through the center of the slump flow. The test was performed on a smooth dampened metal plate also, all the equipment in contact with the concrete was dampened to avoid any removal of water from the fresh concrete. The average slump flow for all the 12-mm SCC was between 650 and 700 mm, and 636 mm for the 19-mm SCC. The slump flows of the SCCs are summarized in Table 4.8.

The conventional slump test was performed on the normal concrete. The concrete met the criteria required for increased workability for beams and columns at 130, 150 and 155 mm. (Table 4.8).

4.3.3 V-Funnel

The deformability and ease of flow through restricted area without blocking can be evaluated using the V-funnel test (Ozawa et al, 1994). The V-Funnel shown in Fig. 4.2 is completely filled with SCC which is then released through the bottom opening. The time of flow is recorded from the release of the opening until all the material clears the funnel. Flow time should be below 6 sec for SCC, and SCC with new VMA have a flow time normally between 2 and 5 sec (Lachemi et al, 2003b). High flow time indicates poor stability between the aggregate and the paste/mortar, and it does not ensure uniform deformation and distribution of SCC. This is caused by separation of paste/water from coarse aggregate or poor cohesion between the two, resulting in the cluster of the aggregate at restricted outlet area.

The flow times for the four 12-mm SCC were between 2.9 and 3.9 seconds, and were slightly higher for the 19 mm SCC with an average of 4.6 seconds. The higher flow time for the 19-mm SCC was expected as for obvious reason the larger aggregate will increase the coagulation and friction of aggregates at the restricted orifice of the funnel. All the SCCs displayed acceptable flow time and the results are listed in Table 4.8.
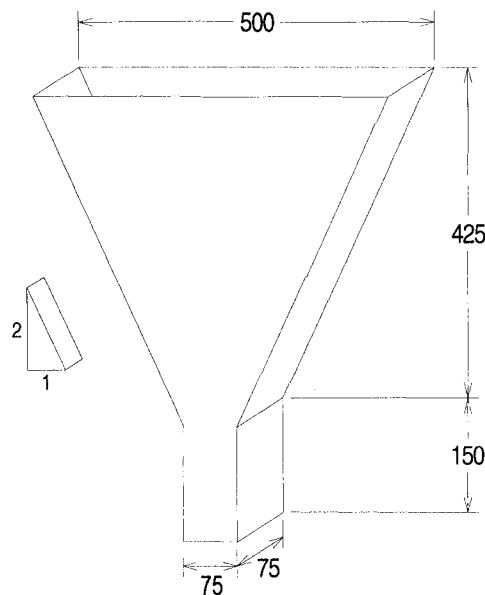
Fig. 4.2 – V-Funnel Setup

4.3.4 L-Box

The L-box flow is the third test adopted for this program to observe the flow properties of the SCC and is a common test utilized by researchers in the field of SCC. The L-box is the test that evaluates the concrete ability to flow through a restricted area. The apparatus consists of vertical and horizontal compartments as illustrated in Fig. 4.3. The compartments are divided by a sliding door that controls the flow of concrete from the vertical part to the horizontal compartment when opened. The flow is restricted by introducing three vertical bars located at 50-mm from the vertical chamber with a clear spacing of 34-mm. The vertical chamber is first filled with concrete and the door is then raised so that the concrete can flow through the bar spacing into the horizontal chamber. The level of concrete is measured at either end of the L-box and is translated into the L-box index by H2/H1. As expected, larger aggregate will increase the friction of flow through restriction. Therefore, the flow index values were generally higher for the 12-mm SCC as compared to 19-mm SCC.
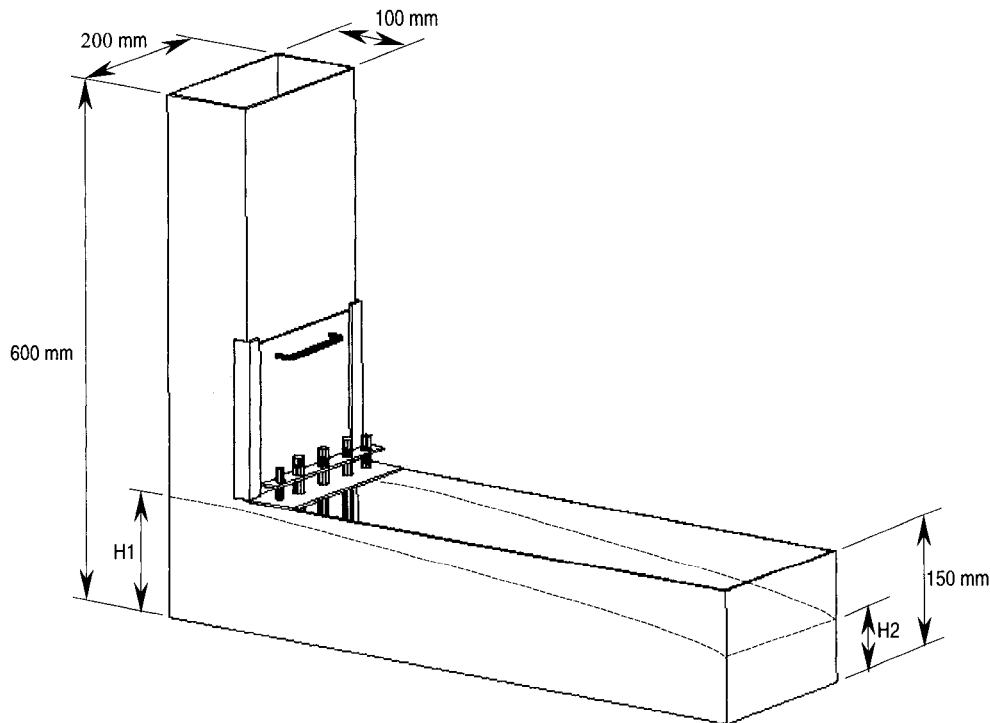
Fig. 4.3 – L-Box Schematic Representation

62

The average flow index for 12-mm SCC and 19 mm SCC are 0.75 and 0.60 respectively. The L-box index values for all the SCC are listed in Table 4.8. The ratio should be greater than 0.80 as recommended by Petersson (1999) for most laboratory testing. He also noted that SCC with an L-box blocking value of 0.6 had been reported to perform without blocking in structure. Blocking of the SCCs near the bars was not observed although, there was a noticeable reduction in flow rate of 19-mm SCC.

4.3.5 Compressive Strength

Performance of hardened concrete was measured for all concrete batches by means of compressive strength at ages of 1 or 2, 7 and 28-days. The average compressive strength was obtained from 100 x 200 mm cylinders for each batch at each age. The observed strength for each concrete mix is given in Table 4.9.

The SCC and NC were required to meet the same 28-day compressive strength of 50 MPa for each application. The 12-mm SCC and NC produced strengths with a difference of 2 and 3 MPa for the columns and the beams, respectively. Although the 19-mm SCC mix design was compensated to insure a compressive strength equal to those of the 12 mm concretes, the generated strength exceeded the 12-mm SCC and NC by 4 and 7 MPa, respectively. The early age strength of all the specimens are similar and show no delay in strength development for SCC with superplastisizer and VMA. No sign of delay of setting or strength development was evident between any of the SCCs and NC.

Table 4.9 – Evolution of Compressive Strength

ID	f'_c (Mpa)			
	1d	2d	7d	28d
CI-SCC	-	32	42	54
CI-NC	-	34	36	52
CII-SCC	24	-	44	49
CII-NC	-	-	38	47
S12-a	22	-	39	54
S12-b	20	-	37	53
N12-a	-	26	37	51
N12-b	-	24	36	50
S19-a	23	-	39	58
S19-b	22	-	44	58

4.3.6 Visual Observations

The SCC concrete for all applications consolidated well under its own weight. The 12-mm SCC tend to consolidate faster and was less affected by the introduction of congestion as compared to the 19-mm SCC. Aside from the difficulty of consolidating the NC, the concrete showed sign of slight segregation near the surface of the concrete after it was consolidated by a poker or vibrating table.

Following the removal of the formwork for the beam elements, a visual inspection of all concrete surfaces was made. All SCC specimens maintained smooth surfaces with no visible voids of entrapped air or honeycombing. The NC specimens maintained good consolidation with no or little voids of entrapped air on the surfaces of the beam.

At 28 days the shear plane surface of the compressed crushed cylinders were examined to characterize the shear path of the concretes. The 12-mm SCC and NC both carried the same shear path around and through the aggregates. Whereas the 19-mm SCC exhibits a shear path that extended through the aggregates.

4.4   Modulus of Elasticity

The Modulus of Elasticity (E_c) was not directly measured by experiments. Therefore, the elastic modulus of the SCC and NC concrete was predicted by means of Artificial Neural Networks (ANN). Due to the high variation in elasticity between similar types of High Performance Concrete (HPC), many statistical models and design codes have showed little success in predicting accurate values of E_c. SCC is in the category of HPCs and given that the ANN developed by (Lambros et al, 2003) was trained with a variety of HPC concretes, including SCC and NC, the author thought it was necessary to use the model to determine the elasticity of the SCC and NC. The E_c is an important parameter and required in code based equations to calculate the peak load of confined columns.

ANNs do not exist as an equation but as a program that can use existing parameters of the given object or material and are trained to understand the relationship of the parameters.

The ANN can manipulate the data to generate an output/predicted value with very low error. Obviously, the type of input values must be the same type to those that the network was trained on. The ANN developed (Lambros et al, 2003) required 10 input values of the following properties of concrete:

- Cement (kg/m^3)
- Fly Ash (kg/m^3)
- Silica Fume (kg/m^3)
- Slag (kg/m^3)
- Water (kg/m^3)
- Coarse Aggregates (kg/m^3)
- Fine Aggregates (kg/m^3)
- Super plasticizer solids (kg/m^3)
- Air Content (% volume)
- Compressive Strength f'_c (MPa) 28 day

The output value generated by the ANN was the 28-day E_c. The SCC developed in this program did not include any supplementary cementing materials (SCM) and this did not affect the value of E_c predicted by the network since many of the concretes included in training the network did not include SCM. The properties of all ten structural concretes developed in the study were collected and entered into the ANN to generate the E_c values listed in Table 4.10. As mentioned, the E_c for the concretes were not directly measured therefore, existing Codes were used to compare and validate the values predicted by the ANN.

Table 4.10 – Predicted Modulus of Elasticity of Concrete in GPa

Designation	$f'c$ (MPa)	ANN	CSA CAN A23.4	ACI Committee 364	Europe FIB(1990)	Norwegian NS 3473 (1990)	Baalbaki 1995
C-SCC-CI	54	35	32	32	34	32	30
C-SCC-CII	49	34	31	31	33	30	29
B-SCC-12a	54	35	32	32	34	32	30
B-SCC-12b	53	34	32	32	34	31	30
B-SCC-19a	58	34	33	33	35	33	34
B-SCC-19b	58	34	33	33	35	33	34
C-NC-CI	52	33	31	31	34	31	29
C-NC-CII	47	34	30	30	32	29	28
B-NC-12a	51	35	31	31	33	31	29
B-NC-12b	50	34	31	31	33	30	29

The predicted values of E_c generated by the ANN were slightly higher than those given by existing codes and models except for the FIB-1990. The study conducted by Lambros et al (2003) found that all the existing code based equations and models poorly estimated the E_c for HPC. However, the European FIB-1990 model generated the lowest error amongst them. Furthermore, many researchers have found that the existing codes can predict E_c reasonably accurate for most concretes with 28-day compressive strength of up to 50 MPa. Therefore, the ANN predicted E_c for the structural concretes are accepted based on two aspects: the similarities to existing code predictions; and the high correlation of predicted E_c and measured E_c demonstrated by the ANN developed by Lambros et al (2003) with $R^2 = 0.98$ and 0.92 for the trained and tested ANN, respectively.

4.5 Discussion

The concrete properties were similar for most of the mixes but did posses some unexpected dissimilarities. The B-SCC-12 batch (b) concrete was more fluid than the batch (a) concrete which contained a higher superplastisizer content. The two mixes were batched on the same day therefore, this unexpected behaviour is difficult to explain. The author accepts human error as a valid explanation for the discrepancy where recording weight and quantity of ingredients may be the cause. In addition to that, the elapsed time from cement and water contact to the first test may have varied due to superplastisizer adjustment following the mixing sequence. Fresh properties are time dependant, due to hydration, therefore, the delay in testing may yield different properties

of the fresh mix. Overall, the 28-day strength had a difference of only 1 MPa and even though the discrepancy, both batches worked well as a SCC and consolidation was likewise.

The B-SCC-19 concrete batches possessed similar fresh and hardened properties although the quantity of superplastisizer was higher for batch (b). The batch (b) mix contained the same type of superplastisizer, naphthalene formaldehyde sulphonic acids, made by a different manufacturer. The author introduced this parameter to observe the effect it would have to the fresh properties of SCC, the results were reasonable with no adverse affect other than increased dosage.

The fresh and hardened properties of C-SCC-CI and C-SCC-CII varied slightly although they had similar material proportions and curing age. The CII mix was batched approximately 1½ month after the CI batch. The difference may be caused by the change in material and lab atmospheric conditions. Mixing and casting at different temperature may have caused the change in performance of the fresh material. The difference of the 28-day compressive strength may have been caused by a lower curing temperature in the moist curing room. The temperature of the water mist in the curing room was controlled however, the author noticed slight temperature changes of the water temperature gauge on various occasions which would alter the strength development of the specimens. This was not a concern with the structural testing program of the project, being that all corresponding specimens and cylinders were cured under the same conditions, and the series CI and CII columns were not required to be identical in strength. This would also account for the difference in the NC compressive strength of series CI and CII columns.

The ease of placement of all the SCCs was alike and much easier than that of NC. This advantage reduced the time of casting of the specimens and the energy required (reduced labour). These properties were even more distinct with the confined column of CII with the added core reinforcement.

5.0 Beams

5.1 Overview

The first phase of the structural program examined the effect of concrete type, aggregate content and size on the shear strength of reinforced concrete beam elements. SCC generally consists of lower coarse aggregate content than normal concrete and with a smaller nominal maximum aggregate size in order to facilitate the ease of flow through congested members. To study the effect of SCC, a NC with different 12-mm aggregate content and a SCC with 19-mm aggregate content were used for comparison. The there types of concrete were used to fabricate 18 simply supported beams of three different cross-sections with adequate flexural reinforcement.

On a second note, this investigation would also serve as a contribution to the study of shear behaviour in beam elements. Despite numerous extensive studies in the past 50 years on the shear failure mechanism in beam elements, the mechanisms of shear failure in reinforced concrete beams still remains unresolved (Zararis, 2001). According to many researchers, including Zararis (2001) and Rebeiz (1999), it is necessary to study the shear failure mechanism of reinforced concrete beams without web reinforcement to better understand the failure mechanisms in beams with stirrups.

5.2 Beam Designation and Testing Procedure

The beams were categorized by concrete type and size and the following coding was used to identify them:

$$(S \text{ or } N)(12 \text{ or } 19)\text{-}(150 \text{ or } 200 \text{ or } 300)(a \text{ or } b)$$

where:

S or N indicates the concrete type, SCC or NC, respectively

12 or 19 indicates the maximum nominal size of aggregate in the concrete mix

150, 200 or 300 indicates the height (h) of the beam

a or b designates the beam within a pair and the concrete batch (Table 4.6)

For example, the 12-mm aggregate SCC beam with a height of 200-mm which is cast with concrete batch (a) is identified by:

S12-200a

5.2.1 Beam Size and Reinforcement Configuration

Six beams per concrete type were fabricated in three pairs of various cross-sections. The beams were designed to comply with the CAN/CSA-A23 standards (CPCA, 1995) in terms of flexural resistance. Stirrups were not included to ensure shear failure of the beams. All beam configurations were designed with the same width (b) of 100 mm and with a height (h) of 150, 200 and 300 mm. Two flexural reinforcement configurations were used for the beams, one layer of 2 x No. 10 rebar for beams of heights 150 and 200 mm and two layers of 2 x No. 10 rebar for beams with a height of 300 mm (Fig. 5.1). The total length of the beams were 900 mm with a span of 800 mm. The design load (P_b) for the 150, 200 and 300-mm beams were 56, 84 and 228 kN, respectively. The flexural reinforcement ratio (ρ) was 1.60, 1.15 and 1.06% for the 150, 200 and 300-mm beams, respectively.
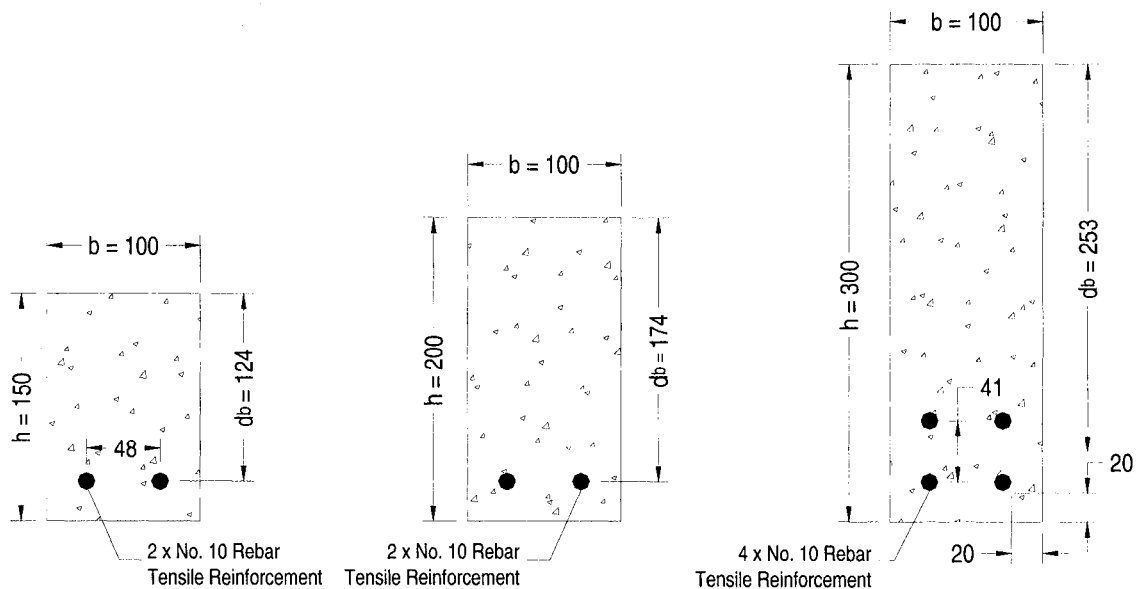
Fig, 5.1 – Details of Reinforcement Configuration and Dimensions of the Beams

69

5.2.2 Materials and Beam Casting

Three classes of concrete were examined in this study: one SCC with 12-mm coarse aggregate (S12), one SCC with 19-mm coarse aggregate (S19), and one NC with 12-mm coarse aggregate (N12). The increase in coarse aggregate content between the S12 and N12 was about 30%; the volume change in the mix design was compensated with a decrease in sand content by 40%. The increase in coarse aggregate content between the S12 and S19 was about 25%; the volume change was compensated with a 10% decrease in sand content. The cement contents in the three concrete mixes were not equal, each mix was designed with a cement content to develop 28-day strengths of 50-55 MPa. Details of the beams mix designs are given in Table 4.6. As discussed in section 4.2.2, one batch of concrete could accommodate three beams with one per size and therefore, two batches were required per set of beams. There was a 1 MPa or less variation of compressive strength between concrete batches of similar mix composition. The average 28-day compressive strength (derived from three 100 x 200-mm cylinders) was 53.5, 58, and 51.5 MPa for S12, S19 and N12, respectively. The detailed fresh and hardened properties of the concretes are given in Tables 4.8 and 4.9, respectively.

S12 and S19 beam concretes were poured and consolidated under their own weight, no vibration was introduced for consolidation. N12 beams were consolidated with a vibrating poker in two consecutive layers and trowel finished for a smooth top surface. There was a significant difference in the ease of placement and time for casting between the SCC and NC. Although the NC was designed with a high slump of 150-mm, placement was labour intensive and the time required to cast and finish each beam element was approximately 2 to 4 times longer than for SCC beams. By visual observation, the SCC properly filled the forms with ease of movement around the reinforcing bars in each reinforcement configuration. The flow or consolidation of S19 was slightly slower and required more time to consolidate properly though, much faster then the N12 concrete. This is attributed to the larger aggregate particles and the higher aggregate content over the S12 concrete.

5.2.3 Test Procedure for Beams

A two point loading apparatus was used to test the simply supported beams. Roller restraints were used at all the bearing points. The two point load was applied symmetrically at 1/3 of the span of the beam (267 mm). Fig. 5.2 illustrates the test set up used for the reinforced beams. A 250 kN load cell was used to measure the applied loads in a stiff frame hydraulic press. The load data was collected via a data acquisition system and a dial displacement gauge was used to manually record the mid-span deflection at increments of 2-5 kN. The load and defection were recorded for flexural cracking and shear cracking during the tests. The initial cracks and crack propagations were traced and labelled directly on the beams during the testing procedure, and the load for each label was recorded to coincide with recorded load-deflection data (Table B1.1, B1.2, and B1.3). Loading was terminated at the splitting of the concrete by means of shear cracking.
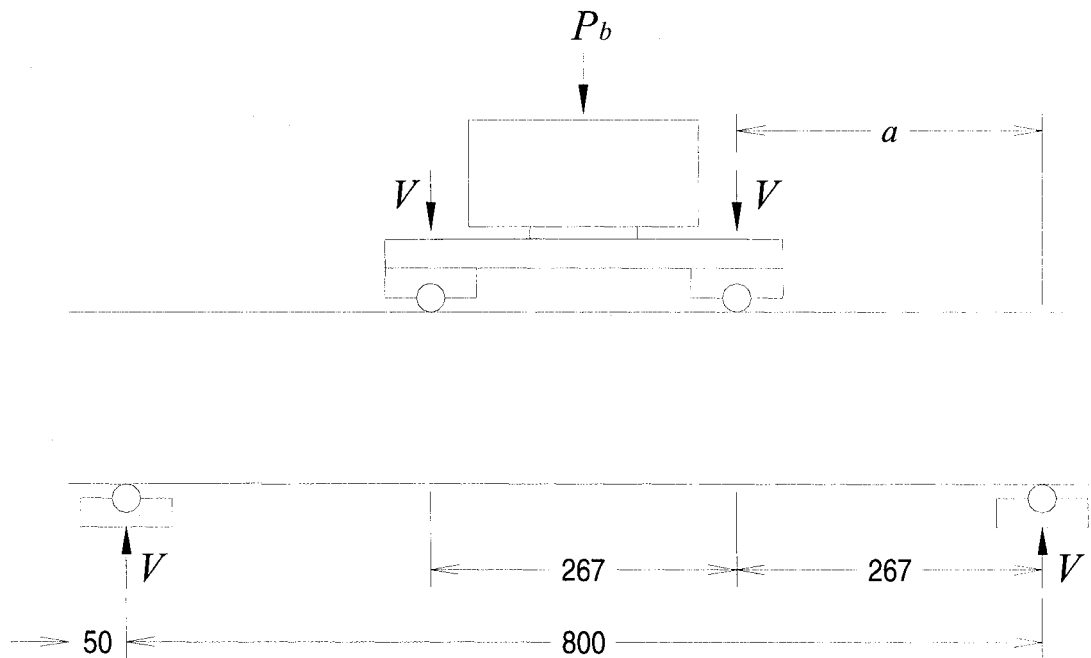
Fig, 5.2 – Testing Set-up for Reinforced Concrete Beams

5.3 Test Results and Analysis

5.3.1 Crack Patterns and Failure Modes

The ultimate failure of the beams was determined by the splitting of concrete propagated by the shear cracking in the shear span region of the beam. The failure occured when the inclined shear stresses along with normal stresses, due to bending of the beam, exceeded the diagonal tensile strength of the member. The first cracks to appear on all the beams were flexural cracks within the middle third of the spam (zero shear region) parallel to the direction of the load. In most cases, several small flexural cracks appeared within the zero shear span and in the shear span prior to the initial shear crack. The initial shear crack was developed in the shear region between the top fibre of the beam and the reinforcement. As load was continuously applied the shear crack propagated towards the support and the loading point, additional cracks appeared (shear and flexural) until ultimate failure occurred. In most cases, failure occurred shortly after the dominant shear crack extended to both bearing points within one shear zone region as indicated in Fig. C1.1-C1.9. The inclination angle of shear cracking was very similar for all concretes for each beam configuration at approximately 35-40° for h = 150 mm, 45-50° for h = 200 mm, and 50-57° of h = 300 mm. Since the shear span (*a*) is equal for all beams the angle of shear crack inclination tend to increase with the height of the beam.

The crack numbers shown on the faces of the beams indicated the order of crack developments and extension during loading (Fig. C1.1-1.9). Table C1.1, C1.2, and C1.3 gives the sequence of cracking, type of cracking, shear load and deflection. Out of the 16 beams tested, four did not fail along the shear inclination angle. The four beams developed shear cracks but then failed prematurely as the cracks extended in the horizontal direction along the longitudinal reinforcing bars, as shown in the case of Fig. C1.2, C1.6b, and C1.7a. The beam characteristics and failure modes are given in Table 5.1. The extension of the longitudinal cracking beyond the support may have been avoided with the use of proper development length beyond the span of the beams. This would force the cracking to remain in the shear region only.

72

Table 5.1 – Summary of Failure Modes

Beam	b mm	d mm	h mm	a/d	ρ %	Ultimate Failure
S12-150a	100	125	150	2.14	1.6	shear
S12-150b	100	125	150	2.14	1.6	shear
S19-150a	100	125	150	2.14	1.6	shear
S19-150b	100	125	150	2.14	1.6	shear
N12-150a	100	125	150	2.14	1.6	splitting
N12-150b	100	125	150	2.14	1.6	splitting
S12-200a	100	174	200	1.53	1.15	shear
S12-200b	100	174	200	1.53	1.15	shear
S19-200a	100	174	200	1.53	1.15	shear
S19-200b	100	174	200	1.53	1.15	splitting
N12-200a	100	174	200	1.53	1.15	shear
N12-200b	100	174	200	1.53	1.15	shear
S12-300a	100	254	300	1.05	1.57	splitting
S12-300b	100	254	300	1.05	1.57	shear
S19-300a	100	254	300	1.05	1.57	shear
S19-300b	100	254	300	1.05	1.57	shear
N12-300a	100	254	300	1.05	1.57	shear
N12-300b	100	254	300	1.05	1.57	shear

ρ is the ratio of tension reinforcement

5.3.2 Shear-Load Deflection Response

To properly analyse and compare the shear-load deflection curves of the various concrete beams it was necessary to normalize the shear strengths to account for variation in concrete compressive strength. This was done by dividing the shear (V) by the product of the width (b), effective depth (d_b) and the concrete compressive strength (f'_c). The shear-load deflection curves are given in Fig. 5.3-5.5. Due to the variation in failure modes only one beam per concrete type was used to evaluate the trend of the load-deflection curves.

h = 150-mm (Fig. 5.3)

Both N12-150 beams failed prematurely due to the extended cracks along the longitudinal bars. S19 beams had 13% and 16% higher shear resistance than S12 and N12 beams, respectively. The mid-span deflection at failure was similar for the S19 and S12 and greater than N12 by 13.8 %. Cracking during loading was noted by abrupt changes and kinks in the load-deflection curves. Initially all the beams displayed similar stiffness however, following initial and extended cracking the S12 and S19 beams displayed

greater stiffness and experienced similar load-deflection responses, N12 beam cracked in the longitudinal direction forcing the concrete to split and fail with less deflection.

h = 200-mm (Fig. 5.4)

Typical load-deflection responses for 200-mm SCC beams endured more deflection than the NC beams before ultimate failure (Fig. 5.4). As more load was applied the cracks began to develop which resulted in a reduction of the stiffness. The ultimate shear strength for S19 beam was higher than that of S12 and N12 beams by 5.3% and 16.7%, respectively. Beam S19 displayed the greatest deflection after cracking and the ultimate failure occurred at a maximum deflection which is 1.5 and 2 times greater than for S12 and N12 beams, respectively.

h = 300-mm (Fig. 5.5)

Typical load-deflection response slope for the 300-mm beams were quite similar before and after crack development up to the ultimate failure (Fig. 5.5). All the beams displayed similar load-deflection curves and S19 beam experienced the highest resistance to shear, typically 2.6% and 12.8% higher than N12 and S12, respectively. The maximum deflection was again greater for the S19 beam by 8.8% and 15.4% over the N12 and S12 beams, respectively.
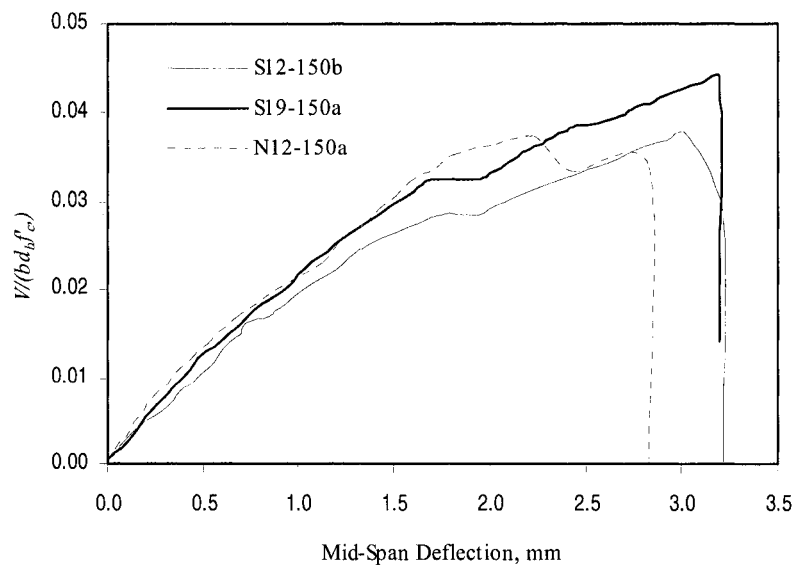
Fig, 5.3 – Shear-Load Deflection with h = 150
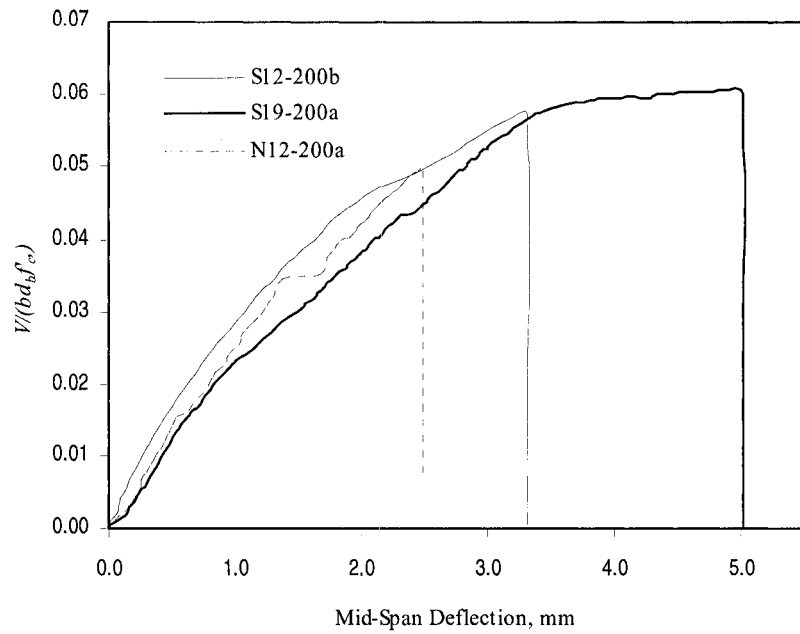
Fig, 5.4 – Shear-Load Deflection with h = 200
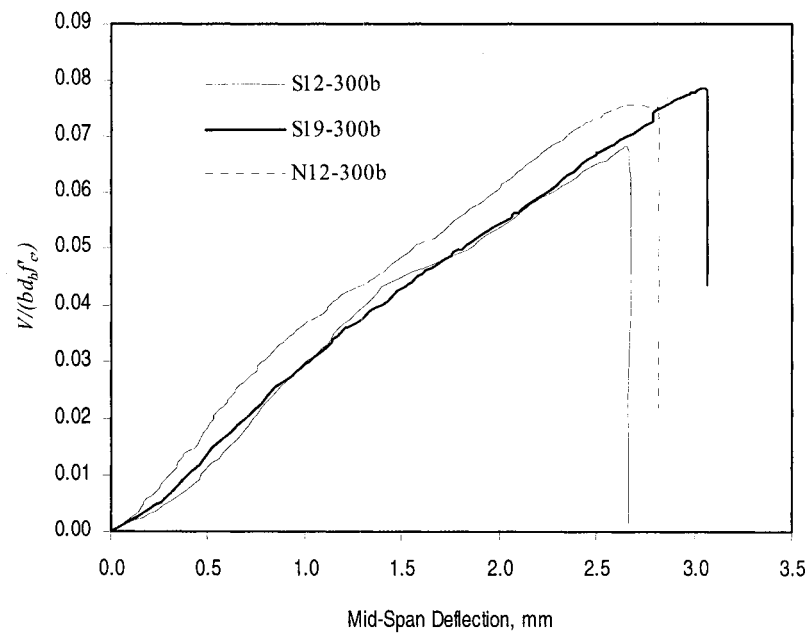
Fig, 5.5 – Shear-Load Deflection with h = 300

75

5.4 Effect of Concrete Type on Shear

5.4.1 Cracking Shear and Ultimate Shear Strength

The concrete shear resistance (V_c) was recorded through visual observation during the testing of the beams by the appearance of the initial shear crack. Due to the human factor in acquiring this value, it may not accurately represent the actual value. It was possible in some cases that the appearance of a crack may have been observed sometime after the crack actually initiated. The observed concrete shear resistance values they were checked against the values predicted by: ACI code (ACI, 1995), CSA code (CSA, 1995) and an equation developed by Rebeiz (1999):

$$V_c = \frac{1}{6}\sqrt{f_c'}bd_b \qquad \text{(ACI, 1995)} \quad (5.1)$$

$$V_c = 0.2\lambda\phi_c\sqrt{f_c'}bd_b \qquad \text{(CSA, 1995)} \quad (5.2)$$

$$V_c = 0.4 + \sqrt{f_c'\rho(d/a)}[2.7 - 0.4A_d]bd_b \qquad \text{(Rebeiz, 1999)} \quad (5.3)$$

where:

A_d is the shear shape adjustment factor $= a/d_b$ if $1.0 < a/d_b < 2.5$, or 2.5 if $a/d_b \geq$ 2.5.

a/d_b is the shear span to depth ratio

The observed and calculated values for cracking shear strength are given in Table 5.2. The CSA code underestimates V_c for all beam sizes and the ACI code predicts similar values for shallow beams but losses accuracy for deeper beams as height increases. The Rebeiz (1999) equation gives fairly reasonable predicted values as compared to Eq. 5.1 and 5.2. Rebeiz' equation (1999) was developed to consider the shear-span-to-depth ratio, which is not taking into account in the Codes when predicting cracking shear strength.

Rebeiz' equation (1999) also suggested that the observed values of S12-200a, S12-300a-b, and N12-300a were too high and therefore, they were excluded in the average V_c value

for each beam pair (Table 5.2). The average cracking shear strength was reasonably similar with a variance of 1.53, 3 and 0.5 kN for the 150, 200 and 300-mm beams, respectively. Therefore, there was no significant difference in the initial shear cracking strength between SCC and NC concrete with regards to aggregate content or aggregate size.

Table 5.2 – Initial Shear Crack of Beam Concrete

Beam	f'_c	Exp Vc	CSA Vc	ACI Vc	Rebeiz Vc	Analytical/Exp CSA	ACI	Model	Exp Vc avg.
	MPa	MPa	MPa	MPa	MPa				MPa
S12-150a	54	15.7	11.0	15.3	15.1	0.70	0.98	0.96	16.1
S12-150b	53	16.5	10.9	15.2	14.9	0.66	0.92	0.91	
S19-150a	58	12.8	11.4	15.9	15.6	0.89	1.24	1.22	15.3
S19-150b	58	17.7	11.4	15.9	15.6	0.65	0.90	0.88	
N12-150a	51	15.7	10.7	14.9	14.7	0.68	0.95	0.93	13.5
N12-150b	50	11.3	10.6	14.7	14.5	0.94	1.30	1.28	
S12-200a	54	37.7	15.3	21.3	23.5	0.41	0.57	0.62	27.5
S12-200b	53	27.5	15.2	21.1	23.3	0.55	0.77	0.85	
S19-200a	58	24.5	15.9	22.1	24.3	0.65	0.90	0.99	23.6
S19-200b	58	22.6	15.9	22.1	24.3	0.70	0.98	1.08	
N12-200a	51	26.5	14.9	20.7	22.8	0.56	0.78	0.86	26.0
N12-200b	50	25.5	14.8	20.5	22.6	0.58	0.80	0.89	
S12-300a	54	64.0	22.4	31.1	52.4	0.35	0.49	0.82	-
S12-300b	53	64.0	22.2	30.8	51.9	0.35	0.48	0.81	
S19-300a	58	48.0	23.2	32.2	54.3	0.48	0.67	1.13	48.0
S19-300b	58	48.0	23.2	32.2	54.3	0.48	0.67	1.13	
N12-300a	51	61.0	21.8	30.2	50.9	0.36	0.50	0.83	49.0
N12-300b	50	49.0	21.6	29.9	50.4	0.44	0.61	1.03	

The ultimate shear strength (V_u) corresponds to the load at which the beams failed. The ultimate shear strength (V_u) of the beams was checked against the designed shear resistance of the beam (V_r) in Table 5.3. The value V_r is obtained from the maximum shear load on the beams based on CAN/CSA-A23 design standards (CPCA, 1995) at maximum flexural resistance. The 150-mm beams, excluding S19-150a, failed before the specified design shear load. The 200-mm beams exceeded or matched the design loads and all the 300-mm beams failed before reaching the design load for shear failure. To directly analyze the effect of concrete type, coarse aggregate content and size on the ultimate shear strength, the values were normalized, as in section 5.3.2, and plotted against the shear-span-to-depth-ratio (a/d_b) in Fig. 5.6. Since some of the beams failed prematurely, only the beam which experienced the maximum shear strength of a pair was selected to plot the values for comparison in Fig. 5.6. S19 beams had the highest resistance to shear, and the variation of shear with height was linear. S12 beam experienced a similar pattern as the S19 beam but with lower shear strength for all beam sizes. The pattern of the N12 beams was less consistent then the S12 and S19 beams, this was partially due to the splitting type failure of N12-150. NC beams tend to develop

more shear strength as beam depth increased. Generally, there was no adverse effect on the shear strength with the use of SCC and lower aggregate content or size. In fact, the shear strength and deflection were enhanced for the majority of beams with SCC.

Table 5.3 – Ultimate Shear Strength of Beams

Beam	f'_c MPa	Ultimate Shear Failure	Exp. V_u kN	V_r kN	Design/ Exp
S12-150a	54	shear	19.5	27.4	1.41
S12-150b	53	shear	25.0	27.4	1.10
S19-150a	58	shear	31.5	28.2	0.90
S19-150b	58	shear	20.0	28.2	1.41
N12-150a	51	splitting	23.5	27.3	1.16
N12-150b	50	splitting	20.0	27.3	1.36
S12-200a	54	shear	49.0	40.3	0.82
S12-200b	53	shear	53.0	40.3	0.76
S19-200a	58	shear	61.0	40.6	0.67
S19-200b	58	splitting	41.0	40.6	0.99
N12-200a	51	shear	44.0	40.1	0.91
N12-200b	50	shear	39.0	40.1	1.03
S12-300a	54	splitting	67.0	113.7	1.70
S12-300b	53	shear	92.0	113.7	1.24
S19-300a	58	shear	93.0	114.9	1.24
S19-300b	58	shear	107.0	114.9	1.07
N12-300a	51	shear	79.0	113.0	1.43
N12-300b	50	shear	97.0	113.0	1.17
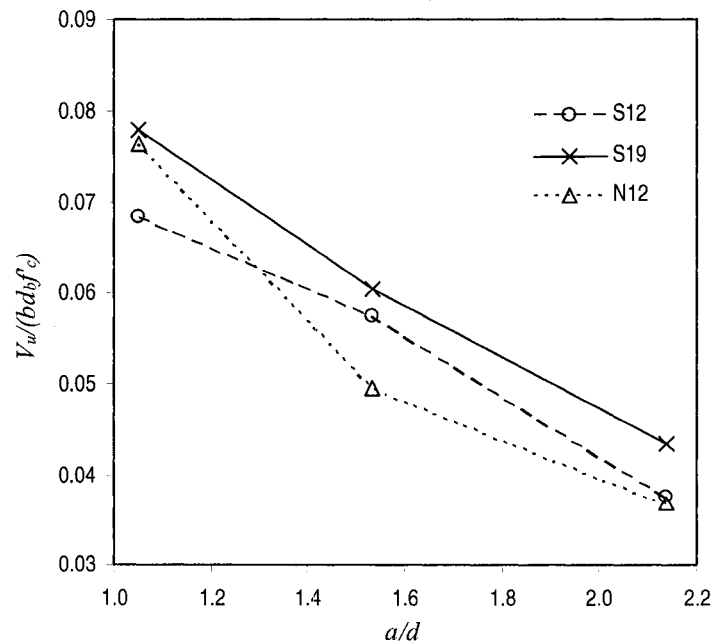
Fig, 5.6 – Effect of Concrete on Ultimate Shear

5.4.2 Discussion on Shear and Concrete

A visual inspection was conducted on the shear plane surface of the beams and the various concrete cylinders. It was common amongst all 19-mm aggregate concrete that the majority of the shear path extended through the aggregate as opposed to around the aggregate. The shear path in the 12-mm aggregate concrete extended through and around the aggregate equally. Shear usually takes the path of least resistance and with the S19 concrete it would be harder to extend cracking around the aggregate rather than through it. This could explain the higher shear resistance with S19 beams. Fig. 5.7 illustrated the difference in shear path between 19 and 12-mm aggregate. The shear path in the 12-mm aggregate follows a fairly straight and smooth path therefore much of the shear occurs in the transition zone.

The size and content of aggregate would influence the degree of interlocking among the particles in the concrete before and after cracking or softening of the concrete. With the presence of reinforcement or confinement the 12-mm aggregates and combined with the de-bonded aggregates along the transition zone, the aggregates would act as dowels and would be forced to interlock together. This would result in an increase of interlocking forces of the aggregate which would increase the shear resistance of the softened concrete. Without the presence of stirrups or confinement, the shear strength would be related to the compressive strength and/or splitting tensile strength of the concrete. Therefore, this may explain the increase in shear strength of the N12-300 beam over the S12-300 beam. The presence of more reinforcement and an inclined shear plane may have increased the interlocking and friction in the cracked concrete therefore, increasing the shear resistance. Since the S12 concrete beams had 30% less aggregate there would be less interlocking and friction in the reinforced area and thus, less shear resistance.
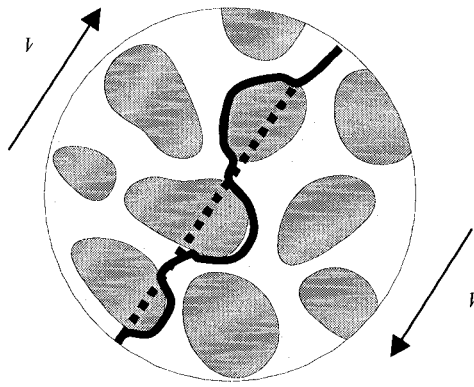
a) 19-mm Aggregate (S19)   *b) 12-mm Aggregate (N12)*
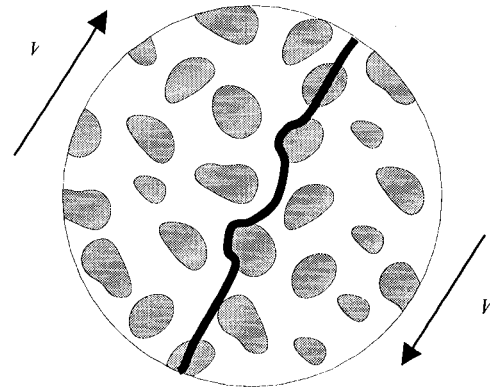
Fig, 5.7 – Influence of Coarse Aggregate on Shear Plane

6.0   Confined Columns

6.1   Overview

The second phase of the structural program investigated the use of SCC as the concrete "fill" material for confined steel tube columns and congested structural elements. Two configurations of confined columns were adopted: concrete filled steel tube columns, designated as series CI, and concrete filled steel tube columns with additional hoop confinement and axial reinforcement, designated as series CII. This phase of the research program served several objectives. Primarily, this investigation was conducted to observe the behaviour of SCC as a structural material, and as with the beam elements, to study the impact of coarse aggregate proportion on the concrete strength, comparative study of peak strength models for confined columns, including the proposition of new peak load models for confined columns with SCC and NC, was also performed. All the experimental phase was performed at Ryerson University. The concrete was mixed and placed in the concrete materials laboratory and the confined columns were tested using a 4600-kN MTS frame at Ryerson University Structures Laboratory.

Both series CI and CII integrated steel tubes for the confinement with a 4.4-mm thick wall, bearing a 0.2% offset yield stress of 300 MPa and an ultimate strength evaluated at 430 MPa. Figure 6.1 illustrates the results of tensile tests performed on 3 standard steel coupons.

Series CI consisted of two sets of two pairs of columns with 1000 and 500-mm in height with an outside diameter of 114 mm. The H/D ratios for series CI columns were 4.8 and 9.5. Series CII consisted of two sets of two pairs of columns with 1000 and 500-mm in height, an outside diameter of 168 mm and including additional hoop and axial reinforcement within the confined concrete section, adding congestion to the columns. The H/D ratios for series CII columns were 3.1 and 6.3. The two sets in both CI and CII series had a combined total of 8 columns for each series where four specimens made with SCC and the others four with NC. Column and material specifications are listed in Table 6.1.
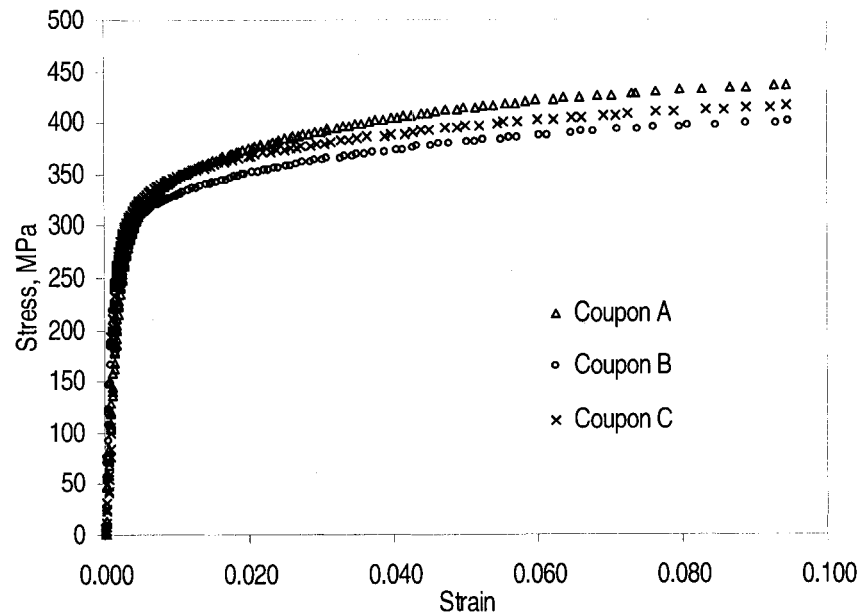
Fig. 6.1 – Steel Stress-Strain

Table 6.1 – Column and Material Specifications

Column	NO	Steel		Concrete		Rebar		H	D	t	K	λ	H/D	Reinforcing Steel			
		f_y	E_s	f'_c	E_c	f_{yr}	E_{sr}							Axial		Hoop	
		MPa	GPa	MPa	GPa	MPa	GPa	mm	mm	mm				No	%	No	%
CI-SCC-4.8	2	300	200	54	33.8	400	200	500	105	4.4	0.5	8.8	4.8	-	-	-	-
CI-NC-4.8	2	300	200	52	32.9	400	200	500	105	4.4	0.5	8.8	4.8	-	-	-	-
CI-SCC-9.5	2	300	200	54	33.8	400	200	1000	105	4.4	0.5	17.5	4.8	-	-	-	-
CI-NC-9.5	2	300	200	52	32.9	400	200	1000	105	4.4	0.5	17.5	4.8	-	-	-	-
CII-SCC-3.1	2	300	200	49	33.9	400	200	500	160	4.4	0.5	5.9	3.1	4	2.0	8	2.9
CII-NC-3.1	2	300	200	47	33.6	400	200	500	160	4.4	0.5	5.9	3.1	4	2.0	8	2.9
CII-SCC-6.3	2	300	200	49	33.9	400	200	1000	160	4.4	0.5	11.8	6.3	4	2.0	15	2.8
CII-NC-6.3	2	300	200	47	33.6	400	200	1000	160	4.4	0.5	11.8	6.3	4	2.0	15	2.8

One of the objectives was to compare the performance of confined columns made with SCC and NC. The investigation was based on the strength, ductility and failure mode of the SCC and NC confined columns. The specimens of Series CI and CII were tested to observe the axial and confinement stresses in the steel when loading the concrete core. The following sections discuss the column fabrication, instrumentation, test results and how the collected data was used to observe the biaxial stresses in the steel tube, employ Von Mises failure criterion to determine column load and stress at the yield of the steel

tube, determine the degree of load sharing between the concrete and steel and propose new peak load models for confined columns of SCC and NC.

Another objective was simply to investigate the ease of placement of SCC in congested columns such as series CII. This information was collected by observing the time and effort required to cast SCC into the confined columns.

The program used the following coding system to identifying the specimens within the test program:

<div align="center">(CI or CII)-(SCC or NC)-XX(a or b)</div>

where:

CI or CII indicates the series of the confined column.

SCC or NC indicates what type of concrete is used in the specimen.

XX represents the H/D of the specimen

a or b represent the column within a pair (two columns of each size and type were fabricated)

For example, the confined column of series CI made with SCC concrete at 500-mm in height and the second of the pair of column is identified by:

<div align="center">CI-SCC-4.8b</div>

6.2   Concrete Properties

As mentioned earlier, one of the objectives in this study was to determine the effect of using SCC with lower coarse aggregate content as concrete fill material in structural elements such as confined columns. In compliance with the requirements for SCC, the concrete mix utilized a 12-mm course aggregate with a low content of 700 kg/m^3 and the normal concrete used 12-mm coarse aggregate content of 1000 kg/m^3. The low content of aggregate was accommodated by increasing the sand content and was set at the lowest

content possible without adversely affecting the properties of SCC. The fresh properties of both SCC and NC are given in Table 4.8.

Each series (CI and CII) of columns were cast with a set of SCC and NC. Nine control cylinders (100 x 200 mm) were cast from each batch of concrete and three cylinders were used to determine compressive strengths at 1, 7 and 28 days. The cylinders were moist cured under the same conditions as the columns. The 28-day cylinders were cured in a humidity room and removed at 25 days to dry cure for 3 days and were tested within one day of the corresponding column testing. The average 28-day compressive strength for the SCC and NC for series CI were 54 and 52 MPa, and for series CII were 49 and 47 MPa, respectively (Table 4.9).

As outlined in section 4.4, the modulus of elasticity was predicted with an artificial neural networks trained for predicting E_c for high performance concrete. The elasticity for SCC and NC for series CI was 34 and 33 GPa and for series CII was 34 and 34 GPa, respectively.

6.3   Column Fabrication

The steel tubes were prepared and supplied by Pittsburgh Steel Limited. This included four sections of 1000-mm height and four sections at 500-mm in height with 114-mm outside diameter and a 4.4-mm thick wall for the CI series columns. The same length sections were prepared for the CII series columns with a diameter of 168-mm. It was intended to apply axial compression forces onto the concrete surface area to avoid the direct transfer of axial loads to the steel and to ensure the development of confining action by the steel to the concrete in the composite section. To facilitate this, removable sleeves were fabricated and used as forms to extend the concrete at both ends of the column by 5 to 7-cm in height as shown in Fig. 6.2.

The sleeves were held in place on either end of the tube with duct tape. Forming oil was applied only to the inside surface of the sleeve for easy removal after the setting of

concrete. The assembly was then placed in the formwork which kept all the specimens in a vertical position as shown in Fig. 6.2. All concrete was mixed in a 100-L capacity batch mixer at Ryerson University concrete materials laboratory. Both series had columns sets made with both SCC and NC. No consolidation was used in the casting of SCC columns while a vibrating table or poker was used to consolidate the NC columns.
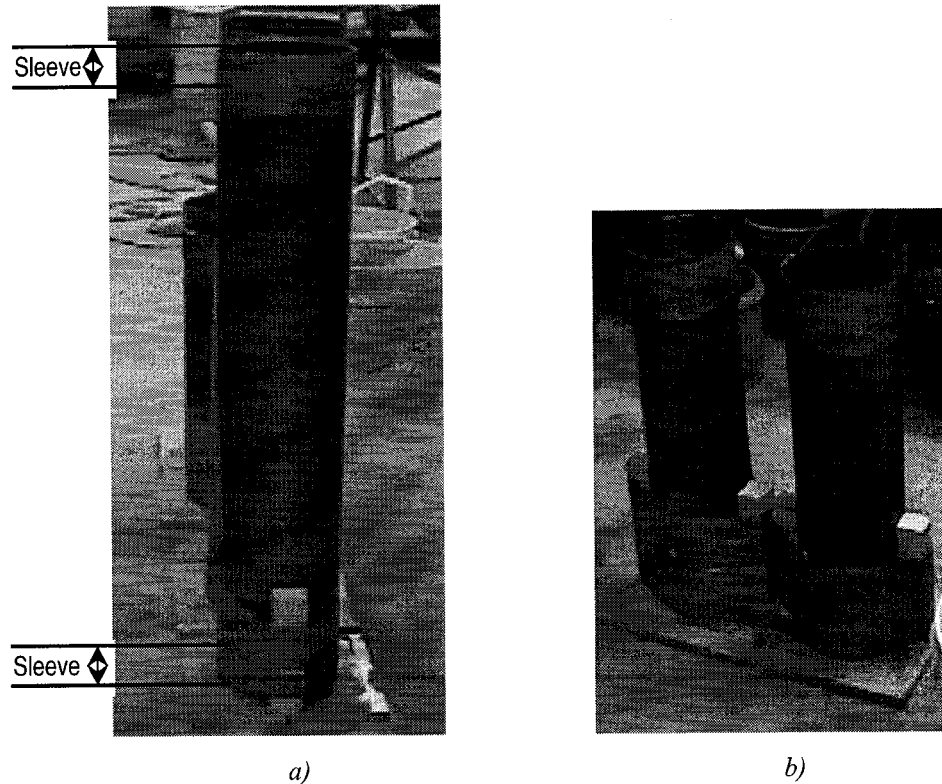
Fig. 6.2 – Confined column forms; a) H = 1000 mm; b) H = 50 0mm

After casting the columns, the tops were covered with vinyl plastic sheets and sealed with duct tape. The specimens were then placed in a humidity cabinet to cure for approximately 24 days and removed 3 days prior to testing where they were then prepared and dry cured for the remaining days until tested. All columns were tested at a minimum of 28 days after casting. This method of curing was chosen to assure consistency throughout all specimens in the experimental program. A corrosion inhibiting oil was applied to the surface of all specimens to eliminate further oxidation of the steel.

The concrete at the column ends were cut so that approximately 4-mm of the confined concrete was extended beyond both ends of the steel. The concrete core was cut using a large diamond wet blade at Ryerson University, and both surfaces were cut perpendicular to the longitudinal axis of the column. Protruded concrete at both ends of the specimens ensured that during testing the axial compressive force was applied directly to the confined concrete surface area.

6.3.1 Casting, Instrumentation and Testing: CI Series Columns

No consolidation was required to place the SCC in the CI-SCC columns, the concrete consolidated exceptionally well under its own weight. A vibrating poker was used to consolidate the NC in three successive layers for the CI-NC columns.

External strain gauges were applied to the steel tube surface at mid-height and top of the columns (Fig. 6.3). Preparation of steel surfaces at the gauge locations and installation of gauges were conducted as per manufacturer's instructions. Generally, all the columns were equipped with at least one circumferential and axial strain gauge at the mid-height level. Other gauges were installed at the top of the columns located 25-mm below the top of the steel either in the axial, circumferential or both directions. Due to a damaged gauge on CI-NC-9.5b column, insufficient data was available to include this column in different analyses. The main focus of modeling was to retrieve strain characteristics of the steel tube at mid-height when the concrete core was compressed. The columns were tested using a 4600-kN capacity displacement controlled MTS frame. Fig. 6.3 shows a typical setup of the confined column and strain gauge locations.

Axial load and displacement were directly recorded by the MTS acquisition system. A second data acquisition system was used to collect the strain gauge data during loading. A loading sequence was used to help match the two data sets. This was done by placing a 30 second hold when the axial load reached 400 kN, loading was then resumed to normal. The loading sequence was set at 60 kN per minute until the maximum displacement of the test head was reached. The axial displacement was used to determine

the axial strain, using the relation $\varepsilon = \Delta L/L$ where ΔL is the relative displacement of the head and L is the column length. The load-displacement data and the strain data were imported to Excel and aligned by shifting the sets of data to match the held load segment to the corresponding constant strain value segment.

The maximum load was set too low (1200 kN) when testing specimen CI-SCC-9.5a and the column did not experience peak load failure. Therefore, the data collected for load, displacement and strain readings halted when the test was terminated at 1200 kN.
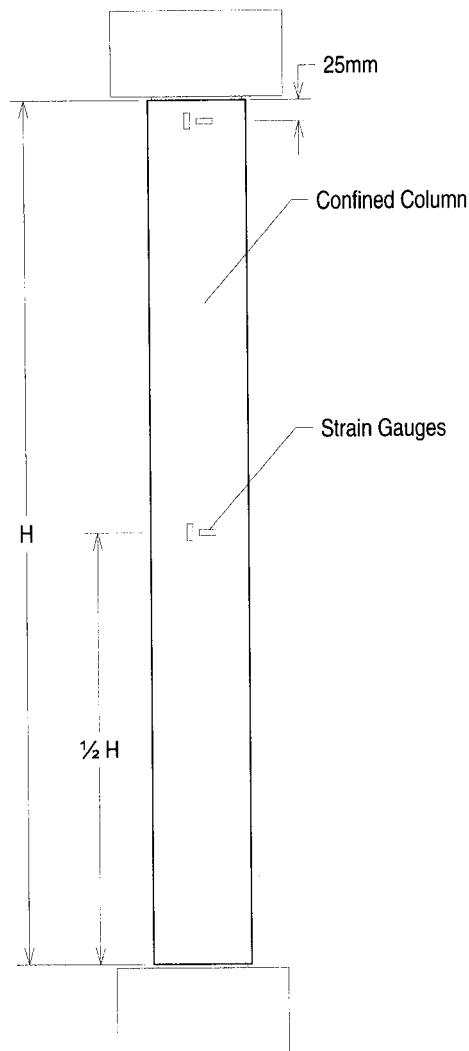
Fig. 6.3 – Typical Column Test Setup

6.3.2 Casting, Instrumentation and Testing: CII Series Columns

No consolidation was required to place the SCC in CII-SCC columns, the SCC consolidated exceptionally well under its own weight. The CII-NC columns were placed on a vibrating table during casting to provide adequate consolidation of the NC. The vibrating poker was not used as the congested configuration of the CII series columns would make it difficult to use.

Fabrication was more complex in the CII series columns because of the added hoop reinforcement. The hoops and longitudinal reinforcement were fabricated from No. 10 deformed rebar by Harris Omer Rebar Limited. The hoops had a diameter of approximately 100-mm and were spaced 66-mm center to center. Fifteen hoops were used in the 1000-mm columns and 8 hoops in the 500-mm columns, all columns in CII series used 4 longitudinal rebar. To prevent premature crushing of the concrete at the top and bottom of the columns, the longitudinal rebars were bent at 90° and directed outwards to the tube wall at the extent of the column (Fig. 6.4). The cages were tack welded together and then inserted into the steel tube. Small tack welds were made to one bent longitudinal bar and the inside wall of the tube at the top and bottom of the column. The welds were reduced to a minimum with a grinder to avoid the transfer of the axial load applied to the concrete core to the steel tube.

Series CII columns were equipped with four external strain gauges. Two gauges were installed at mid-height, one circumferential and one axial strain gauge. The second pair of gauges was installed at the 25-mm below the top of the steel tube, again, one circumferential and one axial strain gauge. The columns were tested using a 4600 kN capacity displacement controlled MTS frame. Data was collected and organizes in similar procedure as discussed in section 6.3.1.
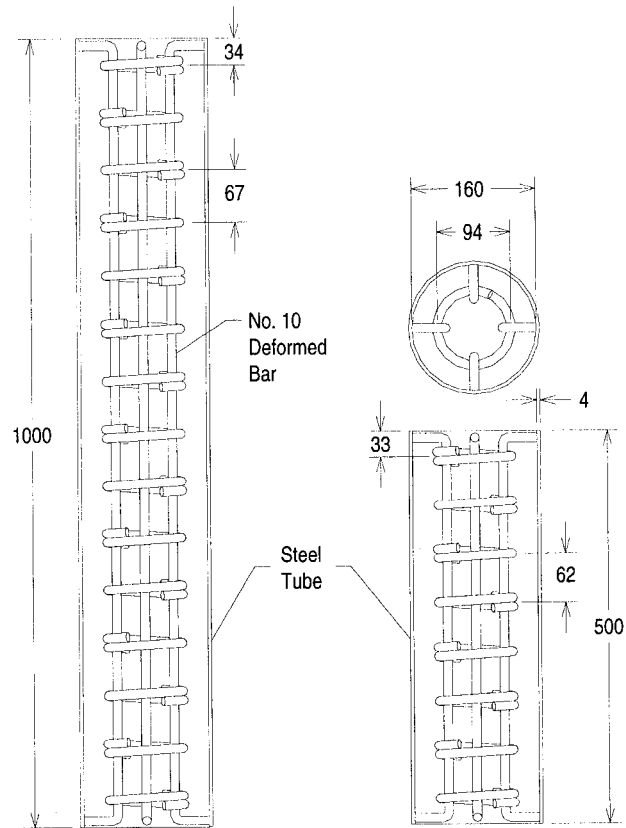
Note: all dimensions are in millimeters
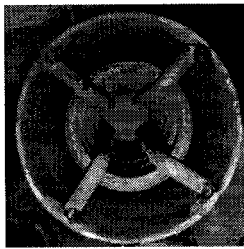
Fig. 6.4 – CII Series column configuration

6.3.3   Casting Time of CII Columns

The time required to cast the columns of CII with SCC and NC was observed for comparison. The concrete was transferred from the mixer to the columns by means of a 1-L hand scoop at a constant rate. It should be noted that this test did not necessarily represent filling or casting time of field applications. On site, the concrete would be

poured by means of a large drop bucket or by pump. Nonetheless, the author thought it appropriate to demonstrate this dimension of SCC. This observation was introduced to the program prior to casting the confined columns with congested reinforcement known as the CII series columns. The SCC was consolidated under its own weight, no vibration methods were used. The NC infill columns were positioned on a vibrating table to consolidate the concrete. It must be noted that the vibrating table is a much easier form of consolidation than a wall/external vibrator and poker vibrator used in field applications, in terms of manpower and time. Consequently, the experimental casting time of NC, in the lab, is believed to underestimate the actual time required for placing.

Placing the normal concrete did pose some difficulty due to the congestion imposed by the presence of the rebars. Thus, more consolidation was required than initially intended. The time interval for vibrating/consolidating the normal concrete during placement was not constant. Vibration was applied as required to consolidate the material without promoting segregation, and was determined based on visual inspections. The ease of placement and time were considerably improved for the SCC. As mentioned earlier, no vibration was required for consolidating the SCC thus, placement was as fast as the transfer of concrete from the mixer to the column. The time required to fill the CII columns were recorded and is given in Table 6.2. Based on the results of the 1000 and 500-mm columns, the average time of placement for the SCC was 2.5 times less than that required for the NC. The advantage to this may translate to a reduction of workers and duration of construction on a full size construction project. This notable observation reflects what field investigations have shown in terms of reduced casting time of SCC structures.

Table 6.2 – Casting Times

Column Height mm	Concrete Type	Casting Time avg. (min:sec)
1000	SCC	1:21
		1:10
	NC	3:01
		3:21
500	SCC	0:49
		0:47
	NC	1:54
		2:13

90

6.4 Test Results

The peak load of the columns was recorded at the first sign of local or global buckling in the columns. Testing was terminated for all the columns at the displacement limit of the MTS loading head. All specimens failed in a ductile manner.

6.4.1 Series CI Columns

_H/D = 4.8_

CI-SCC-4.8a and b columns sustained peak loads of 1170 and 1175 kN respectively with corresponding axial displacements of 11.4 and 12.1-mm. CI-NC-4.8a and b columns sustained peak loads of 1216 and 1230 respectively with corresponding axial displacements of 12.2 and 12.4-mm. The peak load of all columns were preceded by the appearance of bulging of the column followed by local buckling approximately at zero and 1/3 the height of the column from the top or bottom of the column. Post peak response exhibited a combination of local and outward buckling as shown in Fig. 6.5. The load displacement responses of CI-columns with H/D of 4.8 are shown in Fig. 6.6. NC columns showed an increase of the average peak load of 4.3% over the column with SCC nonetheless, the pre-peak, post-peak and ductility behaviour had no significant differences. All columns exhibited outstanding ductility due to the confinement effect.

a)   *b)*

Fig. 6.5 – Bulging/Buckling failure H/D = 4.8   a) CI-SCC-4.8a; b) CI-NC-4.8a;

1400

1200

1000

800

Axial Load, kN

600

400

------- CI-SCC-4.8a

------ CI-SCC-4.8b

———— CI-NC-4.8a

—·— CI-NC-4.8b

200

0

0   10   20   30   40   50   60   70

Axial Displacement, mm

Fig. 6.6 – Load Curve Displacement, Series CI, H/D = 4.

<u>H/D = 9.5</u>

CI-SCC-9.5a and b columns sustained peak loads of 1084 and 1097 kN respectively with corresponding axial displacements of 13.8 and 13.7-mm. CI-NC-9.5a and b columns sustained peak loads of 1119 and 1087 kN respectively with corresponding axial displacements of 14 and 13.2-mm. Peak loads were noted by the global buckling of all columns. The post peak behaviours were common amongst all specimens, with the exception of column CI-NC-9.5a, that failed by buckling. The initial buckling for column CI-NC-9.5a was located at $0.73H_1$ then a hinge point formed during the post peak loading at $0.49H_1$, followed by a second outward buckling in the opposite direction (Fig. 6.7). The locations of the hinge points for the SCC columns were relatively close to mid-height of columns depicting consistency between the two specimens. The NC columns tend to be less consistent in the development of buckling regions and failure modes. This may be attributed to non-homogeneity and inadequate consolidation of NC.

With the exception of CI-NC-9.5a, all columns had similar behaviour as shown in Fig. 6.8. Initially the post-peak load of CI-NC-9.5a began to decrease (similar to the other columns) but then it gradually increased until maximum displacement was achieved. The mode of buckling is directly related to this pattern.

For $H/D = 9.5$ the peak loads of the SCC and NC columns were 92% and 90% to that observed in shorter columns ($H/D = 4.8$) which indicated minimal or no slenderness effect.
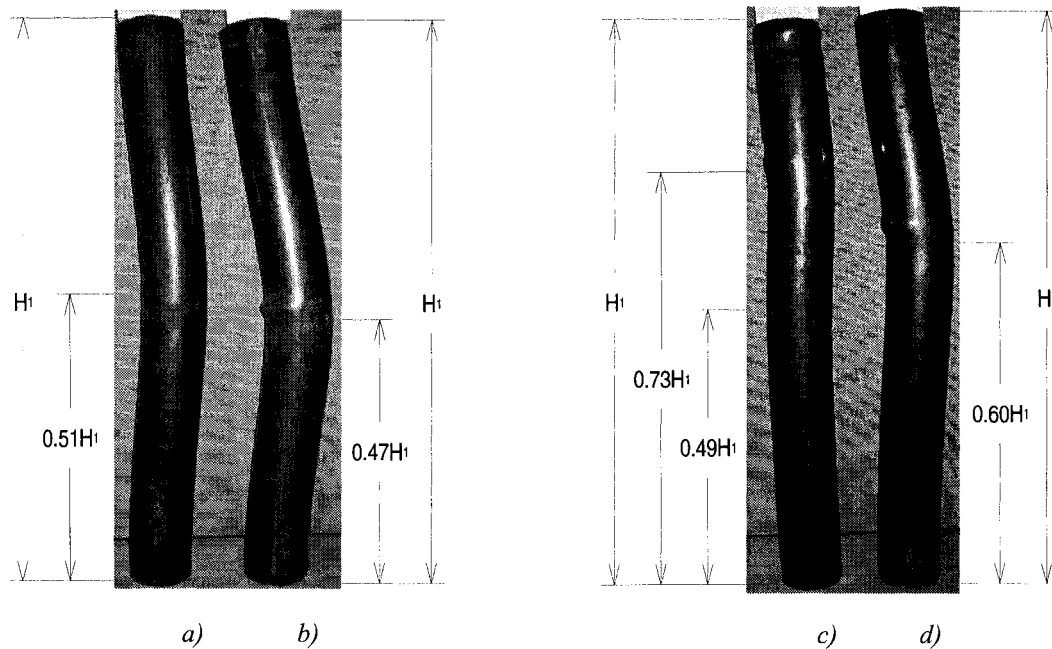
Fig. 6.7 – Global Buckling failure, H/D = 9.5, a) CI-SCC-9.5a; b) CI-SCC-9.5b ; c) CI-NC-9.5a d) CI-NC-9.54b
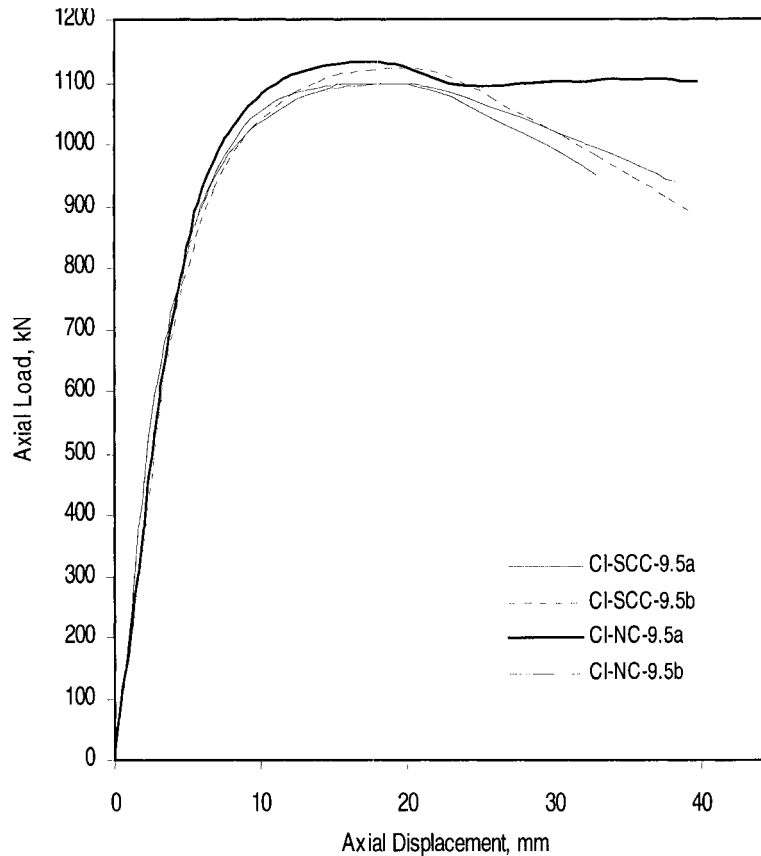
Fig. 6.8 − Load and Displacement, Series CI, H/D = 9.5

6.4.2 Series CII Columns

H/D = 3.1

CII-SCC-3.1a and b columns sustained peak loads of 2294 and 2271 kN respectively with corresponding axial displacements of 15.1 and 15.2-mm. CII-NC-3.1a and b columns sustained peak loads of 2454 and 2481 respectively with corresponding axial displacements of 16.5 and 15.0-mm. As with the short columns in series CI, the peak load of all columns were preceded by the appearance of bulging of the column followed by local buckling in various locations along the height of the columns (Fig. 6.9). The load displacement responses of CI columns with H/D of 3.1 are shown in Fig. 6.10. NC columns had an average peak load 8.1% higher than the SCC columns. The unconfined compressive strength of the SCC concrete was greater than that of NC by about 4 MPa. The reason for lower peak load of SCC in confined columns can be explained by the decrease in shear friction during the softening of SCC because of lower aggregate

content. The load displacement curves follow the same pattern throughout all specimens. The post peak loads of the SCC columns seemed to gradually increase or stay constant until the test was terminated, while with the NC columns the load dropped and fluctuated.
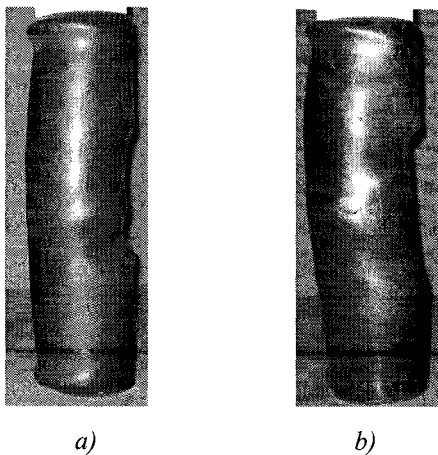

a) *b)*
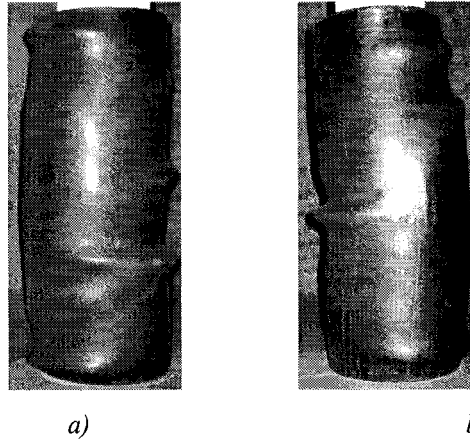
Fig. 6.9 – Bulging/Buckling failure H/D =3.1 a) CII-SCC-3.1b; b) CII-NC-3.1b
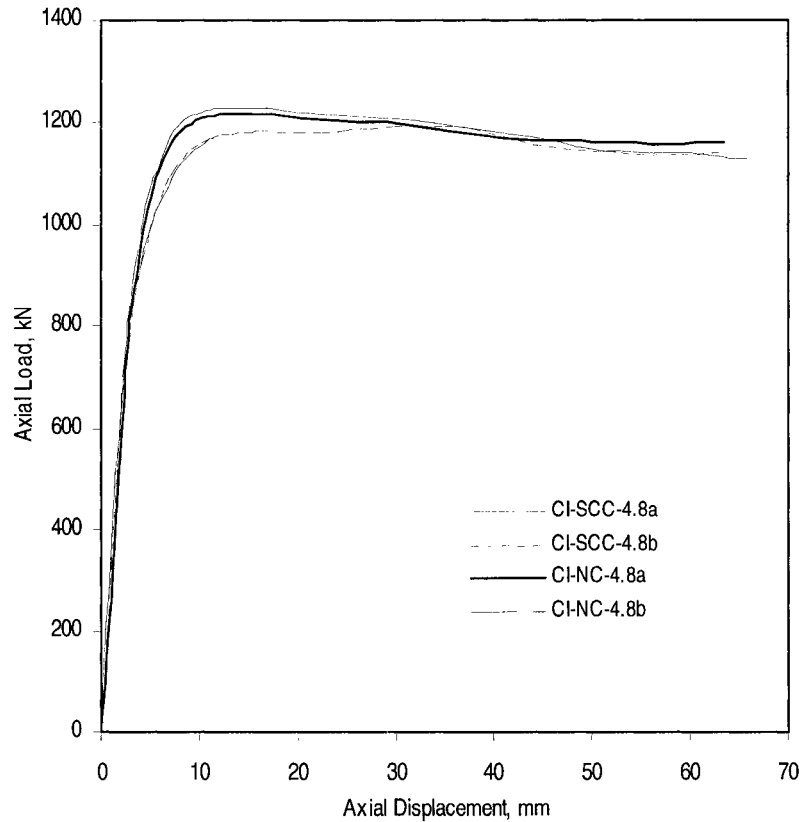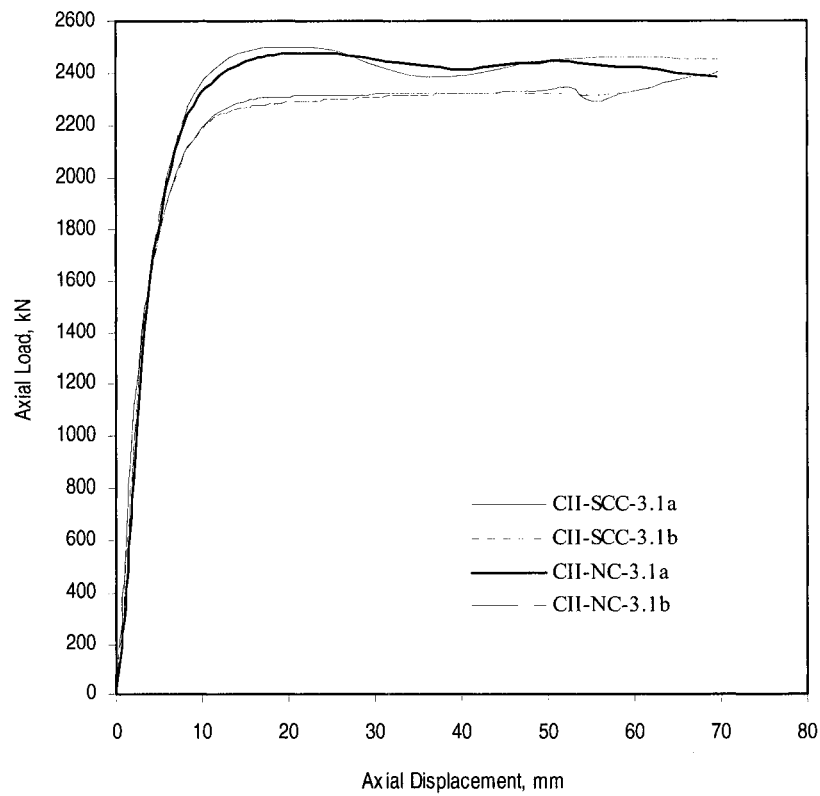

Fig. 6.10 – Load Curve Displacement, Series CII, H/D = 3.1

H/D = 6.3

CII-SCC-6.3a and b columns sustained peak loads of 2094 and 2127 kN respectively with corresponding axial displacements of 20.8 and 24.6 mm. CII-NC-6.3a and b columns sustained peak loads of 2242 and 2263 respectively with corresponding axial displacements of 22 and 22.2 mm. All columns showed enhanced strength and ductility due to the double confinement.

Peak loads were preceded by the appearance of global buckling of the columns, which was followed by post peak local buckling and slightly visible bulges generated by the hoop stress concentrations from within the column. The failure mode and load-displacement pattern were similar between the different pairs however, the location of the buckling in the NC columns are unequal (Fig. 6.11b). This inconsistency was similar to the NC columns of series CI, where non-homogeneity or poor consolidation could be the cause. SCC column buckling locations were consistent and symmetrical at mid-height of the columns.

The 1000-mm columns experienced similar peak load reductions compared to 500-mm columns as the case in Series CI columns. SCC and NC columns of H/D = 6.3 averaged a peak load of 93.5% and 91.3% respectively to the corresponding H/D = 3.1 columns. The load displacement response of the CII columns with H/D of 6.3 is shown in Fig. 6.12.
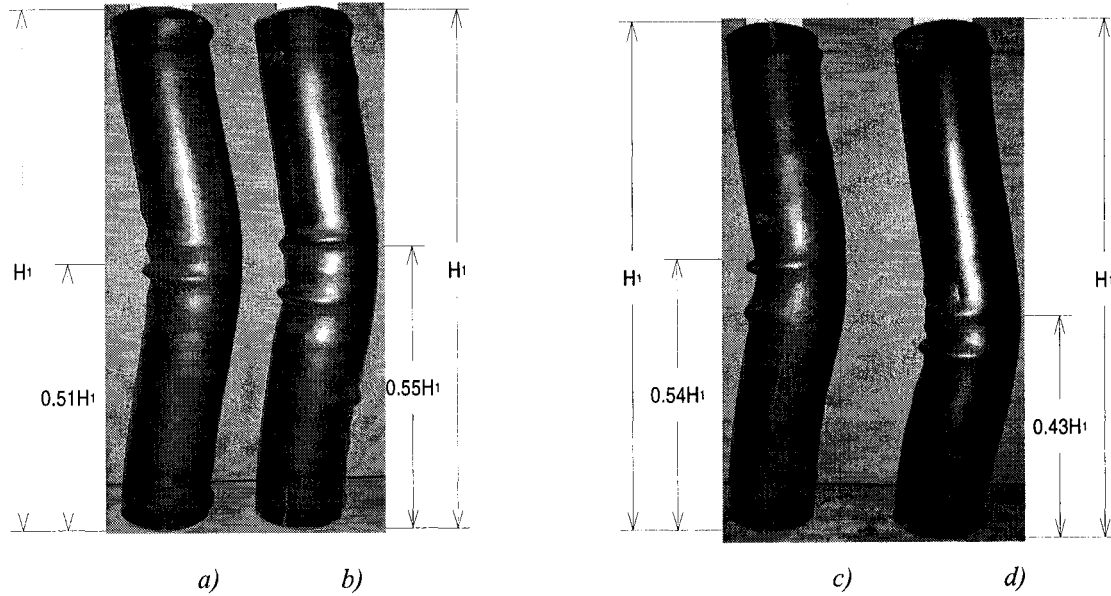
Fig. 6.11 – Buckling failure, H/D = 6.3, a) CII-SCC-6.3a; b) CII-SCC-6.3b ; c) CII-NC-6.3a d) CII-NC-6.3b
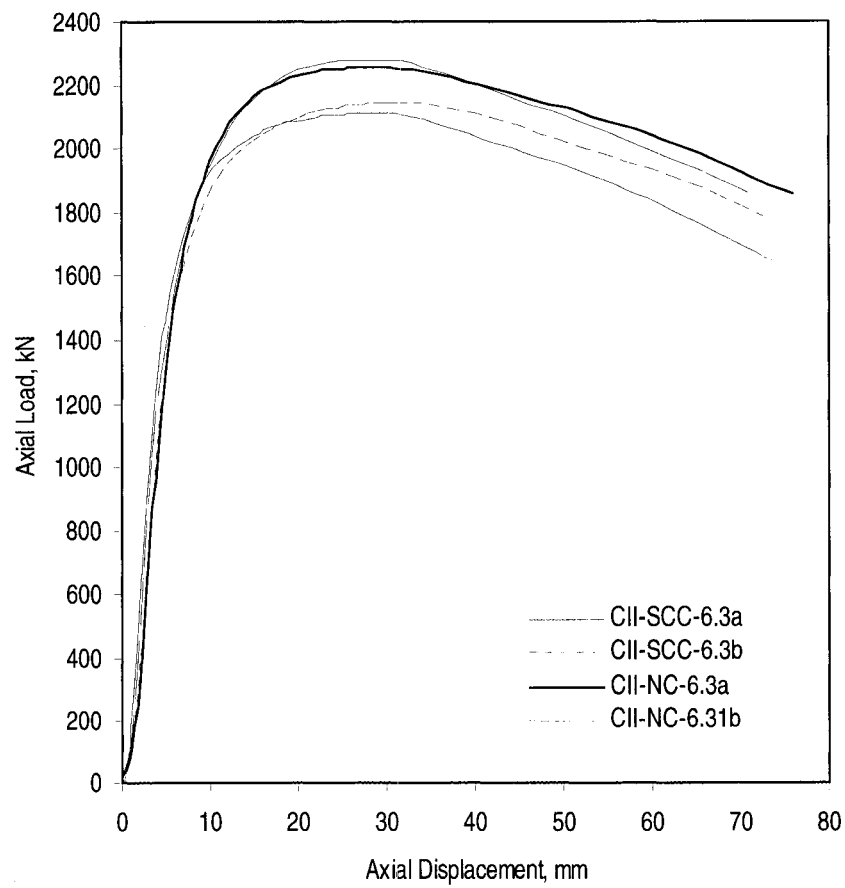
Fig. 6.12 – Load Curve Displacement, H/D = 6.3

6.4.3 Peak Strength of SCC and NC

The peak loads observed in Series CI for NC columns were generally greater than the SCC columns on average by 1.1 and 4.1% for the 500 and 1000-mm columns, respectively. Similar observation was made for Series CII columns. NC columns generated higher peak loads over SCC columns by 7.5 and 6.3% for 500 and 1000-mm columns, respectively. The difference between the two column heights was higher than those of series CI columns. The shear strength of the concrete in confinement was believed to be the reason for the different strengths. Primarily, the higher content of coarse aggregate in NC generated a more complex shear path. Even though the unconfined compressive strength of the SCC was greater than that of NC, this occurrence was thought to be caused by the reduced shear friction or mechanical bond during the softening and cracking of the concrete. The shear failure path observed in the beams with 12-mm SCC and NC (Chapter 5), extended through and mostly around the coarse aggregate. Since NC had a higher CA content, the friction along the shear path was greater that enhanced the shear strength of the concrete. The same observation was made for Series CII columns. The shear resistance might be exaggerated when the concrete was in confinement due to the additional confining forces acting on the concrete material and not allowing the sheared components to freely break away.

6.4.4 Ductility

Each column tested, from both series, exhibited a remarkable capacity for undergoing large deformation. 500-mm column in both series (H/D = 4.8, H/D = 3.1) had ultimate strains exceeding 0.125 with little or no decrease in post peak load. The residual strength of the SCC columns of series CII increased with the increase of deformation. The method used to quantify the section ductility was the ductility index (DI) expressed as:

$$DI = \frac{\varepsilon_{85}}{\varepsilon_p} \tag{6.1}$$

where ε_{85} is the axial strain in the column at 85% of the peak load on the descending branch of the stress strain curve, and ε_p is the strain at peak load. Tables 6.3 and 6.4

summarize load and strain relations for all the columns. The descending branch of the stress strain curve did not fall below $0.85P_{max}$ for 500-mm columns, therefore, the index was calculated with the max strain for each section.

Table 6.3 – Load Strain Relations: Series CI columns

Column	H mm	D mm	t mm	P_{max} kN	ε_p 10^{-6}	P_{85} kN	ε_{85} 10^{-6}	DI
CI-SCC-4.8a	500	114	4.4	1170	22800	-	-	-
CI-SCC-4.8b	500	114	4.4	1175	24220	999	126913	5.24
CI-NC-4.8a	500	114	4.4	1216	24300	1034	126846	5.22
CI-NC-4.8b	500	114	4.4	1230	24720	1046	131758	5.33
CI-SCC-9.5a	1000	114	4.4	1084	13830	921	35128	2.54
CI-SCC-9.5b	1000	114	4.4	1097	13660	932	37155	2.72
CI-NC-9.5b	1000	114	4.4	1119	13980	951	47252	3.38
CI-NC-9.5a	1000	114	4.4	1087	13200	924	40524	3.07

Table 6.4 – Load Strain Relations: Series CII columns

Column	H mm	D mm	t mm	P_{max} kN	ε_p 10^{-6}	P_{85} kN	ε_{85} 10^{-6}	DI
CII-SCC-3.1a	500	168	4.4	2294	30260	1950	139682	4.62
CII-SCC-3.1b	500	168	4.4	2271	30340	1930	134000	4.42
CII-NC-3.1a	500	168	4.4	2454	33000	2086	139200	4.22
CII-NC-3.1b	500	168	4.4	2481	30060	2109	139980	4.66
CII-SCC-6.3a	1000	168	4.4	2094	20790	1780	64449	3.10
CII-SCC-6.3b	1000	168	4.4	2127	24610	1808	72600	2.95
CII-NC-6.3a	1000	168	4.4	2242	22030	1906	74461	3.38
CII-NC-6.3b	1000	168	4.4	2263	22210	1924	81067	3.65

Since the residual capacity did not drop below the $0.85P_{max}$ for the short columns, the ductility was not a good comparative value for CI and CII short columns. However, the results did indicate that there was no change in ductility between SCC and NC for short columns of both series. Furthermore, the results indicated that the ductility of the short column was governed by the performance of the steel section.

The ductility index increased from SCC to NC in both CI and CII-1000 mm columns by 18% and 14%, respectively. The index suggested an increase in ductility from CI to CII type configuration for both SCC an NC by 13% and 8%, respectively.

1000-mm columns (H/D = 9.5, H/D = 6.3) had ultimate strains exceeding 0.02 with gradual decrease in load. CI-NC-9.5a column displayed an unexpected post peak response showing a brief decrease in residual strength before it begun to increase. The unexpected deformation of the column might have been the cause of this residual strength increase and might have led to an increase in internal steel-concrete friction and strain hardening of the tube. The SCC material demonstrated a higher consistency in failure response throughout all the specimens.

6.5   Analysis and Discussion

6.5.1   Biaxial Stresses in the Steel Tube

The confining action of the steel tube for concentrically loaded confined columns begins after the concrete softens or dilates. The outward expansion stresses of the concrete transfer the steel where biaxial stresses begin to develop. The confining action of the steel increases the dilation capacity of concrete fill material and peak failure loads are endured as the steel deforms plastically. The biaxial stresses in the tube were calculated from the measured strains of the concrete with the following stress equations (Fig.2.8):

$$\sigma_a = \frac{E_s}{1-\nu^2}\left(\varepsilon_a + \nu\varepsilon_h\right) \tag{6.2}$$

$$\sigma_h = \frac{E_s}{1-\nu^2}\left(\varepsilon_h + \nu\varepsilon_a\right) \tag{6.3}$$

where

σ_a, σ_h are the axial and circumferential steel stress, respectively.

ε_a, ε_h are the measure axial and circumferential steel strain, respectively.

E is the modulus of elasticity of the steel.

ν is the Poisson ratio of steel, taken as 0.3.

The yield stresses of the steel tube were based on the Von Mises failure criterion, (see Section 2.5.1), using the following Equation:

$$f_{ys}^2 = \sigma_a^2 + \sigma_h^2 - \sigma_a \sigma_h \qquad (6.4)$$

where f_{ys} is the uniaxial steel yield stress of the tube.

The steel tube was considered yielded when f_{ys} = 300 MPa. Typical biaxial stress state at mid-height of the columns based on Von Mises criterion as shown in Fig. 6.13: stress values are normalized to the uniaxial yield value. The initial stage of loading only develops axial stresses in the tube. When yielding of the tube is reached, hoop stresses are well developed but are still dominated by axial stresses. This suggests that axial load applied to the concrete is transferred to the steel due to a strong bond interaction between the two materials. Following the steel yield, confining forces in the concrete began to increase the hoop strains in the steel at a rate equal to the axial strain. This typical evolution of steel strain and column load is shown in Fig. 6.14.
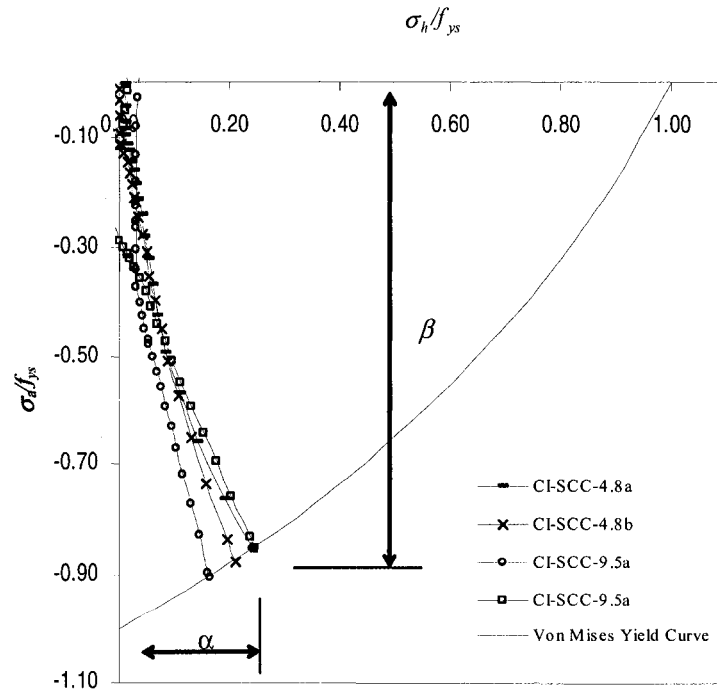
Fig. 6.13 – Evolution of Biaxial Stresses – Von Mises Failure Criterion
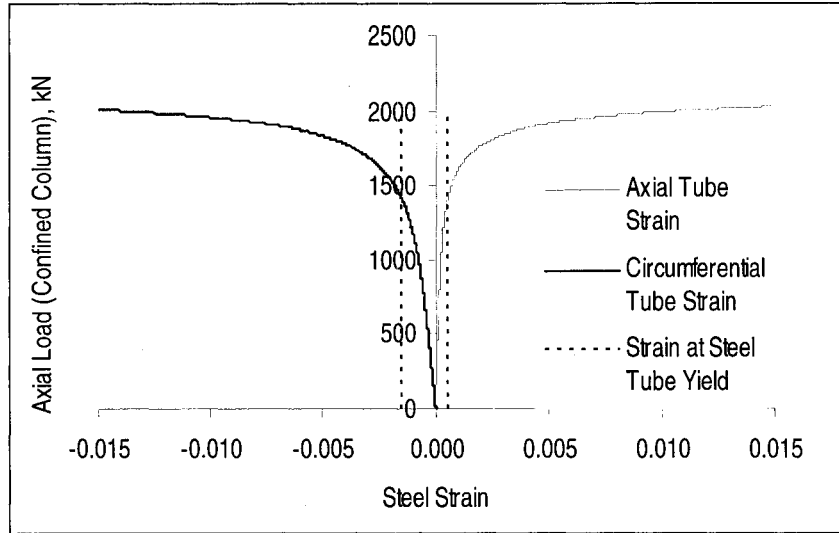
Fig. 6.14 – Steel Tube Strain-Confined Column Load – CII-SCC-6.3a

The values of α and β, as illustrated in Fig. 5.13, were used to quantify axial stress (σ_a) and circumferential/hoop stress (σ_h) to the yield strength of steel (f_{ys}). The α and β factors were calculated for each column and used to analyze the stress relations of CFST with SCC and NC, and also to calibrate and develop models for predicting peak strength of the confined columns. The quantified stress factors (α and β) for SCC and NC are listed in Table 6.5.

Table 6.5 – Axial and Hoop Stress Factors

Col	Concrete	H/D	Range			
			α		β	
CI	SCC	4.8-9.5	0.23	0.21	0.87	0.88
	NC		0.24	0.15	0.86	0.92
CII	SCC	3.1-6.3	0.22	0.08	0.88	0.96
	NC		0.30	0.11	0.81	0.94

The mean α value for each concrete type and column configuration was used to solve for β in Eq. 5.3. The results are represented as a range based on the column series, type of concrete and H/D ratios of the columns. The quantified stresses can be represented by:

$$\sigma_a = \beta f_{ys} \tag{6.5}$$

$$\sigma_h = \alpha f_{ys} \tag{6.6}$$

102

The stress relationships of each concrete type and column were observed through the results of Table 6.5. The axial stress in the steel tube was much higher than the circumferential stress when the steel yields for all confined columns. The CI stress factors (α and β) were very similar for SCC and NC although the NC columns tend to have less confining stress as slenderness increases. This suggested that NC had less dilation over the SCC. However, this effect was not repeated in CII columns, but somewhat reversed. In CII short columns, NC showed greater confining stresses and increased dilation over SCC. The confinement stresses were very low at steel yield for both SCC and NC as slenderness increased. This might be a result of the effect of hoop confinement located in the core of the columns. The increased confinement reduced the concrete dilation resulting in much higher peak loads than series CI columns. The hoop stresses of the confining steel tube were used to determine the lateral pressure of the confining concrete where observations were made based on the concrete stresses. By substituting Eq. 6.6 in Eq. 2.9, the magnitude of lateral pressure of the confined concrete can be derived as:

$$f_2 = \frac{2t}{D - 2t} \alpha f_{ys} \qquad (6.7)$$

The hoop confined core of CII columns reduced the lateral pressure acting on the steel tube. Thus, to quantify the pressure exerted in the column as a whole, the hoop core pressure must be added. The lateral confining stress for the hoop confined concrete (f_{2h}) can be calculated with the following expression:

$$f_{2h} = \frac{2 A_{sr} f_{yr}}{D_r s} \qquad (6.8)$$

where:

A_{sr} is the section area of the steel bar

f_{yr} is the yield strength of the steel bar

D_r diameter of the concrete from center-to-center of the confining rebar

s is the lateral spacing of the confining hoops

Table 6.6 compares the axial peak load (P_{max}) and strain (ε_p), axial load (P_{ys}) and strain at biaxial steel yield (ε_{ys}), and the calculated lateral pressure (f_2) exerted by the confined concrete. The value of f_{2max} is the maximum uniaxial lateral pressure calculated based on Eq. 6.7 at steel yield. The maximum uniaxial lateral pressure for CII columns includes additional lateral pressure derived by Eq. 6.8. The concrete lateral pressure in columns CI is determined by Eq. 5.7. The values coincide with the relationship depicted by the stress factors (α and β) in Table 6.5. The lateral pressures of CII columns derived from the tube alone are very small. Therefore, the inclusion of hoop induced lateral pressure in the concrete core, by Eq. 6.8, reasonably describes the internal action of the confined columns of series CII. Excluding the hoop effect would greatly underestimate the internal pressures acting on the concrete core. Moreover, it would adversely affect the peak load calculations based on equations and models. The higher lateral stress for CII-NC-3.1 may be explained by a bond-slip of the steel-concrete interface resulting in the lower axial stress transfer to the steel tube.

The P_{ys}/P_{max} was very consistent within the SCC columns of various slenderness and configurations ranging between 0.65 and 0.67. The P_{ys}/P_{max} for NC were less consistent ranging between 0.59 and 0.74. The consistent performance of SCC is attributed to the homogeneity and proper compaction of the material. The inconsistency of the behaviour and properties of the NC columns may cause difficulty in modeling attempts and strength predictions. These are the well-known challenges in modeling concrete behaviour and therefore, producing better performing materials is an ongoing challenge for the researchers.

Table 6.6 – Observed steel yield and lateral stresses

Column	P_{max}	ε_p	P_{ys}	ε_{ys}	P_y/P_{max}	$\varepsilon_y/\varepsilon_p$	f_{2max}	f_2	f_{2h}
	kN	10^{-6}	kN	10^{-6}			MPa	MPa	MPa
CI-SCC-4.8	1173	23510	785	5768	0.67	0.25	25	5.8	-
CI-SCC-9.5	1091	13745	711	3945	0.65	0.29	25	5.3	-
CI-NC-4.8	1223	24510	788	5559	0.64	0.23	25	6.0	-
CI-NC-9.5	1103	13590	831	4900	0.74	0.35	25	3.8	-
CII-SCC-3.1	2283	30300	1510	7190	0.66	0.24	29	3.6	12.9
CII-SCC-6.3	2111	22700	1415	5052	0.67	0.22	28	1.3	11.9
CII-NC-3.1	2468	31530	1582	7690	0.64	0.24	29	8.1	12.9
CII-NC-6.3	2253	22120	1337	4930	0.59	0.22	28	1.8	11.9

The header spans "Average Values for each Pair of columns".

6.5.2 Axial Load Sharing

The stress-strain response of the confined concrete was determined by using axial sharing equations Eq. 2.12 and Eq. 2.13. The axial stresses in the tube were converted to equivalent concrete stresses and subtracted from the stress-strain values of the confined columns. A typical stress strain curve for the yielding steel tube and confined concrete as a composite section is illustrated in Fig. 6.15.

Generally, these curves were used to observe the behaviour of axial load sharing between steel and concrete of various size and configurations of columns. Columns of both series CI and CII displayed similar response curves including a dip at the steel yield point. This is believed to be an artefact arising from the assumed abrupt yield of the tube (McAteer, 2002). As noted in the previous section, the yielding of the steel tube happened much earlier than the peak load of the column. Therefore, it was valid to assume that the peak stress of the confined concrete corresponded to the to the peak strain of the confined column. The stress (at which concrete dilates) was then extracted from the stress-strain response curves at the peak load of the columns. These values were taken as the observed confined concrete strength, f'_{cc}, and are given in Table 6.7 with their corresponding unconfined concrete strength.
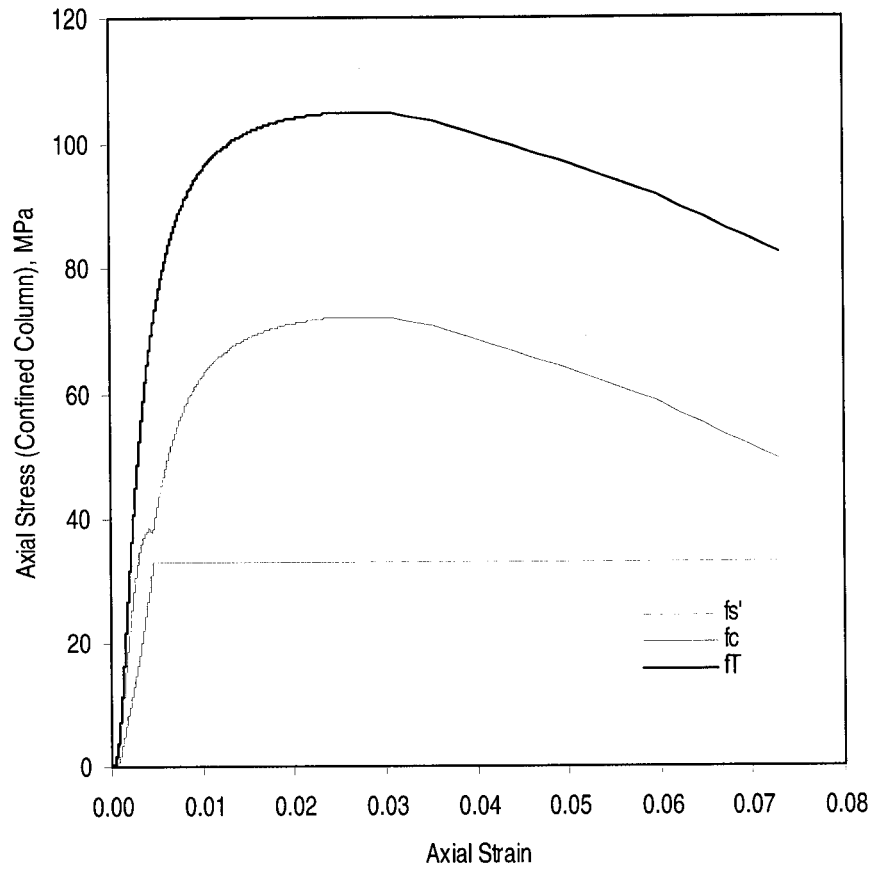
Fig. 6.15 – Typical Composite Column Response curve – CII–SCC-6.3a

Table 6.7 – Observed Concrete Strength

Column	H mm	f_c MPa	f_{cc} MPa	f_{cc}/f_c
CI-SCC-4.8	500	54	90	1.66
CII-SCC-3.1	500	49	83	1.69
CI-SCC-9.5	1000	54	80	1.47
CII-SCC-6.3	1000	49	72	1.47
CI-NC-4.8	500	52	96	1.85
CI-NC-9.5	500	52	81	1.56
CII-NC-3.1	1000	47	101	2.14
CII-NC-6.3	1000	47	80	1.69

Observed confined strength of the concrete in the 1000-mm columns is on average 20% less than the 500-mm column for SCC columns. The SCC displays remarkable consistency in the increase of compressive strength at each column height, a direct result

106

of improved consolidation and homogeneity of the material. The NC columns display an average variation of confined concrete strength at 30-40% between the two heights of the column in each series. In the case of 1000-mm columns of both series, the increase of compressive strength, due to confinement, is significantly higher for NC columns. However, the strength increases are very inconsistent in NC columns compared to SCC columns.

In addition, CII-series columns generate some added complexity to the load sharing condition of axial forces. The loading of the steel tube is directly measured as discussed, but the concrete core load is shared between the hoop and axial reinforcements. Load sharing of the hoop confined concrete core and tube confined concrete was not directly measured in this program. Therefore, analytical confined concrete strength models, f'_{cc}, were used to generate the values. The following section explores a combination of hoop reinforcement models and the CFT models to predict f'_{cc} values.

6.6   Analytical Models for Axial Capacity of Confined Columns

6.6.1   Confined Concrete Strength (CCS)

The confined compressive strength of concrete was observed for each specimen and compared to analytical values obtained from various confinement models. The models were used with the generated α and β values provided in Table 6.5. Three models were chosen for this investigation: Eq. 2.14, 2.15 and 2.16. They do not take into account the effect of confining hoops in the concrete core of columns CII. The experimental program did not provide strain evolutions in the reinforcing hoops and therefore, it would be difficult do develop or modify existing equations. To account for this the author proposed a combination of existing equations which considers the presence of hoop confinement in the concrete core. The selected confined concrete strength models were originally developed by Richart et. al. (1928), Mander et. al. (1988) and O'Shea and Bridge (2000) which are represented as Eq. 6.9, 6.10 and 6.11, respectively. Reasons for choosing these models are outlined in Section 2.5.3.

$$f'_{cc(R)} = f'_c + 4.1 f_2 \tag{6.9}$$

$$f'_{cc(M)} = f'_c \left(2.254 \sqrt{1 + 7.94 \frac{f_2}{f'_c}} - 2 \frac{f_2}{f'_c} - 1.254 \right) \tag{6.10}$$

$$f'_{cch(O)} = f'_c \left(2.172 \sqrt{1 + 7.46 \frac{f_{2h}}{f'_c}} - 2 \frac{f_{2h}}{f'_c} - 1.228 \right) \tag{6.11}$$

where

$$f_2 = \frac{2t}{D - 2t} \alpha f_{ys} \tag{6.12}$$

Eqs. 6.9, 6.10, and 6.11 are based on the confining action of the steel tube and also can take into account the additional confined concrete strength induced by the hoop confinement as is the case for CII columns. The listed models take into account the unconfined compressive strength of concrete and therefore, they would overestimate f'_{cc} if used again to generate a value for the hoop confined core. To account for this, the author adjusted the models to eliminate the unconfined strength of the concrete: The proposed modified equations based on Eqs. 6.9, 6.10 and 6.11 are presented as Eqs. 6.13, 6.14 and 6.15 respectively:

$$f'_{cch(R)} = 4.1 f_{2h} \tag{6.13}$$

$$f'_{cch(M)} = f'_c \left(2.254 \sqrt{1 + 7.94 \frac{f_{2h}}{f'_c}} - 2 \frac{f_{2h}}{f'_c} - 1.254 - 1 \right) \tag{6.14}$$

$$f'_{cch(O)} = f'_c \left(2.172 \sqrt{1 + 7.46 \frac{f_{2h}}{f'_c}} - 2 \frac{f_{2h}}{f'_c} - 1.228 - 1 \right) \tag{6.15}$$

where

$$f_{2h} = \frac{2A_{sr}f_{yr}}{D_c s}$$ (6.16)

To evaluate the combined effect of steel tube and hoop confinement, the equations representing f''_{cch} and f'_{cc}, are combined and made equivalent to the concrete area:

$$f_{cct} = f'_{cc}\left(\frac{A_{cc}}{A_c}\right) + f'_{cch}\left(\frac{A_{cch}}{A_c}\right)$$ (6.17)

where:

A_c is the area confined by the steel tube

A_{rv} is the total area of steel rebar taken as an equivalent concrete area by the volumetric ratio of total rebar to total concrete.

A_{cc} $= (A_c - A_{rv}) =$ Area of the concrete only

A_{cch} is the area confined by the hoop confinement.

The summary of the confined concrete strength for series CI and CII columns are listed in Table 6.8 and 6.9, respectively. Equation 6.17 was used to generate all values for columns of series CI and CII. The columns of series CI do not contain added confining hoops and thus by elimination of the appropriate values in Eq. 6.17, it reverts back to either Eq. 6.9, 6.10 or 6.11.

Table 6.8 – CI-Confined Concrete Strength Models Summary

Column	Obs. f_{cc} MPa	Proposed f_{cc} Richart	Proposed f_{cc} Mander	Proposed f_{cc} Oshea	Proposed/Obs. Richart	Proposed/Obs. Mander	Proposed/Obs. Oshea	Error MPa Richart	Error MPa Mander	Error MPa Oshea
CI-SCC-4.8	90	77	86	79	0.87	0.96	0.89	12.1	3.3	10.1
CI-SCC-9.5	80	75	84	77	0.95	1.05	0.97	4.2	4.3	2.3
CI-NC-4.8	96	77	86	79	0.80	0.89	0.82	19.0	10.3	17.2
CI-NC-9.5	81	67	74	68	0.83	0.91	0.85	14.0	7.0	12.5
							SCC	8.1	3.8	6.2
							NC	16.5	8.6	14.9
							All	12.3	6.2	10.5

Table 6.9 – CII-Confined Concrete Strength Models Summary

| Column | Obs. f_{cc} | Proposed f_{cct} | | | Proposed/Obs. | | | Error MPa | | |
	MPa	Richart	Mander	Oshea	Richart	Mander	Oshea	Richart	Mander	Oshea
CII-SCC-3.1	83	81	87	78	0.98	1.05	0.95	1.9	3.8	4.5
CII-SCC-6.3	72	71	74	67	0.99	1.03	0.93	0.9	1.9	4.9
CII-NC-3.1	101	85	91	82	0.84	0.91	0.82	15.9	9.5	18.4
CII-NC-6.3	80	71	75	68	0.89	0.94	0.85	8.5	4.9	11.8
							SCC	1.4	2.9	4.7
							NC	12.2	7.2	15.1
							All	6.8	5.0	9.9

The predicted confined concrete strength of SCC CI columns have a lower mean error with both models. This is again evident in series CII SCC columns. The errors generated for the NC columns of both series are rather inconsistent within the various configurations. The comparison shows that Mander's confined concrete strength model yields better results with lower average error.

The predicted confined concrete strength of CII columns are made up of two components: tube confined concrete strength (f''_{cc}), and hoop confined concrete strength (f''_{cct}). The effect of hoop confinement on the concrete core increased the predicted confined concrete strength by an additional 17 - 20 MPa for all the columns. The proposition of adding the effect of hoop confinement in analytical model yields better prediction. Otherwise, the use of only f''_{cc} would underestimate the peak strength prediction. Although Mander model yields better prediction, Richart, and O'Shea and Bridge models were also included to study the peak strength of the columns.

6.6.2 Proposed Peak Strength Models for Confined Columns

By adopting the methods and models outlined in section 2.5.4, the author has proposed the following models to predict the peak strength of series CI and CII type confined columns.

110

Using the axial capacity models proposed by Hossain (2003) (Eq. 2.21 and Eq. 2.23), and substituting Eq. 6.17, and including the effect of longitudinal rebar, the axial capacity (P_{r1} and P_{r2}) can be written as:

$$P_{r1} = \beta A_s f_{ys} + A_{cc} f'_{cc} + A_{cch} f'_{cch} + A_{ra} f_{yr}$$ (6.18)

and

$$P_{r2} = A_s f_{ys} + A_{cc} f'_{cct} + A_{cch} f'_{cch} + A_{ra} f_{yr}$$ (6.19)

where

A_{ra} is the total area of longitudinal rebar

f_{yr} is the yield strength of the rebar

These models are for both CI and CII series columns. As mentioned in the previous section, when applied to series CI type columns many parameters are eliminated with the confined concrete strength and the longitudinal reinforcement, therefore simplifying the equations.

The author followed the same procedure as outlined by Hossain (2003) and replaced the stress factors (α and β) to those generated in this study (Table 6.5). Table 6.10 lists the comparison of peak loads predicted by both proposed models in combination with the confined concrete strength models proposed in the previous chapter.

Table 6.10 – Proposed Peak Load Strength Model Comparison

Column	P_{obs}	P_{r1}			P_{r2}			P_r/P_{obs}					
		kN	kN	kN	kN	kN	kN	P_{r1}			P_{r2}		
	kN	Richart	Mander	Oshea	Richart	Mander	Oshea	Richart	Mander	Oshea	Richart	Mander	Oshea
CI-SCC-4.8	1173	1064	1140	1081	1124	1200	1141	0.91	0.97	0.92	0.96	1.02	0.97
CI-SCC-9.5	1091	1052	1125	1068	1106	1179	1122	0.96	1.03	0.98	1.01	1.08	1.03
CI-NC-4.8	1223	1055	1131	1071	1120	1196	1136	0.86	0.92	0.88	0.92	0.98	0.93
CI-NC-9.5	1103	997	1058	1010	1034	1094	1047	0.90	0.96	0.92	0.94	0.99	0.95
CII-SCC-3.1	2283	2325	2433	2270	2411	2518	2355	1.02	1.07	0.99	1.06	1.10	1.03
CII-SCC-6.3	2111	2190	2245	2112	2219	2274	2141	1.04	1.06	1.00	1.05	1.08	1.01
CII-NC-3.1	2468	2353	2474	2300	2476	2596	2423	0.95	1.00	0.93	1.00	1.05	0.98
CII-NC-6.3	2253	2178	2246	2110	2219	2287	2151	0.97	1.00	0.94	0.98	1.02	0.95
Mean Error	CI	SCC						0.06	0.03	0.05	0.03	0.05	0.03
		NC						0.12	0.06	0.10	0.07	0.01	0.06
	CII	SCC						0.03	0.06	0.00	0.05	0.09	0.02
		NC						0.04	0.00	0.07	0.01	0.03	0.03

All the models predicted the peak strength of the tested columns with reasonable accuracy. For series CI columns, the least errors were generated by the P_{r2} model with the lowest average error of 3% when combined with the Mander confinement model. For series CII columns, the least error was generated by model P_{r1} with overall mean error of 2.5% with the O'Shea et al. confinement theory. Based on material performance, the models yield the lowest overall error when predicting the peak strength of SCC columns.

The comparative study of a selected model with the existing models was based on the lowest overall error and consistency of prediction. The selected proposed model is P_{r2} with the O'Shea et al. confinement theory. The model can be expressed as:

$$P_{r2} = A_s f_{ys} + A_{cc} f'_{cc(O)} + A_{cch} f'_{cch(O)} + A_{ra} f_{yr} \qquad (6.20)$$

where for confined columns without hoop confinement the values of $f'_{cch} = A_{ra} = A_{cch} = 0$.

6.6.3 Comparative Study of Peak Load Models

Table 6.11 summarizes the analytical results for peak loads of the proposed model, P_{r2}, with the models proposed by Hossain (2003) and code based equations based on CISC, AISC and Eurocode 4. The study clearly shows that the proposed model P_{r2} provides better prediction of peak strength with least error for both CI and CII columns. The models proposed by Hossain (2003) were equipped with the stress factors (α and β) generated by the columns in this study (Table 6.5).

Series CI columns

Notably, the models proposed by Hossain (2003) generate reasonably low error with average error of 10% and 5% for the first and second model, respectively. The Code based models of CISC, AISC and Eurocode4 underestimated the peak strengths on average by 36%, 31%, and 20%, respectively.

Series CII columns

The high error generated by the existing models and Code based equations was expected, because they do not take into account the effect of added confining hoops or spirals within the core of the concrete fill. The values predicted by existing and code based models underestimated the peak loads by an averaged range of 1% to 36%. The models based on CISC and AISC yielded the highest errors. The proposed model appears to be good in predicting peal load as it shows low mean error of 2% for SCC and 6% for NC columns.

The comparative study validated the performance of the proposed model and hence can be used for the prediction of peak strength of concrete filled steel tube columns with or without added hoop or spiral reinforcement in the concrete core

Table 6.11 – Comparative Study of Proposed and Existing Codes Models

Column	P_{obs} avg. kN	P_{r2} kN	Hossain[1] kN	Hossain[2] kN	CISC C_{rc} kN	AISC P_{cr} kN	Euro Code 4 kN	$P_{r/P_{obs}}$ P_{r1mod}	Hossain[1]	Hossain[2]	CISC	AISC	Euro Code 4
CI-SCC-4.8	1173	1141	1053	1129	763	832	921	0.97	0.90	0.96	0.65	0.71	0.79
CI-SCC-9.5	1091	1122	1041	1111	689	778	921	1.03	0.95	1.02	0.63	0.71	0.84
CI-NC-4.8	1223	1136	1045	1125	754	818	904	0.93	0.85	0.92	0.62	0.67	0.74
CI-NC-9.5	1103	1047	985	1039	681	765	904	0.95	0.89	0.94	0.62	0.69	0.82
CII-SCC-3.1	2283	2355	1829	1930	1471	1509	1828	1.03	0.80	0.85	0.64	0.66	0.80
CII-SCC-6.3	2111	2141	1700	1746	1412	1478	1828	1.01	0.81	0.83	0.67	0.70	0.87
CII-NC-3.1	2468	2423	2019	2261	1486	1475	1788	0.98	0.82	0.92	0.60	0.60	0.72
CII-NC-6.3	2253	2151	1690	1749	1424	1446	1788	0.95	0.75	0.78	0.63	0.64	0.79
Mean Error % CI SCC								0.03	0.07	0.03	0.36	0.29	0.18
Mean Error % CI NC								0.06	0.13	0.07	0.38	0.32	0.22
Mean Error % CII SCC								0.02	0.20	0.16	0.34	0.32	0.17
Mean Error % CII NC								0.03	0.22	0.15	0.38	0.38	0.24

6.6.4 Steps for using the Proposed Peak Load Model

The same steps can be used for predicting the peak load of columns with CI or CII configurations. The following steps can be followed to determine the peak load of SCC or NC CFST:

1. Select the appropriate stress factors for the concrete from Table 5.4.

2. Calculate the lateral pressure of the tube confined concrete with Eq, 6.12 using the α value selected.

3. Use the answer of Eq. 6.12 to calculate the confined concrete strength using Eq. 6.11.

4. If there is no hoop confinement in the columns go to step 7 or 6. Otherwise, calculate the lateral pressure in the hoop/spiral confined concrete with Eq. 6.16.

5. Use the answer from Step 4 to calculate the confined concrete strength increase by the hoop/spiral confined concrete using Eq. 6.15.

6. To calculate the peak load, substitute the confined concrete strengths (Eq. 6.11 and 6.15) in Eq. 6.20 and if axial reinforcement is present in the confined concrete include it in the calculation as indicated in Eq. 6.20.

7.0   Conclusions and Recommendations

7.1   Summary

The first phase of the investigations in this thesis studied the performance of four different novel viscosity modifying admixtures (VMA) compared to a commercial VMA. The influence of various dosages and types of VMA in addition to the dosages of SP on viscosity and yield stress of cement pastes/mortars made with a W/C of 0.45 was studied. The second investigation was carried out to develop two SCC mixtures with VMA and one NC mix, with different aggregate size and content for casting structural elements.

The second phase of this thesis examined the structural performance of SCC in beam and confined column elements. The first part examined the effect of types of SCC, with varying aggregate content and size on the shear strength of reinforced beam elements through a comparative study of initial shear cracking and ultimate shear strength. The second part of the structural phase examined the behaviour of SCC with different aggregate contents as infill in CFST columns with or without congested reinforcement. This phase also included the study of the performance of existing peak strength models, and the development of a new peak load model for confined columns with SCC and NC infill which took into account the effect of additional hoop confinement and longitudinal reinforcement.

7.2   Conclusions

The apparent viscosity of the cement paste/mortar was increased with the increase of dosages of VMA from 0.025% to 0.075%. The viscosity of paste/mortar with new A, B, C and D VMAs was found to be higher than that of commercial "COM" VMA. Viscosity of the paste also increased with the increase of elapsed time between mixing of paste and testing. Based on viscosity data, all new VMAs were found to be more efficient than the commercial "COM" VMA and would provide better rheological properties. Based on the current investigation, cement paste/mortar with new VMA dosage ranging between 0.025 and 0.075% would provide better rheological properties. The washout resistance of

VMA was enhanced with the increase in VMA dosage and reduction in SP content. With the proper VMA-SP combination a flowable washout resistant mixture can be secured. The washout resistance of Type A, B, C, or D VMA was higher than the commercial VMA COM at similar VMA-SP dosages. The tests on paste/mortar showed that the new VMAs could be used in the development of a SCC with satisfactory properties.

The fresh property tests on SCC with 12 and 19-mm aggregate found a slight difference in the flowability. The 19-mm SCC required more time to flow in place and consolidate as indicated by visual observation which was verified by the slower V-funnel flow time and a lower L-box index value. However, the properties of the 19-mm concrete were satisfactory. The new Type A-VMA with the dosage of 0.05% produced satisfactory SCC with high fluidity (for 12 and 19-mm aggregate) in combination with an SP dosage of 0.75 and 1.05%, respectively. A total of four 12-mm and two 19-mm SCC batches were mixed and they all displayed good consistency and stability in the fresh state.

The shear resistance of the beams with various concrete types and aggregate contents did not have any adverse effect on the shear cracking patterns, and resistance. However, the S19 concrete (19-mm SCC) did develop higher resistance to shear failure for every beam configuration than the S12 and N12 beams (3 to 16%). This was expected and was believed to be due to the influence of a more resistant shear path developed by the presence of the larger coarse aggregate particles. The S19 beams also experienced more mid-span deflection at failure with most cases. The S12 beams with h = 150 and 200-mm generated higher resistance to shear failure over the N12 beams. However, the NC beam showed an increased resistance in the 300-mm beam and surpassed the S12 beam by a 10% increase. This is believed to be due to the combined effect of added reinforcement in the 300-mm beam, the inclined shear angle and the presence of more coarse aggregate that enhanced the dowel action and interlocking effect of the aggregate in the cracked concrete. The consistency of results with both SCC mixes (S19 and S12) exhibited a more predictable pattern than the normal concrete mix in terms of the beam depth.

The confined columns made with SCC for both series CI and CII displayed more consistency in terms of failure mode and load-displacement response than the NC columns. This was attributed to the homogeneity and proper consolidation of SCC. However, NC columns of both series CI and CII showed higher load capacities over the SCC by 1.1, 4.1, 7.5 and 6.3% for H/D ratios of 4.8, 9.5, 3.1 and 6.3, respectively. The post peak behaviour was usually similar for all columns although, the ductility index indicated that NC columns were slightly more ductile. As indicated in the beams, the NC concrete may have more resistance to shearing in confinement due to the interlocking of the aggregates in the softened concrete. Higher aggregate content in NC was believed to be the reason for the higher capacity of NC columns. There was a great advantage to the ease of placement and the time required to pour SCC in the columns. Productivity, based on the casting time, was increased by 2.5 times with SCC.

By studying the stress development in the confining tubes and with the use of existing confinement theories, it was possible to develop a model for predicting the peak load capacity of the confined column within 6% maximum error. The model was developed based on the use of stress factors extracted from the experimental data and based on existing confinement models by O'Shea and Bridge (2000) and Hossain (1999 and 2003). By introducing the effect of hoop confinement, it was possible to develop a model to predict the capacity of both CI and CII type columns with average errors of 2.5 and 4.5% for SCC and NC, respectively.

7.3   Recommendations

The four new VMAs presented in this thesis should be tested in SCC mixes with various dosage of VMA and SP combinations. This should include extensive testing of the flow properties in congested configurations and study of the flowability of SCC with the new VMAs.

Further analysis of the beams should be carried out to study the internal forces at the diagonal shear cracks, and to use existing shear crack theories to describe the diagonal

shear failure in the beams. The effect of concrete type and aggregate content in concrete mixture on shear resistance should be further analyzed in order to develop new shear strength model for beams without web reinforcement.

The study of confined columns did not examine in detail the elasto-plastic deformation of the confined columns. Therefore, the following recommendations are made for future studies:

- Use of the data collected from this investigation to develop models to predict the load-deformation response (stress-strain of the confined columns in the pre-peak and post-peak regions for both CI and CII type columns).
- The effect of the concrete type in confined columns is not fully understood in this investigation and therefore, experiments should be conducted with thin walled confined steel tubes of various sizes to investigate the role of SCC on the performance of confined concrete.

SCC can increase the productivity of concrete construction projects. Where confined columns are employed, such as in bridge pier construction, the use of SCC as the concrete infill material should be studied for overall project efficiency in terms of ease of placement, height of pouring lifts, time of placement and cost effectiveness of the project.

REFERENCES

ACI committee 318. 1995. *Building Code Requirements for Structural Concrete (ACI 318-95 and Commentary (318-95)*. American Concrete Institute, Farmington Hills, Michigan, 369 pp.

Aïtcin, P.C., and Mehta, P.K. 1990. *Effect of Coarse Aggregate Characteristics on Mechanical Properties of High-Strength Concrete*. ACI Material Journal, Vol. 87, No. 2, pp. 103-107.

Aïtcin, P-C, 1998. *High Performance Concrete*. London ; New York : E. & F.N. Spon, 591 p.

Andersson, R, and Sjökvist, L.G.. 1999. *SCC for Production of Elements*, Report TVBM-5039, Division of Building Materials, Lund Institute of Technology, Lund, pp. 114.

Bingham, E.C. and Reiner, M. 1933. The Rheological Properties of Cement and Cement-Mortar-Stone, *Physics,* No. 4, pp. 88-96.

Bouzoubaâ, N. and Lachemi, M. 1999. *Self-Compacting Concrete Incorporating High-Volumes of Class Fm Fly Ash: Preliminary results*. Cement and Concrete Research, Vol. 31, No. 3, pp. 413-420.

Byfors, J and Grauers, M. 1997. *SCC: A Large Step Towards a More Industrialized Type of Construction*. Betong 4, pp.8-10.

Campion, M.J. and Jost P. 2000. *Self-Compacting Concrete*. Concrete International: Design and Construction, Vol. 22, No. 4, pp. 31-34.

CSA (Canadian Standards Association). 1995. *Design of Concrete Structures, CSA Standard A23.2-94*. Toronto, Ontario, Canada, 220 pp.

CSA A23.3 Technical Committee. 1994. *Design of Concrete Structures (A23.3-94)*. Canadian Standards Association, Rexdale, Ontario, 199 pp.

Dieden, C. 1999. *SCC for House Construction*. Report TVBM-7040, Division of Building Materials, Lund Institute of Technology, Lund, pp. 107.

Ehara. K. 1998. Personal information, Shimizu, Tokyo, 1998.

Eurocode 4. 1992. *Design of Composite Steel and Concrete Structures, Part 1.1: general rules and rules for buildings*. ENV 1994-1-1.

Fujiwara, H. 1992. *Fundamental Study of Self-Compacting Property of High-Fluidity Concrete.* Proceedings of the Japan Concrete Institute, Vol. 14, No. 1, pp. 27-32.

Grauers, M. 1998. *Industrialized concrete cast on site* Bygg Teknik 7, pp.12-15.

Hayakawa, M., Matsuoka, Y. and Shindoh, T. 1993. *Development and Application of Super Workable Concrete.* Proceedings of an International RILEM Workshop on special concrete: Workability and Mixing, Scotland, March, pp. 183-190.

Hossain, K.M.A. 1999 *Modelling of Axial Behaviour of Thin Walled Composite Columns.* Proce. of 24th International Conference on Our world in Concrete & Structures, Vol. XVII, Singapore, 24 August, pp. 179-186.

Hossain, K.M.A. 2003. *Behaviour of Thin walled composite Columns under Axial loading.* Composite – Part B: Engineering- An International Journal, 34(2003), pp. 715-725.

Johansson, M., and Gylltoft, K. 2002. *Mechanical Behavior of Circular Steel- Concrete Composite Stub Columns.* Journal of Structural Engineering, ASCE, Vol. 128, No. 8, pp. 1073-1081.

Kato B. 1996. *Column curves of Steel-Concrete Composite Members.* Journal of Construction Steel Research. Vol. 39, No. 2, pp. 121-135.

Khayat, K.H., and Aïtcin, P.C. 1999. *Use of Self-Consolidating Concrete in Canada – Present Situation and Perspectives.* Université de Sherbrooke, Quebec, Canada.

Khayat, K.H., and Guizani, Z. 1997. *Use of Viscosity Modifying Admixtures to Enhance Stability of Fluid Concrete.* ACI Materials *Journal,* Vol. 94, No. 3, pp. 332-340.

Khayat, K.H., Paultre, P., and Tremblay, S. 2001. *Structural performance and in-place properties of self-consolidating concrete used for casting highly reinforced columns.* ACI Materials Journal, Vol. 98, No. 5, pp. 371-378.

Khayat, K.H. and Yahia A. 1997. *Effect of welan gum-high range water reducer combinations on rheology of cement grout.* ACI Materials Journal, Sept-Oct., pp. 365-372.

Klevbo, G. 1999. *Optimization of SCC – Personal information, Cement and Concrete Research Institute.* CBI, Stockholm and Trelleborg.

Kosmatka, S.H., Kerkhoff, B, Panarese, W.C., MacLeod, N.F. and McGrath, R.J. 2002. *Design and Control of Concrete Mixtures.* CPCA. 7th Canadian Edition.

120

Lachemi M., K.M.A Hossain, V. Lambros and N. Bouzoubaa. 2003a. *Development of Cost-Effective Self-Consolidating Concrete incorporating fly ash, blast furnace slag or viscosity modifying admixtures.* ACI Materials Journal, Vol. 100, No. 5, pp. 419-425.

Lachemi M., K.M.A Hossain, V. Lambros, P.-C. Nkinamubanzi and N. Bouzoubaa. 2003b. *Self-Compacting Concrete incorporating new viscosity modifying agents.* Cement and Concrete Research Journal, (in press)

Lacombe, P., Beaupré, D. and Pouliot, N. 1999. *Rheology and Bonding Characteristics of Self-Levelling Concrete as a Repair Material.* Materials and Structures, Vol. 32, No. 222, pp. 593-600.

Lambros V., Androus, A., Hossain, K.M.A, Sennah, K., Raahemifar, K. and Lachemi, M. 2003. *Predicting the Modulus of Elasticity of High Performance Concrete Using Artificial Neural Networks.* Proceedings of the 31st Annual CSCE Conference, June 4-June 7, 2003, Moncton N.B.

Légeron, F. and Paultre, P. 2003. *Uniaxial Confinement Model for Normal and High Strength Concrete Columns.* ASCE Journal of Structural Engineering, Vol. 129, No. 2, pp. 241-252.

Li, V.C. 1995. *New Construction Materials Proliferate in Japan.* Civil Engineering, Vol. 65, No. 8, pp. 38-41.

Mander, J.B., Priestly, M.J.N. and Park, R. 1988. *Theoretical Stress-Strain Model for Confined Concrete.* ASCE Journal of Structural Engineering. Vol. 114, No. 8, pp 1804-1826.

Mantegazza, G. and Alberti, E. 1994. *Slump Loss and Rheology of Superplasticizer Mortar and Concrete with Different Polysaccharide Syrups.* Fourth CANMET/ACI international Conference on Superplasticizer and other chemical admixtures in concrete, Ed. V.M. Malhotra, pp. 105-119.

McAteer, M.P. 2002. *Axially Loaded Circular High Strength Concrete Column Confined by Steel Tube: Mechanics, Modeling, and Slenderness Effects.* MASC Thesis, University of Toronto, Toronto, Ontario, 121 p.

Mitschka P. 1982. *Simple conversion of Brookfield R.V.T. readings into viscosity functions, Rheology Acta.* 21, 207-209.

Nagataki, S. and Fujiwara, H. 1995. *Self-Compacting Property of Highly Flowable Concrete.* ACI SP 154, Las Vegas, pp. 301-314.

O'Shea, M.D., and Bridge, R.Q. 2000. *Design of Circular Thin Walled Concrete Filled Steel Tubes*. ASCE Journal of Structural Engineering, Vol. 126, No. 11, 1295-1303.

Okamura, H. 1996. *Self-Compacting High-Performance Concrete.* Concrete International, Vol. 19, No. 7, pp. 50-54.

Persson, B. 2001. *A Comparison Between Mechanical Properties of Self-Compacting Concrete and the Corresponding Properties of Normal Concrete.* Cement and concrete Research, No. 31, pp. 193-198.

Petersson, O. 1999. *SCC Final Report of Task 2: Workability.* Swedish Cement and Concrete Research Institute, RT2_v2.doc, (http://scc.ce.luth.se/).

Rabeiz, K.S. 1999. *Shear Strength Prediction for Concrete Members.* ASCE Journal of Structural Engineering, Vol. 125, No. 3, pp. 301-308.

Richart, F.E., Brandtzaeg, A. and Brown, R.L. 1928. *A Study of the Failure of Concrete Under Combined Compressive Stresses.* Bulleting #185, University of Illinois, Engineering Experimental station, Urbana, Ill. 104 p.

Rols, S., Ambroise, J. and Péra, J. 1999. *Effects of different viscosity agents on the properties of self-levelling concrete.* Cement and Concrete Research, Vol. 29, No. 2, pp. 261-266.

Sakata, K., Ayano, T. and Ogawa, A. 1995. *Mixture Proportions for Highly-Flowable Concrete Incorporating limestone Powder.* Proceedings of the 5th International Conference: Fly ash, silica fume, slag and natural pozzolans in concrete, ACI, Vol. 1, pp. 249-268.

Sakata, K., Maruyama, K. and Minami, M. 1996. *Basic Properties and Effects of Welan Gum on Self-Consolidating Concrete.* Production methods and workability of concrete: proceedings of the international RILEM conference, Ed. P.J.M. Bartos, pp. 237-253.

Sari, M., Prat, E. and Labastire, J.F. 1999. *High Strength Self-Compacting Concrete, Original Solutions Associating Organic and Inorganic Admixture.* Cement and Concrete Research, Vol. 29, No. 6, pp. 813-818.

Shanmugam, N.E. and Lakshi, B. 2001. *State of the Art Report on Steel-Concrete Composite Columns.* Journal of Construction Steel Research, Vol. 57, pp. 1041-1080.

Skarendahl, A. 1999. *Self-Compacting Concrete for Improved Productivity, Working Environment and Performance.* Swedish Cement and Concrete Research Institute, Stockholm. Paper presented at IREX- meeting: "Réunion d'information sur les bétons autoplacants". Paris, France, February 23, 1999.

Sonebi, M., and Bartos, P.J.M. 2001a. *Flexural Response and Performance of Reinforced Beams Cast with Self-Compacting Concrete.* Proceedings of the Second International Symposium on Self-Compacting Concrete. Tokyo, Japan, October 23-25, 2001.

Sonebi, M., and Bartos, P.J.M. 2001b. *Performance of Reinforced Columns with Self-Compacting Concrete.* Fifth CANMET/ACI international conference, recent advances in concrete technology. Ed. V.M. Malhorta. SP 200-25, pp. 415-431.

Sonebi, M., Bartos, P.J.M., Zhu, W., Gibbs, J., and Tamimi, A., 2000. *Task 4 – Properties of Hardened Concrete, Final Report.* Advanced Concrete Masonry Centre. University of Paisley, Scotland, United Kingdom. (*http://scc.ce.luth.se/*)

Sun, Y.P. and Sakino, K. 1998. *Modeling for the Axial Behavior of High strength CFT Columns.* Proceeding 23rd Conference on our World in Concrete and Structures, 25-26 August, pp. 120-126, Singapore, 1998.

Tumidajski, P.J., and Chan, G.W. 1996. *Durability of High Performance Concrete in Magnesium Brine.* Cement and Concrete Research. Vol. 26, No, 4, pp. 557-565

Yahia, A. 1997. *Rhéologie et performance des coulis de ciment destinés à la consolidation structurale d'ouvrages submergés.* PhD Thesis, Université de Sherbrooke, Canada, 1997, in French.

Yasumoto, A., Edamatsu, Y., Mizukoshi, M., and Nagaoka, S. 1998. *A Study on the Shrinkage Crack Resistance of Self-Compacting Concrete.* Fourth CANMET/ACI international conference, advances in concrete technology. Ed. V.M. Malhorta. pp. 651-669.

Zararis, P.D and Papadakis G.C. 2001. *Diagonal Shear Failure and Size Effect in RC Beams without Web Reinforcement.* ASCE Journal of Structural Engineering, Vol. 127, No. 7, pp.733-741.

Zhu, W., Gibbs, J.C., and Bartos, J.M. 2001. *Uniformity of In-Situ Properties of Self-Compacting Concrete in Full-Scale Structural Elements.* Cement and concrete Composites, No. 23, pp. 57-64.

Appendix A: Aggregates

12 mm Aggregate

Seive (mm)	Fractional Mass Retained (kg)	Fractional % Retained	Cummulative % Retained	Cummulative % Passing
40 (1-1/2")	0	0%	0%	100%
28 (1")	0	0%	0%	100%
20 (3/4")	0.000	0%	0%	100%
14 (1/2")	0.406	6.2%	6.2%	93.8%
10 (3/8")	3.423	52.5%	58.7%	41.3%
5 (No. 4)	2.207	33.8%	92.5%	7.5%
Pan	0.486	7.5%	100%	0%

Grain Size Distribution Curve
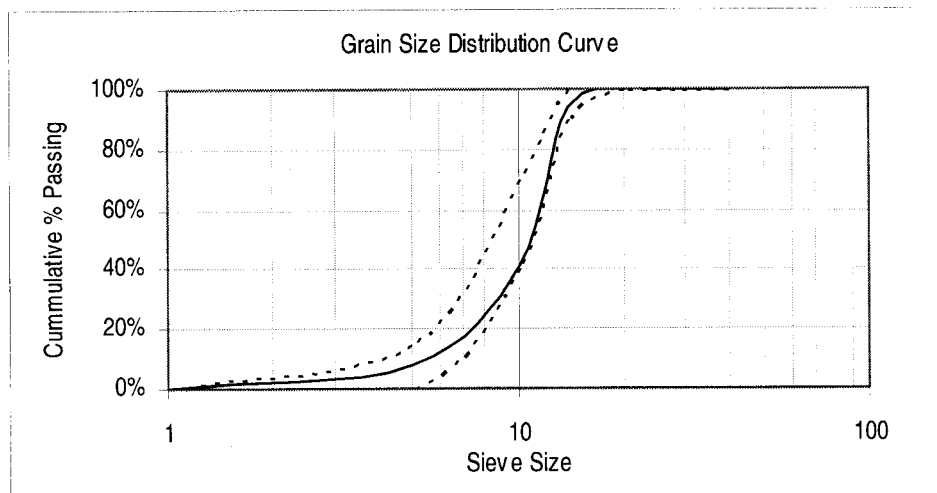
Nominal Maximum Size:	12 mm	
Original Dry Mass:	6.523 kg	
Sum of Fractional Mass Retained:	6.522 kg	
% Loss:	0.013%	
Dry Rodded Density:	1700	kg/m^3
Bulk Relative Density (dry):	2592	kg/m^4
Bulk Relative Density (SSD):	2641	kg/m^5
Absorption:	1.89%	

124

19 mm Aggregate

Seive (mm)	Fractional Mass Retained (kg)	Fractional % Retained	Cummulative % Retained	Cummulative % Passing
40 (1-1/2")	0	0%	0%	100%
28 (1")	0	0%	0%	100%
20 (3/4")	0.176	1.8%	1.8%	98.2%
14 (1/2")	3.966	41.1%	42.9%	57.1%
10 (3/8")	2.780	28.8%	71.7%	28.3%
5 (No. 4)	2.615	27.1%	98.7%	1.3%
Pan	0.122	1.3%	100%	0%

Grain Size Distribution Curve
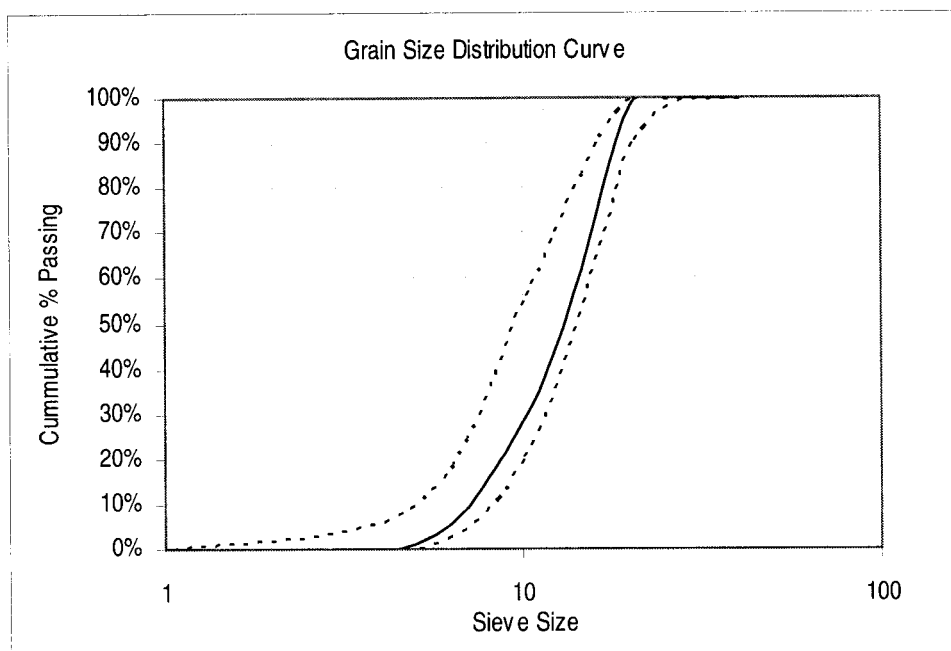
Nominal Maximum Size:	19 mm
Original Dry Mass:	9.668 kg
Sum of Fractional Mass Retained:	9.663 kg
% Loss:	0.05%
Dry Rodded Density:	1734 kg/m^3
Bulk Relative Density (dry):	2692 kg/m^4
Bulk Relative Density (SSD):	2707 kg/m^5
Absorption:	0.56%

Sand

Seive (mm)	Fractional Mass Retained (kg)	Fractional % Retained	Cummulative % Retained	Cummulative % Passing
10 (3/8")	0	0%	0%	100%
5 (No. 4)	0.024	2.9%	2.9%	97.1%
2.5 (No. 8)	0.105	12.8%	15.7%	84.3%
1.25 (No. 16)	0.091	11.1%	26.8%	73.2%
0.63 (No. 30)	0.157	19.1%	45.9%	54.1%
0.315 (No. 50)	0.239	29.1%	74.9%	25.1%
0.16 (No. 100)	0.153	18.6%	93.6%	6.4%
Pan	0.053	6.4%	100%	0%

Grain Size Distribution Curve
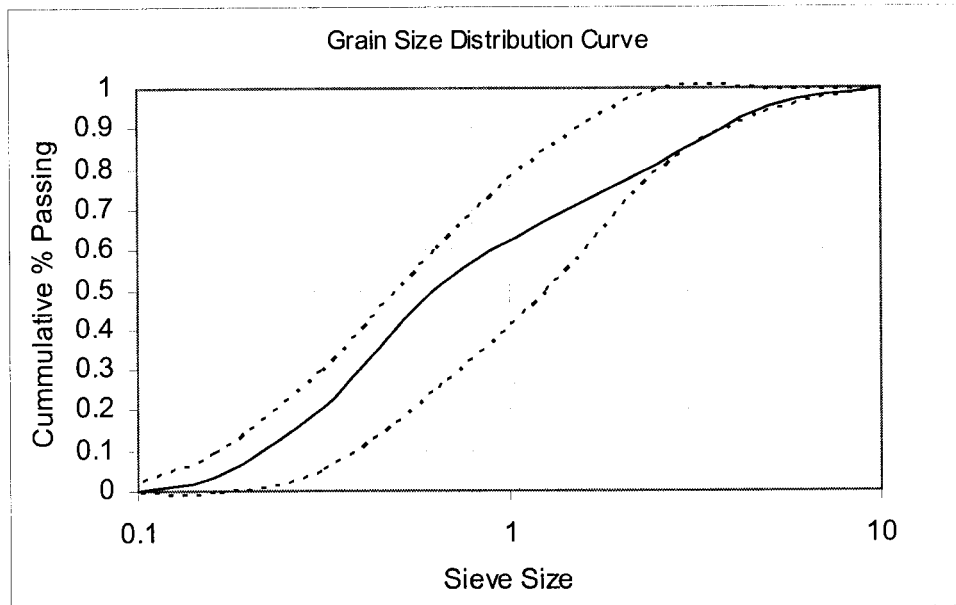
Fineness Modulus	2.59	
Original Dry Mass:	825 g	
Sum of Fractional Mass Retained:	822 g	
% Loss:	0.32%	
Bulk Relative Density (dry):	2694	kg/m^4
Bulk Relative Density (SSD):	2714	kg/m^5
Absorption:	0.75%	
Absorption:	-100.00%	

126

Appendix B: Concrete Mixes

Table B1.1 – VMA SCC Trial Mixes

Mix ID.	Agg	W/B	Cement kg/m³	Water kg/m³	Coarse Aggregate kg/m³ (SSD)	Fine Aggregate kg/m³ (SSD)	SP L/m³	SP %	VMA %	Slump mm	Density kg/m3
VMA1	12	0.45	400	180	750	1046	4.99	0.61	0.050%	630	2337
VMA2	12	0.45	400	180	898	899	4.00	0.49	0.050%	610	2399
VMA3	12	0.45	400	180	1098	696	1.36	0.17	0.050%	480	2388
VMA4	12	0.40	370	148	800	1109	6.75	0.90	0.050%	560	2352
VMA5	12	0.40	370	148	955	954	5.16	0.69	0.050%	615	2439
VMA6	12	0.40	370	148	800	1108	9.47	1.26	0.075%	600	2353
VMA7	12	0.40	370	148	955	954	10.79	1.44	0.075%	475	2245
VMA8	12	0.45	430	194	750	1000	4.14	0.47	0.050%	610	2398
VMA9	12	0.45	430	194	880	880	3.26	0.37	0.050%	615	2448
VMA10	12	0.45	450	203	715	1000	2.87	0.31	0.050%	605	2432
VMA11	12	0.45	450	203	855	855	3.72	0.41	0.050%	660	2478
VMA12	12	0.40	450	180	715	1050	6.36	0.70	0.050%	660	2349
VMA13	12	0.40	450	180	890	890	4.99	0.55	0.050%	660	2387
VMA14	19	0.45	400	180	910	910	3.77	0.46	0.050%	600	2466
VMA14b	19	0.45	400	180	910	910	4.31	0.53	0.050%	660	2502
VMA15	19	0.40	400	160	935	935	5.40	0.66	0.050%	645	2509

Table B1.2 – Slag SCC Trial Mixes

Mix ID.	Agg	W/B	Cement kg/m³	Slag kg/m³	Water kg/m³	Coarse Aggregate kg/m³ (SSD)	Fine Aggregate kg/m³ (SSD)	SP L/m³	SP %	Slump mm	Density kg/m³
SL1	12	0.45	200	200	180	750	1038	3.50	0.86	400	2460
SL2	12	0.45	200	200	180	893	893	3.20	0.79	500	2462
SL3	12	0.45	200	200	180	1100	685	1.74	0.43	415	2461
SL4	12	0.40	185	185	148	800	1102	8.63	2.30	575	2357
SL5	12	0.40	185	185	148	949	948	7.66	2.04	575	2395
SL6	12	0.40	111	259	148	949	942	11.38	5.05	630	2386
SL7	12	0.45	225	225	203	700	1000	3.81	0.83	740	2457
SL7b	12	0.45	225	225	203	700	1000	2.98	0.65	610	2464
SL8	12	0.45	225	225	203	850	850	3.02	0.66	660	2473
SL9	12	0.40	225	225	180	715	1050	9.91	2.17	700	2482
SL10	12	0.40	225	225	180	875	875	3.26	0.71	700	2514
SL11	19	0.40	200	200	160	925	925	9.85	2.43	700	2560
SL11b	19	0.40	200	200	160	925	925	3.28	0.81	580	2530

Table B1.3 – NC Trial Mixes

Mix ID.	Agg	W/B	Cement kg/m³	Water kg/m³	Coarse Aggregate kg/m³ (SSD)	Fine Aggregate kg/m³ (SSD)	Slump mm	Density kg/m³
NC1	12	0.38	481	183	1017	711	60	2484
NC2	12	0.42	481	202	951	739	150	2463
NC3	12	0.42	481	202	1017	671	105	2453
NC4	12	0.42	481	202	1017	724	170	2472

Appendix C: Shear and Flexural Cracking of Beams

Table C1.1 – h = 150

Beam	Crack No.	Crack Type	Load kN	Mid-span Defl mm
S12-150a	1	Flex	9.0	0.49
	2	Flex	10.8	0.64
	3	Flex	14.0	0.88
	5	Shear	15.7	1.05
	6	Shear	16.9	1.15
	7	Shear	17.9	1.31
S12-150b	1	Flex	8.8	0.61
	2	Flex	9.4	0.67
	3	Flex	10.5	0.71
	4	Flex	12.7	0.96
	6	Shear	16.5	1.32
	7	Shear	17.4	1.45
	8	Shear	17.9	1.55
	9	Shear	19.2	1.83
N12-150a	1	Flex	8.8	0.52
	2	Flex	10.8	0.68
	4	Shear	15.7	1.18
	4	Shear	15.7	1.18
	5	Shear	17.7	1.35
	5a	Shear	19.6	1.51
	6	Shear	20.6	1.58
	6	Shear	21.6	1.73
	8	Shear	22.6	1.81
	9	Shear	23.3	2.03
N12-150b	1	Flex	7.8	0.45
	2	Flex	8.8	0.54
	3	Flex	8.8	0.54
	4	Flex	9.1	0.59
	5	Shear	11.3	0.78
	7	Shear	12.3	0.85
	8	Shear	14.7	1.09
	9	Shear	15.7	1.14
	10	Shear	18.1	1.36
	11	Shear	18.6	1.43
	12	Shear	20.1	1.64
S19-150a	1	Flex	9.0	0.47
	2	Flex	11.0	0.63
	4	Flex	13.7	0.85
	5	Flex	15.7	1.00
	3	Shear	12.8	0.77
	6	Shear	16.7	1.07
	7	Shear	19.6	1.32
	9	Shear	21.5	1.50
	10	Shear	23.5	1.70
	11	Shear	24.5	2.05
	14	Shear	23.6	1.70
	15	Shear	24.5	2.05
	16	Shear	28.2	2.45
S19-150b	1	Flex	8.8	0.55
	2	Flex	10.8	0.71
	3	Flex	12.8	0.85
	4	Flex	14.7	1.01
	5	Shear	17.7	1.26
	6	Shear	18.6	1.34
	7	Shear	19.6	1.44
	8	Shear	19.6	1.56

Table C1.2 – h = 200

Beam	Crack No.	Crack Type	Load kN	Mid-span Defl mm
S12-200a	1	Flex	22.1	1.01
	5	Flex	41.2	2.24
	1s	Shear	32.7	1.72
	2	Shear	36.8	1.90
	3	Shear	38.3	2.03
	4	Shear	40.2	2.17
	6	Shear	42.2	2.31
	7	Shear	44.1	2.45
	8	Shear	45.6	2.66
	9	Shear	47.6	2.94
	10	Shear	48.6	3.08
S12-200b	1	Flex	19.6	0.68
	2	Flex	25.0	0.93
	3	Shear	27.5	1.06
	4	Shear	28.9	1.10
	8	Shear	41.5	1.96
S19-200a	1	Flex	14.7	0.58
	2	Flex	16.7	0.66
	3	Flex	17.7	0.73
	4	Flex	18.6	0.76
	5	Flex	20.6	0.86
	6	Shear	24.5	1.09
	7	Shear	25.5	1.16
	8	Shear	30.4	1.49
	9	Shear	30.9	1.54
	10	Shear	31.4	1.56
	11	Shear	32.4	1.63
	12	Shear	32.9	1.66
	13	Shear	33.4	1.68
	14	Shear	34.3	1.74
	15	Shear	35.8	1.83
	16	Shear	36.8	1.89
	17	Shear	39.2	2.05
	18	Shear	40.7	2.14
	19	Shear	42.2	2.23
S19-200b	1	Flex	17.7	0.67
	2	Flex	18.6	0.78
	3	Flex	18.6	0.78
	4	Flex	21.6	0.89
	5	Flex	21.6	0.89
	9	Flex	29.4	1.46
	6	Shear	22.6	1.00
	7	Shear	25.5	1.10
	8	Shear	27.5	1.24
	9	Shear	29.4	1.46
	10	Shear	31.4	1.51
	11	Shear	32.4	1.70
	12	Shear	32.4	1.70
	13	Shear	33.4	1.76
	14	Shear	35.3	1.82
	15	Shear	36.3	2.02
	16	Shear	39.2	2.27
N12-200a	1	Flex	19.6	0.86
	2	Flex	20.6	0.93
	3	Flex	21.6	0.93
	4	Flex	23.5	1.03
	10	Shear	26.5	1.21
	11	Shear	28.4	1.31
	12	Shear	30.8	1.39
	13	Shear	33.4	1.74
N12-150b	1	Flex	13.7	0.40
	2	Flex	21.6	0.79
	4	Flex	22.6	0.85
	6	Flex	26.5	1.03
	8	Flex	27.5	1.07
	5	Shear	25.5	0.96
	9	Shear	27.0	1.21
	10	Shear	27.5	1.26
	11	Shear	27.5	1.41
	14	Shear	29.4	1.56
	16	Shear	31.4	1.72

Table C1.3 – h = 300

| Beam	Crack No.	Crack Type	Load kN	Mid-span Defl mm
S12-300a	1	Flex	44	1.13
	2	Flex	62	1.59
	3	Shear	64	1.63
	4	Shear	66	1.68
S12-300b	1	Flex	44	1.11
	2	Flex	47	1.15
	3	Shear	64	1.66
	4	Shear	66	1.76
S19-300a	1	Flex	38	0.83
	2	Shear	48	1.10
	3	Shear	54	1.29
	4	Shear	55	1.31
	5	Shear	62	1.49
	6	Shear	66	1.61
	7	Shear	68	1.66
	8	Shear	76	1.92
S19-300b	1	Flex	35	0.81
	2	Flex	41	0.95
	3	Shear	48	1.11
	4	Shear	51	1.18
	5	Shear	53	1.22
	6	Shear	57	1.33
	7	Shear	61	1.45
	8	Shear	61	1.45
	9	Shear	62	1.47
	10	Shear	67	1.60
	11	Shear	69	1.65
	12	Shear	73	1.77
	13	Shear	75	1.83
	14	Shear	78	1.94
	15	Shear	79	1.97
	16	Shear	81	2.05
	17	Shear	85	2.15
	18	Shear	86	2.18
	19	Shear	87	2.21
	20	Shear	89	2.26
	21	Shear	90	2.29
	22	Shear	91	2.31
N12-300a	1	Flex	25	0.51
	2	Flex	30	0.61
	3	Flex	36	0.74
	4	Flex	39	0.82
	5	Flex	44	0.93
	7	Flex	56	1.15
	8	Shear	61	1.38
	9	Shear	71	1.72
	10	Shear	75	1.93
N12-150b	1	Flex	26	0.54
	2	Flex	38	0.79
	3	Flex	45	0.96
	4	Flex	46	0.99
	5	Flex	47	0.99
	7	Flex	48	1.03
	8	Shear	49	1.10
	9	Shear	53	1.19
	10	Shear	55	1.23
	11	Shear	56	1.27
	12	Shear	57	1.32
	13	Shear	59	1.42
	14	Shear	61	1.45
	15	Shear	62	1.51
	16	Shear	64	1.56
	17	Shear	66	1.58
	18	Shear	67	1.68
	19	Shear	74	1.89
	20	Shear	75	1.92
	21	Shear	76	1.92
	22	Shear	79	2.06
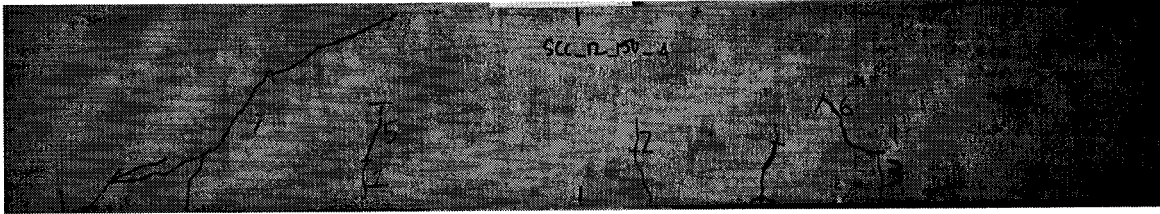
a) S12-150a
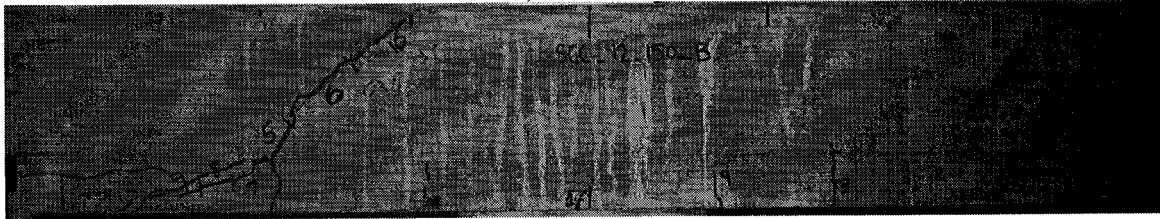
b) S12-150b
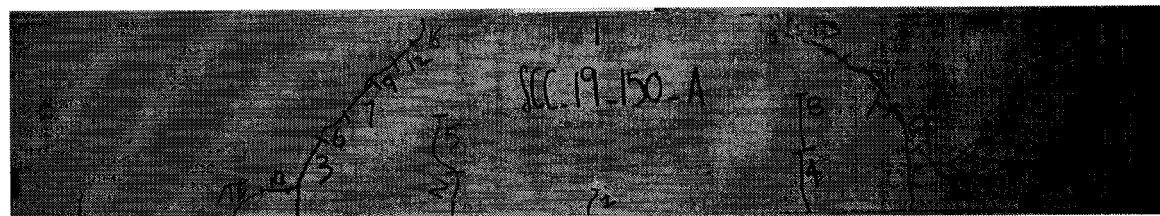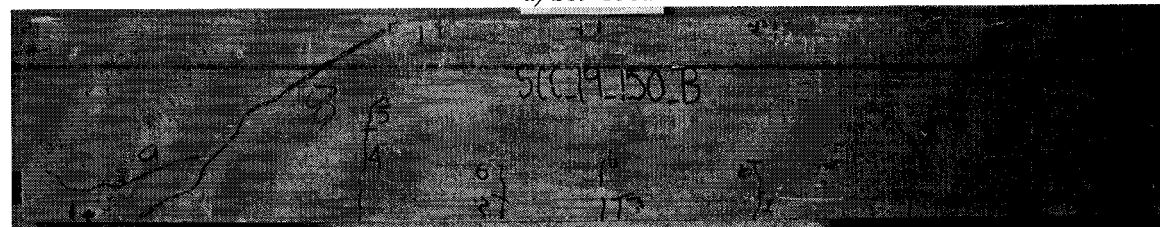*Fig, C1.1 – Crack patterns for Beams S12-150)*
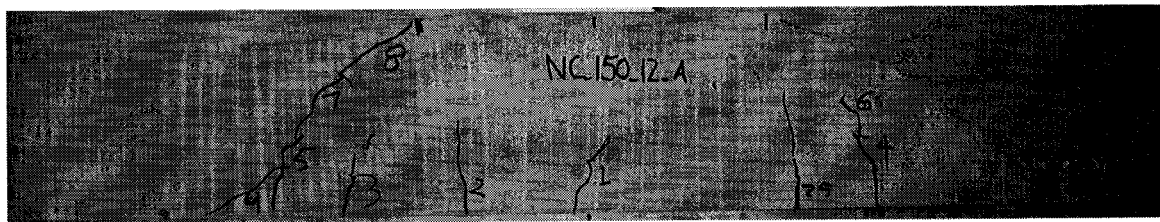
a) N12-150a
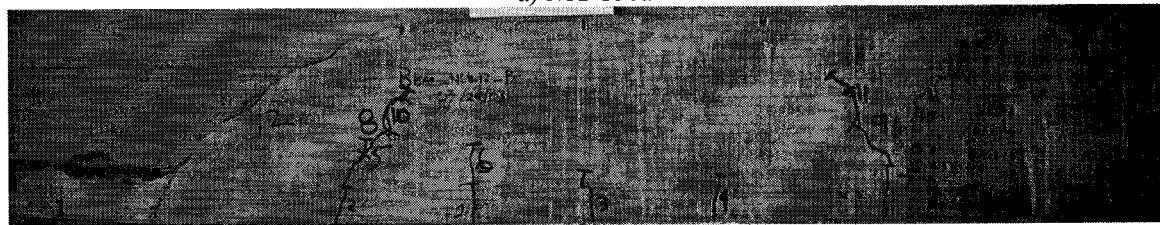
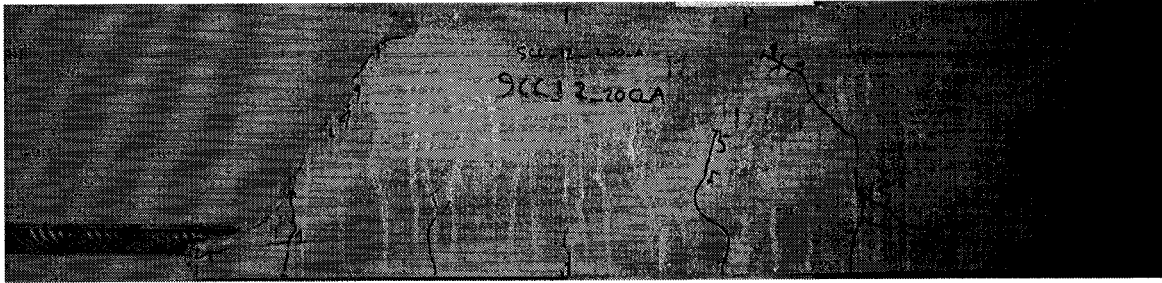*b) N12-150b*
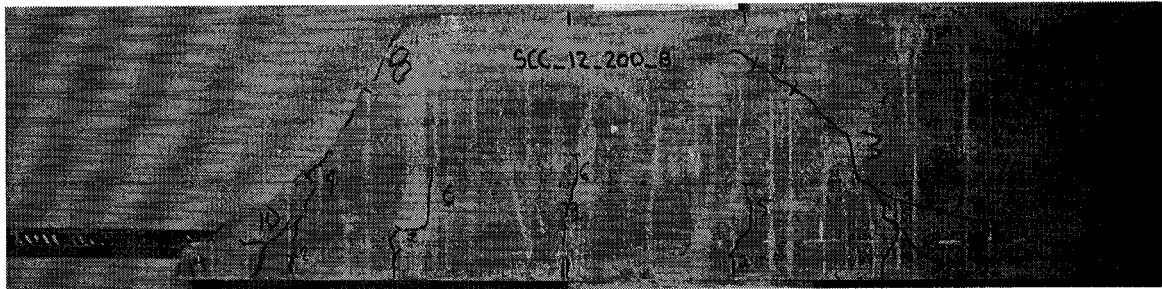*Fig, C1.2 – Crack patterns for Beams N12-150*

a) S19-150a

b) S19-150b
Fig, C1.3 – Crack patterns for Beams S19-150
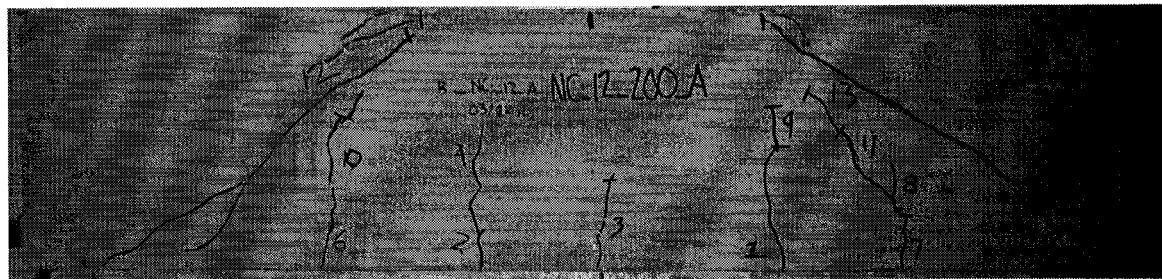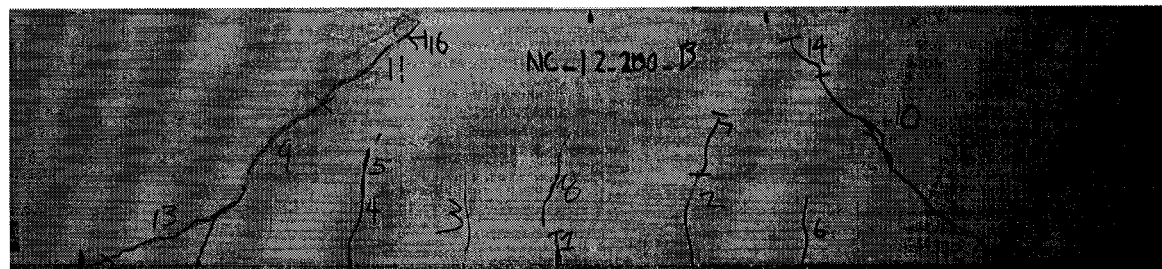
129

a) S12-200a

b) S12-200b

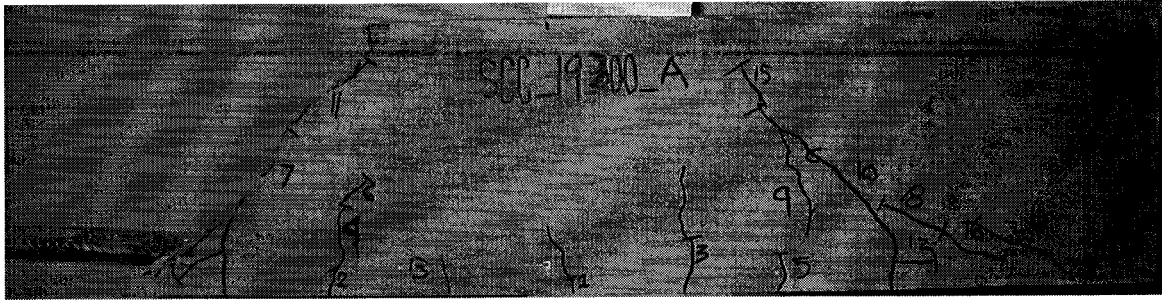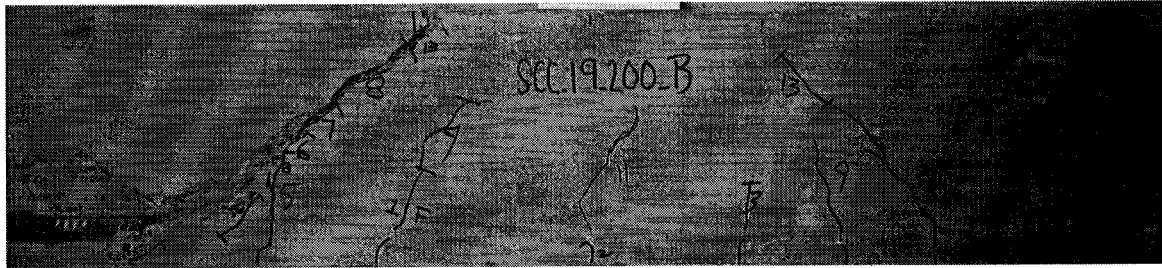*Fig, C1.4 – Crack patterns for Beams S12-200*

a) N12-200a

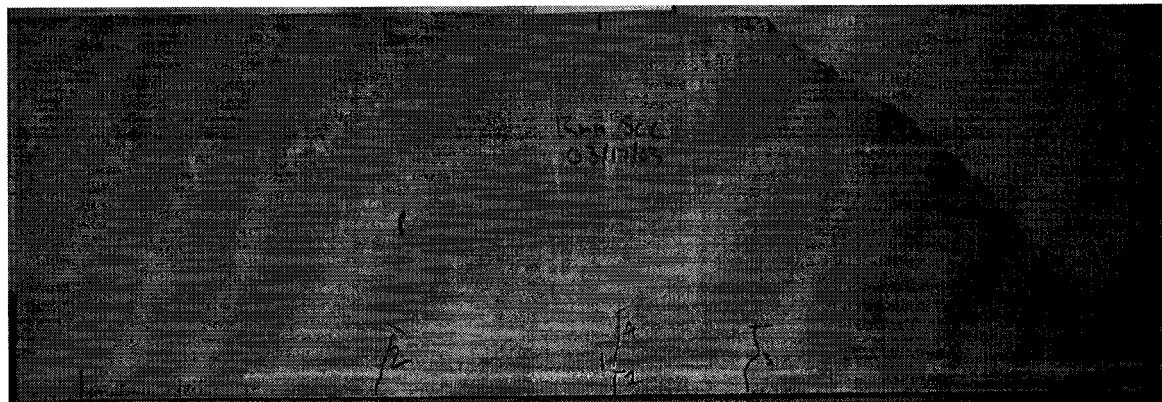*b) N12-200b*

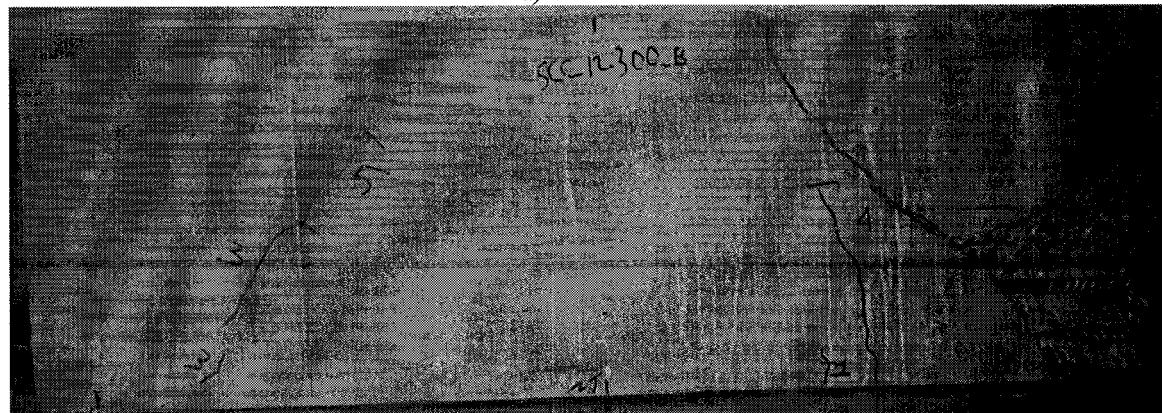*Fig, C1.5 – Crack patterns for Beams N12-200*

a) S19-200a

b) S19-200b

Fig, C1.6 – Crack patterns for Beams S19-200
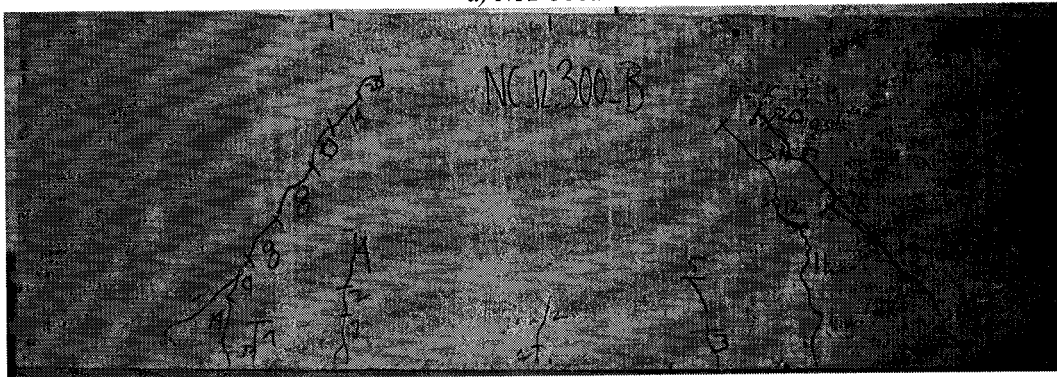

a) S12-300a

b) S12-300b

Fig, C1.7 – Crack patterns for Beams S12-300
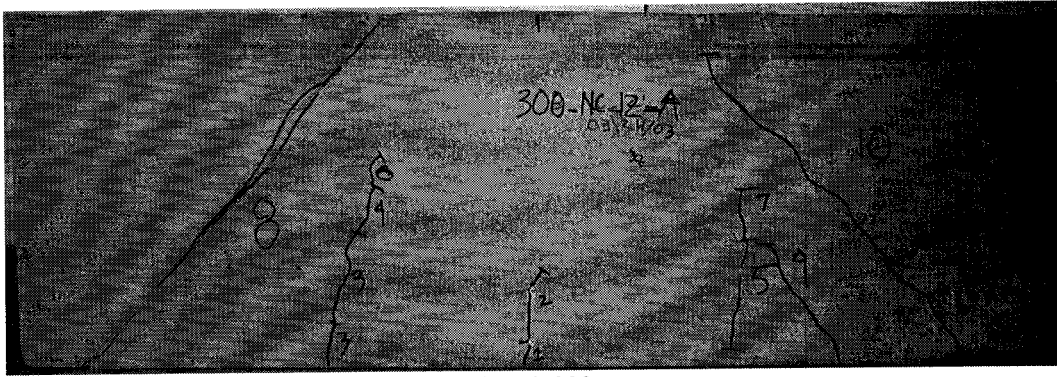
a) N12-300a

b) N12-300b

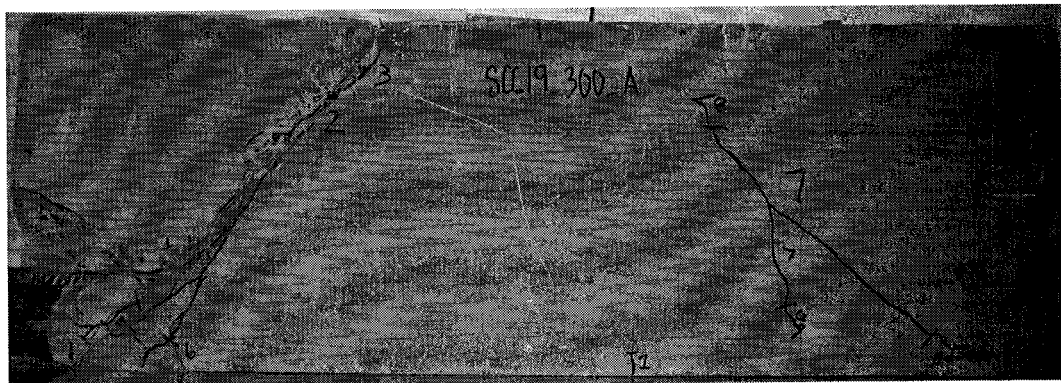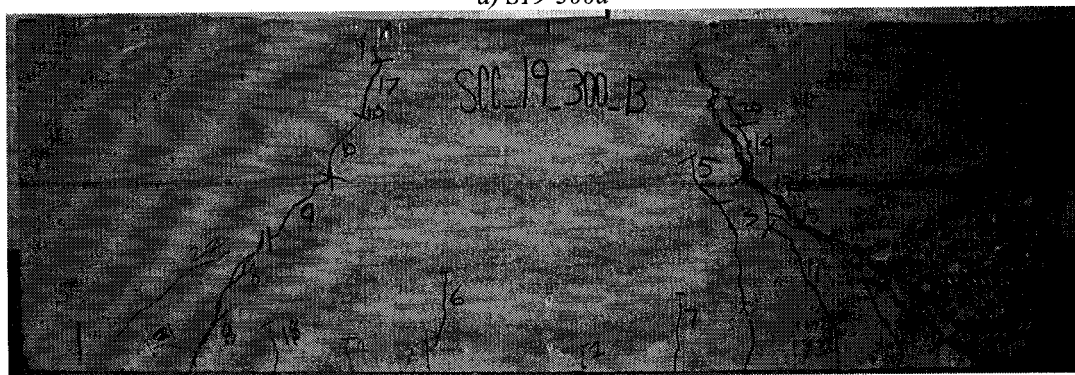*Fig, C1.8 – Crack patterns for Beams N12-300*

a) S19-300a

b) S19-300b

Fig, C1.9 – Crack patterns for Beams S19-300

132